REMAINING LIFE OF REINFORCED CONCRETE BEAMS WITH DIAGONAL-TENSION CRACKS

Final Report

SPR 341

REMAINING LIFE OF REINFORCED CONCRETE BEAMS WITH DIAGONAL-TENSION CRACKS

Final Report

SPR 341

by

Christopher Higgins, Solomon C. Yim, Thomas H. Miller,
Melissa J. Robelo, Tanarat Potisuk

Oregon State University
Structural Engineering Group
Department of Civil Engineering
202 Apperson Hall
Corvallis, OR 97331

for

Oregon Department of Transportation
Research Unit
200 Hawthorne Ave. SE -- Suite B-240
Salem, OR 97301-5192

and

Federal Highway Administration
400 Seventh Street SW
Washington, DC 20590

April 2004

1. Report No.	2. Government Accession No.	3. Recipient's Catalog No.
FHWA-OR-RD-04-12		

4. Title and Subtitle	5. Report Date
REMAINING LIFE OF REINFORCED CONCRETE BEAMS WITH DIAGONAL-TENSION CRACKS	April 2004
	6. Performing Organization Code

7. Author(s)	8. Performing Organization Report No.
Christopher Higgins, Solomon C. Yim, Thomas H. Miller, Melissa J. Robelo, Tanarat Potisuk Structural Engineering Group, Department of Civil Engineering Oregon State University 202 Apperson Hall Corvallis, OR 97331	

9. Performing Organization Name and Address	10. Work Unit No. (TRAIS)
Oregon Department of Transportation Research Group 200 Hawthorne SE, Suite B-240 Salem, Oregon 97301-5192	11. Contract or Grant No. SPR 341

12. Sponsoring Agency Name and Address			13. Type of Report and Period Covered
Oregon Department of Transportation Research Unit 200 Hawthorne SE, Suite B-240 Salem, Oregon 97301-5192	and	Federal Highway Administration 400 Seventh Street SW Washington, DC 20590	Final Report 14. Sponsoring Agency Code

15. Supplementary Notes

16. Abstract

This report covers the initial efforts of a research study investigating the remaining capacity and life of cast-in-place reinforced concrete deck-girder (RCDG) bridges with diagonal tension cracks. A database of 442 bridges constructed from 1947 to 1962 was developed to identify salient parameters related to bridges with diagonal tension cracks in the Oregon Department of Transportation bridge inventory. The database was queried to provide summary details for individual parameters and relationships between parameters. In addition, a bridge analysis was conducted on an in-service RCDG bridge with diagonal tension cracks. A linear finite element model of the bridge provided reasonable prediction of cracking.

17. Key Words	18. Distribution Statement
conventionally reinforced concrete bridge, diagonal tension cracking, field testing, modeling, bridge characteristic, database	Copies available from NTIS, and online at http://www.odot.state.or.us/tddresearch

19. Security Classification (of this report)	20. Security Classification (of this page)	21. No. of Pages	22. Price
Unclassified	Unclassified	124 + appendices	

Technical Report Form DOT F 1700.7 (8-72) Reproduction of completed page authorized Printed on recycled paper

SI* (MODERN METRIC) CONVERSION FACTORS

APPROXIMATE CONVERSIONS TO SI UNITS

Symbol	When You Know	Multiply By	To Find	Symbol
		LENGTH		
In	inches	25.4	Millimeters	mm
Ft	feet	0.305	Meters	m
Yd	yards	0.914	Meters	m
Mi	miles	1.61	Kilometers	km
		AREA		
In^2	square inches	645.2	Millimeters squared	mm^2
ft^2	square feet	0.093	Meters squared	m^2
Yd^2	square yards	0.836	Meters squared	m^2
Ac	acres	0.405	Hectares	ha
Mi^2	square miles	2.59	Kilometers squared	km^2
		VOLUME		
fl oz	fluid ounces	29.57	Milliliters	mL
Gal	gallons	3.785	Liters	L
ft^3	cubic feet	0.028	Meters cubed	m^3
Yd^3	cubic yards	0.765	Meters cubed	m^3
NOTE: Volumes greater than 1000 L shall be shown in m^3.				
		MASS		
Oz	ounces	28.35	Grams	g
Lb	pounds	0.454	Kilograms	kg
T	short tons (2000 lb)	0.907	Megagrams	Mg
		TEMPERATURE (exact)		
°F	Fahrenheit temperature	5(F-32)/9	Celsius temperature	°C

APPROXIMATE CONVERSIONS FROM SI UNITS

Symbol	When You Know	Multiply By	To Find	Symbol
		LENGTH		
mm	millimeters	0.039	inches	in
m	meters	3.28	feet	ft
m	meters	1.09	yards	yd
km	kilometers	0.621	miles	mi
		AREA		
mm^2	millimeters squared	0.0016	square inches	in^2
m^2	meters squared	10.764	square feet	ft^2
ha	hectares	2.47	acres	ac
km^2	kilometers squared	0.386	square miles	mi^2
		VOLUME		
mL	milliliters	0.034	fluid ounces	fl oz
L	liters	0.264	gallons	gal
m^3	meters cubed	35.315	cubic feet	ft^3
m^3	meters cubed	1.308	cubic yards	yd^3
		MASS		
g	grams	0.035	ounces	oz
kg	kilograms	2.205	pounds	lb
Mg	megagrams	1.102	short tons (2000 lb)	T
		TEMPERATURE (exact)		
°C	Celsius temperature	1.8C + 32	Fahrenheit	°F

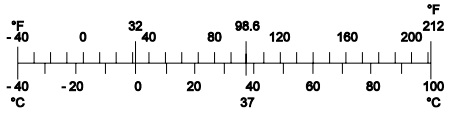

***** SI is the symbol for the International System of Measurement (4-7-94 jbp)

ACKNOWLEDGEMENTS

The authors would like to thank Mr. Steven M. Soltesz of the Oregon Department of Transportation Research Unit for his assistance in coordinating research efforts within ODOT. Additionally, the authors would like to thank Mr. William Farrow III and Mr. James Newell for their help in conducting the field investigation, as well as Ms. Theresa Daniels, Mr. Brian Nicholas, Mr. Ryan Parmenter, and Mr. John Poland for their help in development of the database. The opinions, findings, and conclusions are those of the authors and do not necessarily reflect the views of the individuals acknowledged above.

DISCLAIMER

This document is disseminated under the sponsorship of the Oregon Department of Transportation and the United States Department of Transportation in the interest of information exchange. The State of Oregon and the United States Government assume no liability of its contents or use thereof.

The contents of this report reflect the views of the author(s) who are solely responsible for the facts and accuracy of the data presented herein. The contents do not necessarily reflect the official policies of the Oregon Department of Transportation or the United States Department of Transportation.

The State of Oregon and the United States Government do not endorse products of manufacturers. Trademarks or manufacturers' names appear herein only because they are considered essential to the object of this document.

This report does not constitute a standard, specification, or regulation.

REMAINING LIFE OF REINFORCED CONCRETE BEAMS WITH DIAGONAL-TENSION CRACKS

TABLE OF CONTENTS

LIST OF FIGURES

PART I: BRIDGE DATABASE

LIST OF TABLES

PART I: BRIDGE DATABASE

PART II: FIELD STUDY AND ANALYSIS

INTRODUCTION TO THE REPORT

There are over 500 cast-in-place reinforced concrete deck-girder (RCDG) bridges in the Oregon Department of Transportation (ODOT) inventory that are identified as exhibiting diagonal-tension cracking. Of these cracked bridges, nearly half are along the I-5 and I-84 corridors. The majority of the cracked bridges were built between the years 1947 and 1962. Weight restrictions on cracked bridges have caused significant detours, and emergency response to maintain transportation corridors in the State has been costly. The problem has also impacted municipal and county agencies.

Due to the large number of bridges involved, a research study was undertaken to investigate the remaining capacity and life of RCDG bridges with diagonal tension cracks. Initially, a relatively small research project was started, but as the magnitude of the problem increased, the scope of the research effort was expanded in order to conduct a thorough investigation of the problem. The complete study includes field testing, laboratory testing, and analysis components. This report covers work completed under the initial effort. It is divided into two parts:

- Part I: A database of Oregon's RCDG bridges most prone to diagonal-tension cracks

  The database was developed to identify salient parameters related to bridges with diagonal tension cracks in the ODOT bridge inventory. The database focused on 442 bridges constructed from 1947 to 1962 that were identified by ODOT as cracked.

  Structural drawings for each individual bridge were reviewed and parameters corresponding to overall bridge geometry, material properties, member proportions, and reinforcement layout were recorded in the database. The database was queried to provide summary details for individual parameters and relationships between parameters. Further, dead load magnitudes and live load capacities were developed for comparison with AASHTO load models, weigh-in-motion service-level loads, and ODOT permit tables.

  Part I is comprised of Chapters 1-7 in this report.

- Part II: An analysis of a bridge with diagonal-tension cracks

  The bridge analysis was conducted on an in-service RCDG bridge with diagonal tension cracks. Crack characteristics and steel stirrup locations were documented for the spans under investigation, and eight diagonal cracks were instrumented to monitor crack motions and strains in steel stirrups that intersected the cracks.

  Data were collected under ambient traffic and controlled truck loading. Dynamic and impact loading, load distribution across girders, deck thickness, diaphragm stiffness, shrinkage, creep, and temperature were included in the analysis. Design values for one of the bridge girders were compared using the 1953 and 2002 versions of the AASHTO Standard Specification. A linear finite element model of the bridge provided reasonable prediction of cracking.

  Part II is comprised of Chapters 8-15 in this report.

PART I: BRIDGE DATABASE

1.0 INTRODUCTION

A database was developed to identify salient parameters related to shear-cracked bridges in the Oregon Department of Transportation (ODOT) bridge inventory. A search of the inventory for concrete bridges with structural type category: stringer/multi-beam/girder, girder and floorbeam, and Tee-beam was performed for the years 1900 to 2001. Based on this search, a total of 1536 bridges were identified. Of these, 493 (32%) were categorized as shear-cracked by ODOT (Crack Stages 1 to 3).

Considering the year of construction, 382 were from the period 1900 to 1945 and only 6 (2% of this group) were identified as cracked; 924 were from the period 1946 to 1962 and 479 (52% of this group) were identified as cracked, and 230 were from the period 1963 to 2001 and only 8 (3% of this group) were identified as cracked. Thus, the vast majority of cracked bridges was from the late 1940's to early 1960's. Based on this observation, bridges constructed between 1947 to 1962 were selected for detailed investigation.

A database was developed for bridges constructed from 1947 to 1962 that were identified by ODOT as cracked. There were 442 bridges entered into the database, reduced from the 479 bridges identified previously, due to actual structural configurations and details not being consistent with the structural type category identified as exhibiting shear cracking in the field. In addition, various bridges were of unique design and problematic to input into the database structure, and still other bridges were missing design drawings.

Structural drawings for each individual bridge were reviewed and parameters corresponding to overall bridge geometry, material properties, member proportions, and reinforcement layout were recorded in the database. The database was queried to provide summary details for individual parameters and relationships between parameters. Further, dead load magnitudes and live load capacities were developed for comparison with AASHTO load models, weigh-in-motion service-level loads, and ODOT permit tables. Database summaries were used to develop member proportions and material properties for laboratory specimens and to identify typical bridges for field instrumentation.

2.0 OVERALL BRIDGE GEOMETRY AND LAYOUT

2.1 STRUCTURAL INDETERMINACY

Within the set of data, six different types of structural indeterminacy were identified. These ranged from cantilever spans to bridges consisting of six continuous spans, as shown in Figure 2.1. Of the 442 bridges contained in the database, there were 774 configurations that could be considered structurally independent. The majority of the configurations were simple spans and three spans continuous, as shown in Figure 2.2. The percentage of simple spans was 34% and the percentage of three-span continuous was 39%. Approximately 8% of the spans in the database were cantilever spans.

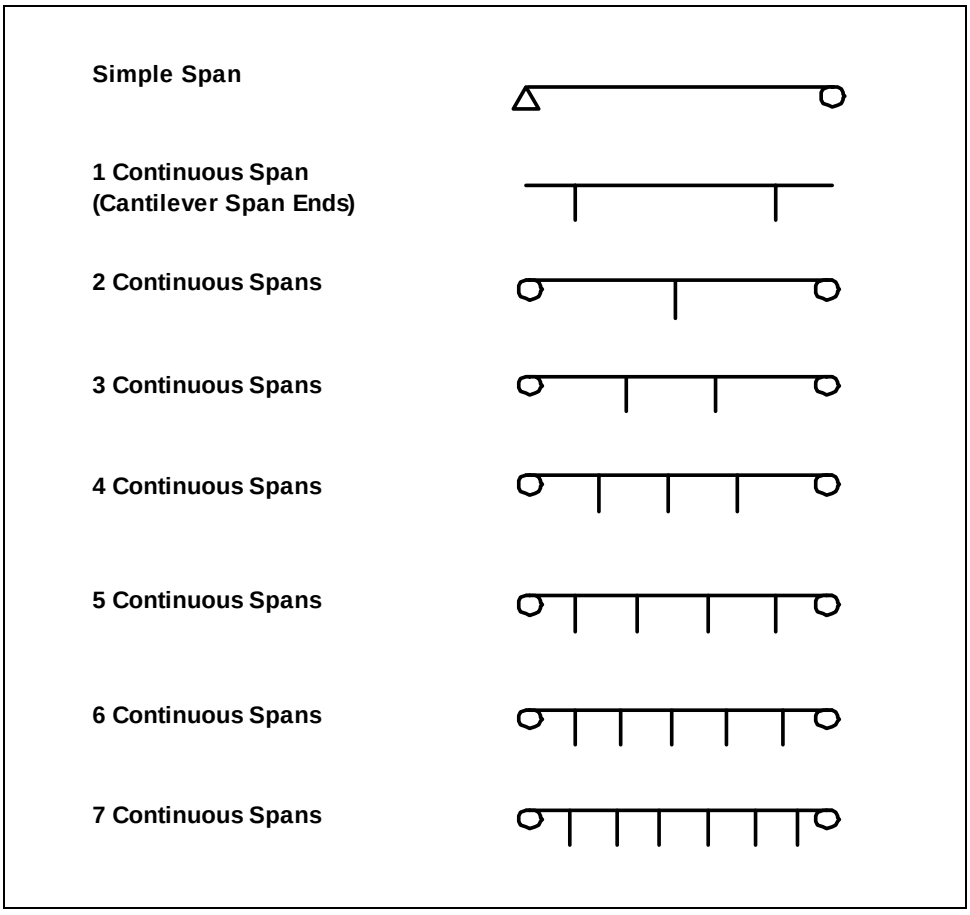

Figure 2.1: Types of indeterminacy

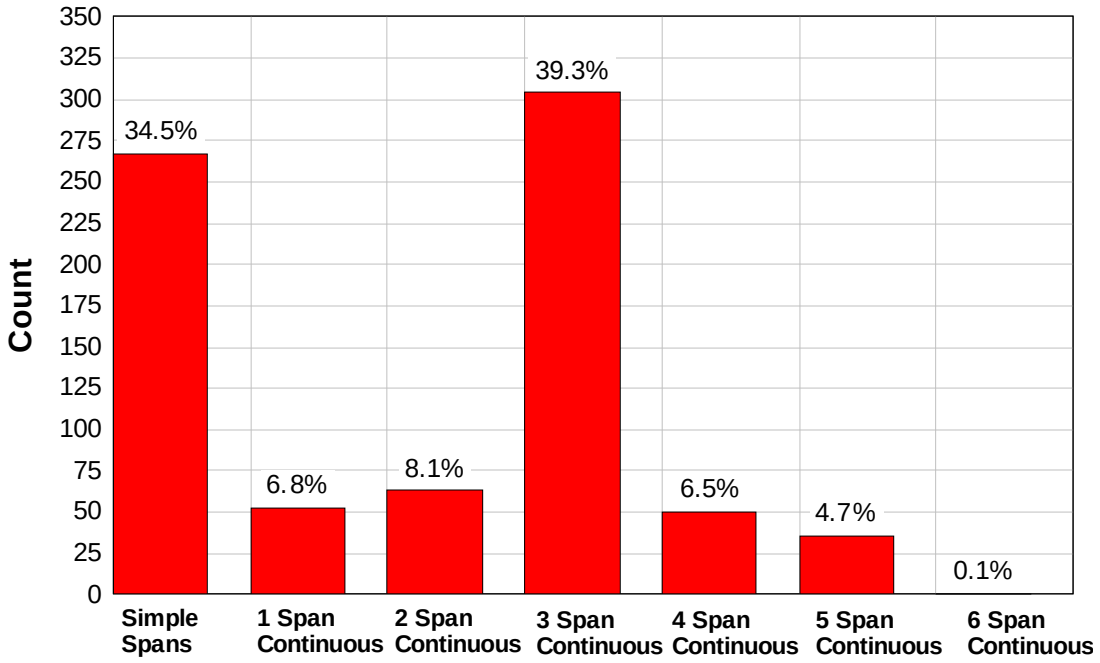

Figure 2.2: Structurally independent configurations

A span could have two simply supported ends (SS), a simply supported end in combination with a continuous support on the other end (SC), continuous supports on both ends (CC), and the span could be a cantilever (Figure 2.3a). Most of the spans (51%) were found to be of the SC type (Figure 2.3b).

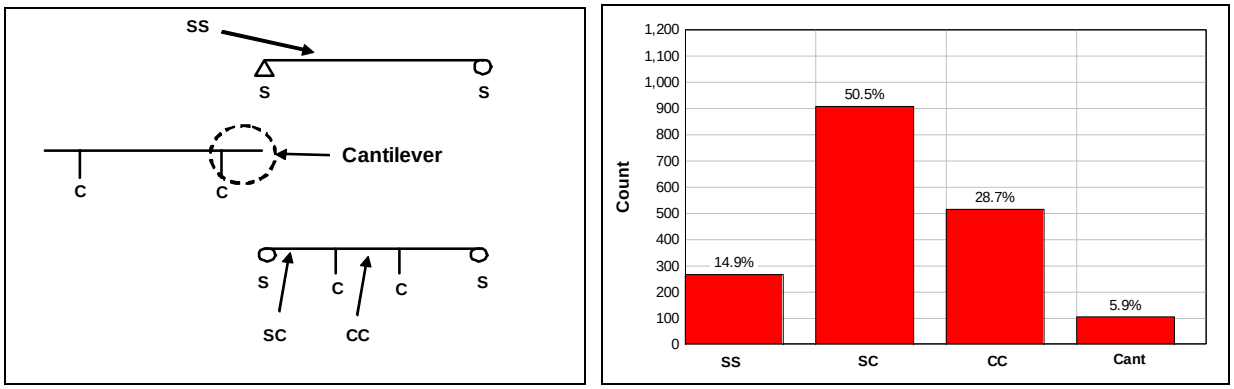

(a) (b)

Figure 2.3: Span indeterminacy – (a) Types of span indeterminacy; (b) Frequency of span indeterminacy types

2.2 SPAN LENGTH

The span length was taken from the plan view of the design drawings as the length along the centerline of the span between the centerlines of supports. The range of spans was from 11 ft to 120 ft. The most frequently occurring range of span lengths for all crack stages was between 40 and 45 ft at a rate of 16%, as shown in Figure 2.4a. The span length, when grouped by crack stage and averaged, tended to be longer as the crack stage increased, as seen in Figure 2.4b. The most frequently occurring span lengths, grouped by crack stage at 5 ft intervals indicated that higher crack stage tended to correspond with longer spans, as shown in Table 2.1, a summary of which can be seen in Figures 2.4c, 2.4d, and 2.4e. Cantilever spans were not included for these comparisons, as these have very short spans in comparison.

Table 2.1: Span lengths for each crack stage

Crack Stage	Most frequently occurring Span lengths within Crack Stage	Rate of Occurrence within Crack Stage
1	25 ft to 30 ft	23%
2	40 ft to 45 ft	23%
3	55 ft to 60 ft	15%

2.3 SKEW

The skew was determined from the plan view of the overall bridge design drawing. The skew angle was taken as the deviation of the roadway direction from the support orientation, in degrees, with a clockwise rotation being positive. Typically, support lines are oriented vertically on the drawings.

The total number of spans that had a skew on either or both ends of the span was 713 and the total number of span-ends with skew was 1,402. The rest of the spans, 915, did not have a skew on either end of the span. For analysis, the absolute values of the skews were utilized. The skew angles ranged between 0.1 to 63 degrees. The two most common ranges of skew angle for all skewed span ends were 30 to 32 degrees and 44 to 46 degrees, both occurring at rates of about 9%, as shown in Figure 2.5a.

The same ranges of skew angle were predominant for spans of Crack Stage 1 and 2. The range of 30 to 32 degrees occurred at a rate of 11% for Crack Stage 1, and 9% for Crack Stage 2. For spans of Crack Stage 1 and 2, the range of 44 to 46 degrees occurred with a frequency of 9%, as shown in Figures 2.5b and 2.5c. The peak range of skew angle for spans of Crack Stage 3 was between 44 and 46 degrees occurring at a rate of 14%, as shown in Figure 2.5d.

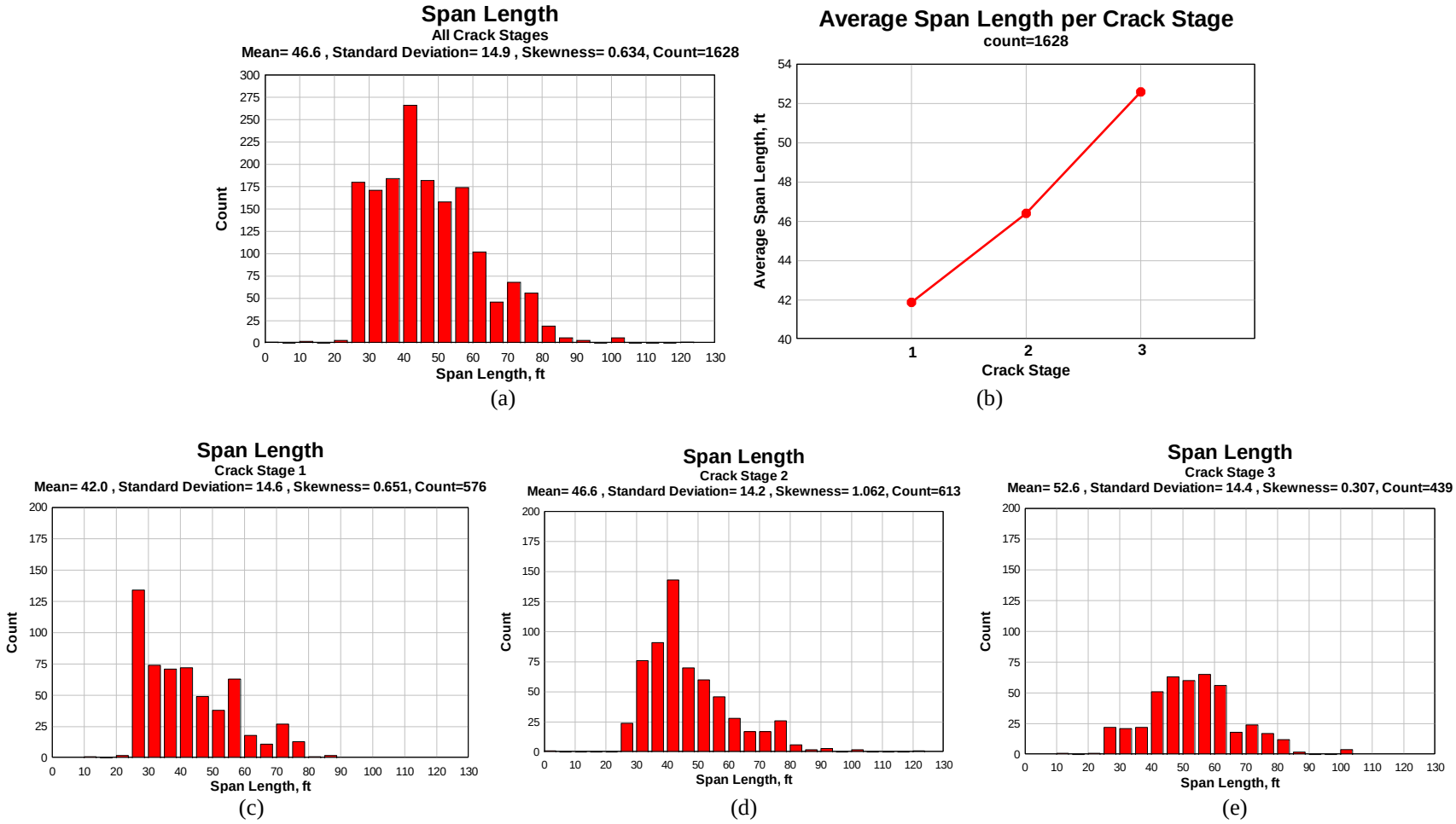

Figure 2.4: Span length – (a) All crack stages; (b) Average per crack stage; (c) Crack Stage 1; (d) Crack Stage 2; (e) Crack Stage 3

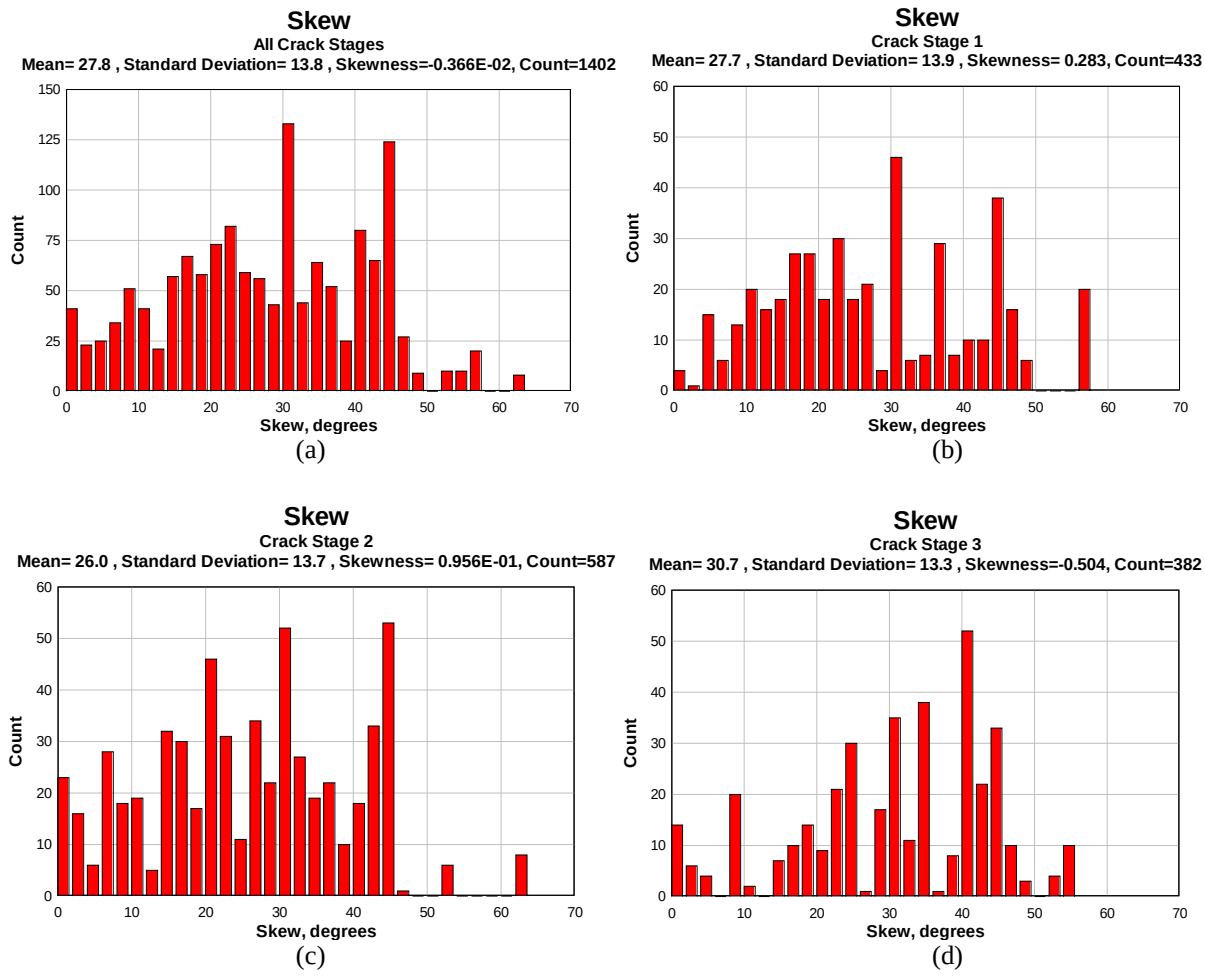

Figure 2.5: Skew – (a) All crack stages; (b) Crack Stage 1; (c) Crack Stage 2; (d) Crack Stage 3

2.4 LANES

The number of lanes carried by each bridge was predominantly determined from the roadway width of the bridge and occasionally from the general notes section of the design drawings. A large majority of the bridges in the database (approximately 76%) carries two lanes of traffic as shown in Figure 2.6.

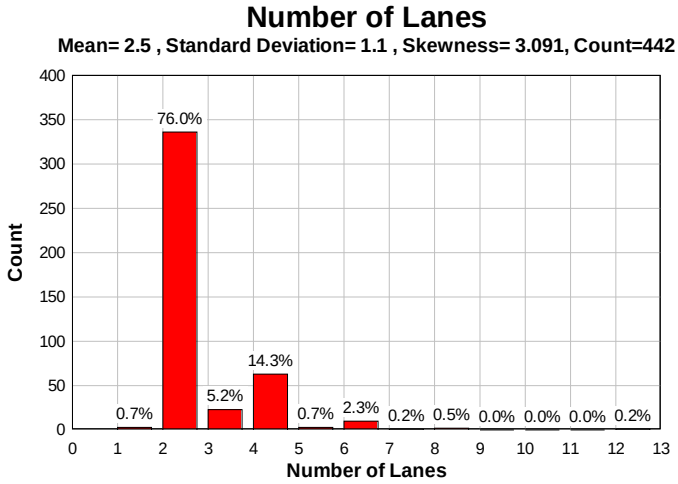

Figure 2.6: Number of lanes

2.5 DECK

Based on design drawings of the bridge cross-section, the slab thickness was determined. Typically, bridges had slab thickness between 6 and 6.5 in., although slab thicknesses up to 8 in. were observed, as shown in Figure 2.7. The 6 in. slabs accounted for 51% of the total number of bridges and 6.5 in. thick slabs accounted for 32%.

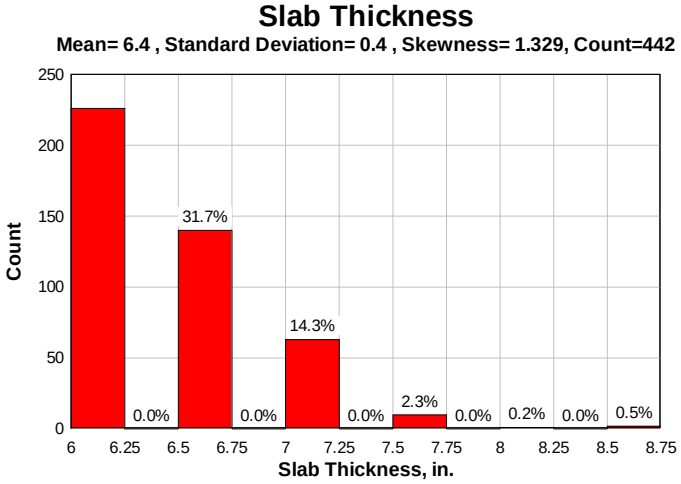

Figure 2.7: Slab thickness

2.6 GIRDER SPACING

The girder spacing was taken from the plan view of the overall bridge drawings, where the exact spacing was generally specified. Girder spacing ranged from 4.75 ft to 16 ft. The most common spacing was 7 ft, accounting for approximately 38% of the spans, as shown in Figure 2.8a. The second most common girder spacing was 9 ft, which appeared in 31% of the spans. A comparison of the data considering crack stage indicated that bridges with larger spacing between girders tended to be at a higher crack stage, as seen in Figure 2.8b. For Crack Stage 3, the most common girder spacing was 9 ft, while for Crack Stages 1 and 2 the most common girder spacing was 7 ft, as shown in Figures 2.8c, 2.8d, and 2.8e. Due to the fact that the most common number of girders does not change with crack stage (Figure 2.9), while the most common girder spacing increases (Figure 2.8), it can be deduced that girders in Crack Stage 3 bridges tend to have larger tributary areas, thus carrying larger forces and moments than the girders of lower crack stage bridges.

2.7 NUMBER OF GIRDERS

The number of girders supporting each span was determined from the plan view of the overall bridge drawing. The number of girders per span ranged from 2 to 13, but the most common configuration was 4 girder lines with an occurrence of 65%, as shown in Figure 2.9a, and did not vary with crack stage. All crack stages had predominantly 4 girders per span, but a comparison of the data considering crack stage indicated that bridges with more girder lines tended to be at a lower crack stage, as shown in Figure 2.9b. Higher numbers of girders per span (5 to 13 girders per span) occurred more frequently with lower crack stages, as can be seen in Table 2.2 and in Figures 2.9c, 2.9d, and 2.9e.

Table 2.2: Number of spans with 5 to 13 girders

Crack Stage	Number of Spans with 5 to 13 Girders (% of Spans within Crack Stage)
1	262 (45%)
2	206 (33%)
3	90 (20%)

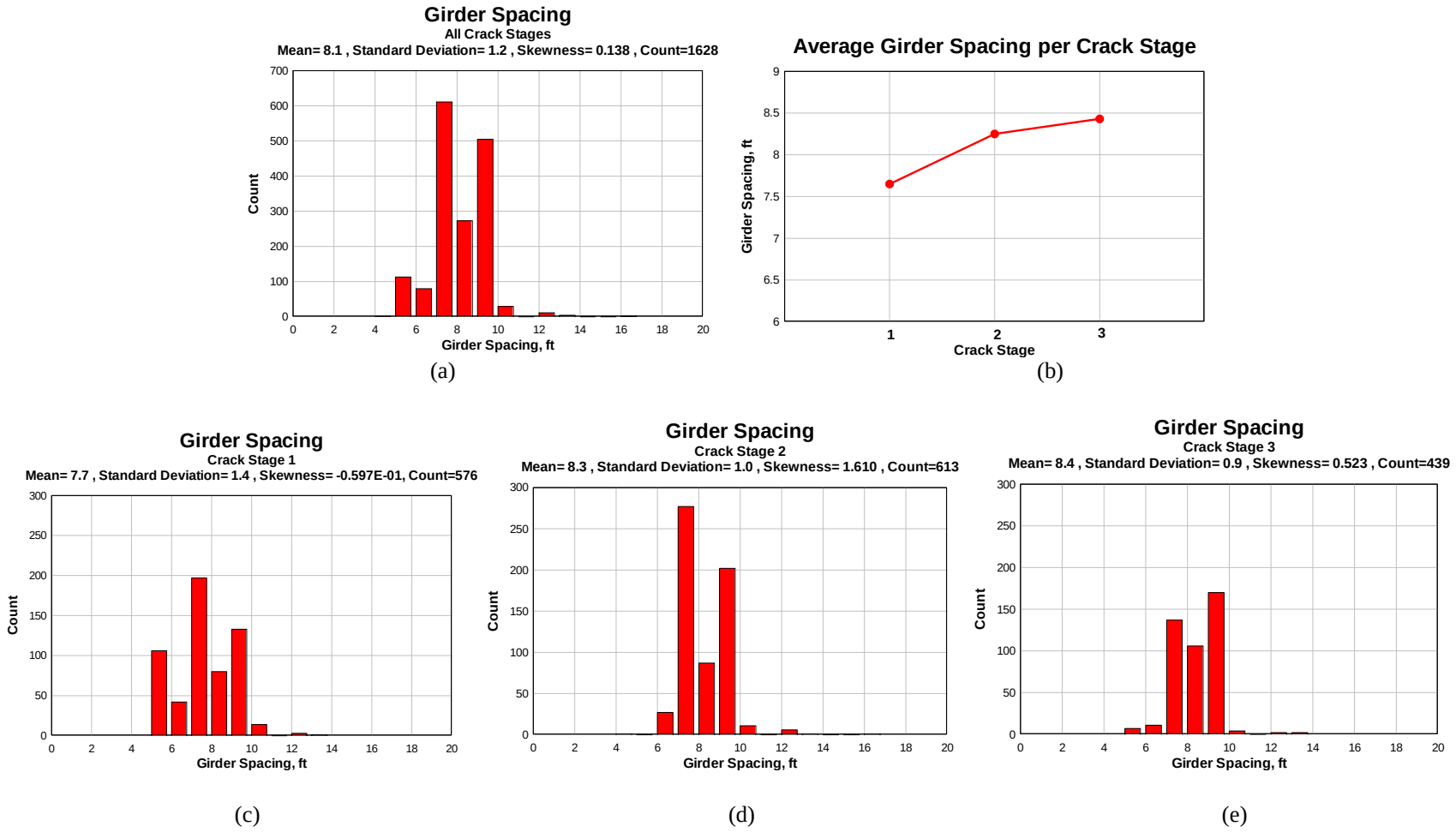

Figure 2.8: Girder spacing – (a) All crack stages; (b) Average per crack stage; (c) Crack Stage 1; (d) Crack Stage 2; (e) Crack Stage 3

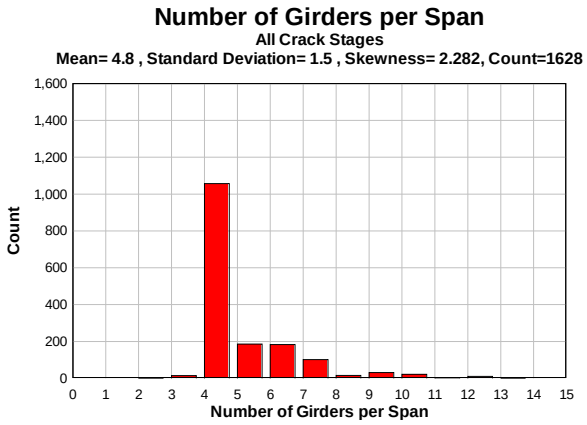

(a)

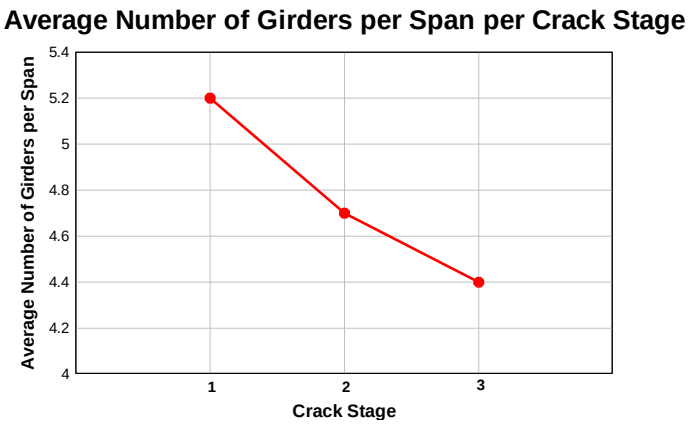

(b)

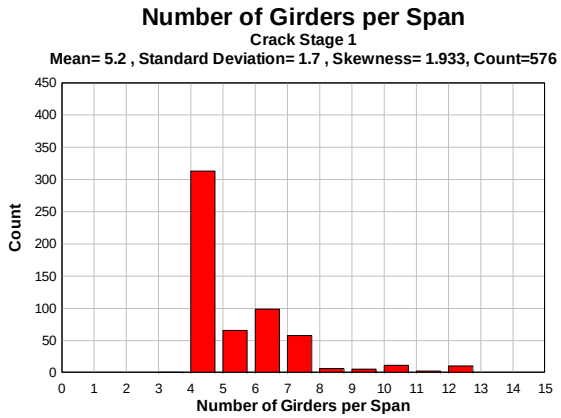

(c)

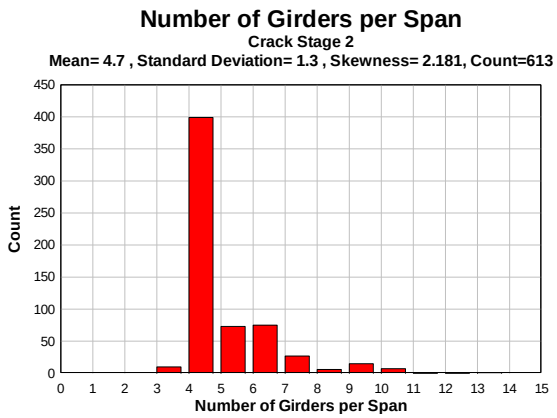

(d)

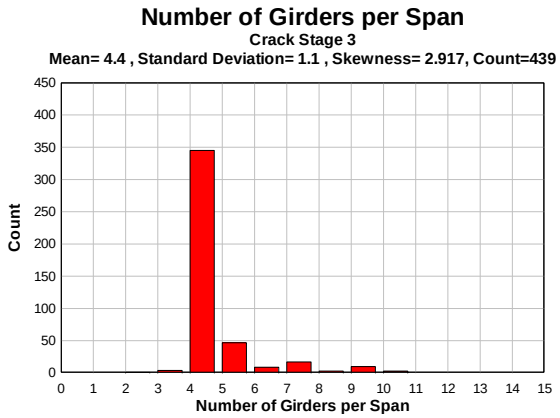

(e)

Figure 2.9: Number of girders per span – (a) All crack stages; (b) Average per crack stage; (c) Crack Stage 1; (d) Crack Stage 2; (e) Crack Stage 3

2.8 DIAPHRAGMS

Out of the entire population of spans (excluding cantilevers as they typically do not have diaphragms), about 9% did not have diaphragms (Figure 2.10). Those spans without diaphragms were generally very short spans or significantly skewed.

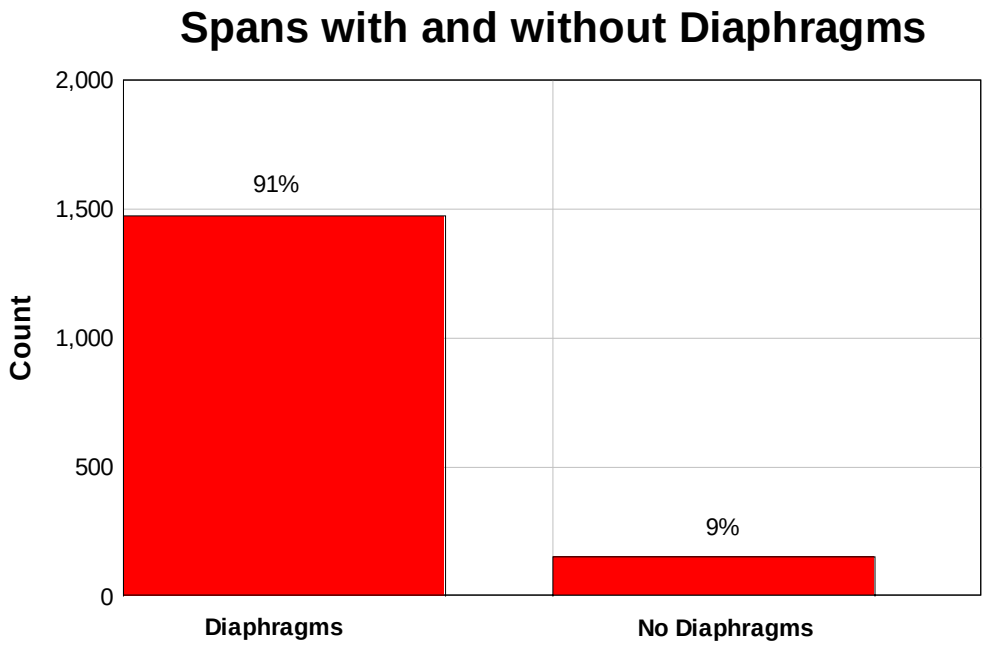

Figure 2.10: Spans with and without diaphragms

2.9 DIAPHRAGM SPACING

The diaphragm spacing was taken from the plan view of the overall bridge drawing, where the exact spacing was generally indicated. The majority of the diaphragms were located within two regions of the span length: 53% were between 0.2 and 0.3 of the span length, and 41% were between 0.5 and 0.6 of the span length, as shown in Figure 2.11a. This did not change with crack stage. The range between 0.2 and 0.3 of the span length accounted for 46% of the Crack Stage 1 spans, 46% of the Crack Stage 2 spans, and 71% of the Crack Stage 3 spans, as shown in Figures 2.11b, 2.11c, and 2.11d. The range between 0.5 and 0.6 of the span length accounted for 49% of the Crack Stage 1 spans, 49% of the Crack Stage 2 spans, and 23% of the Crack Stage 3 spans.

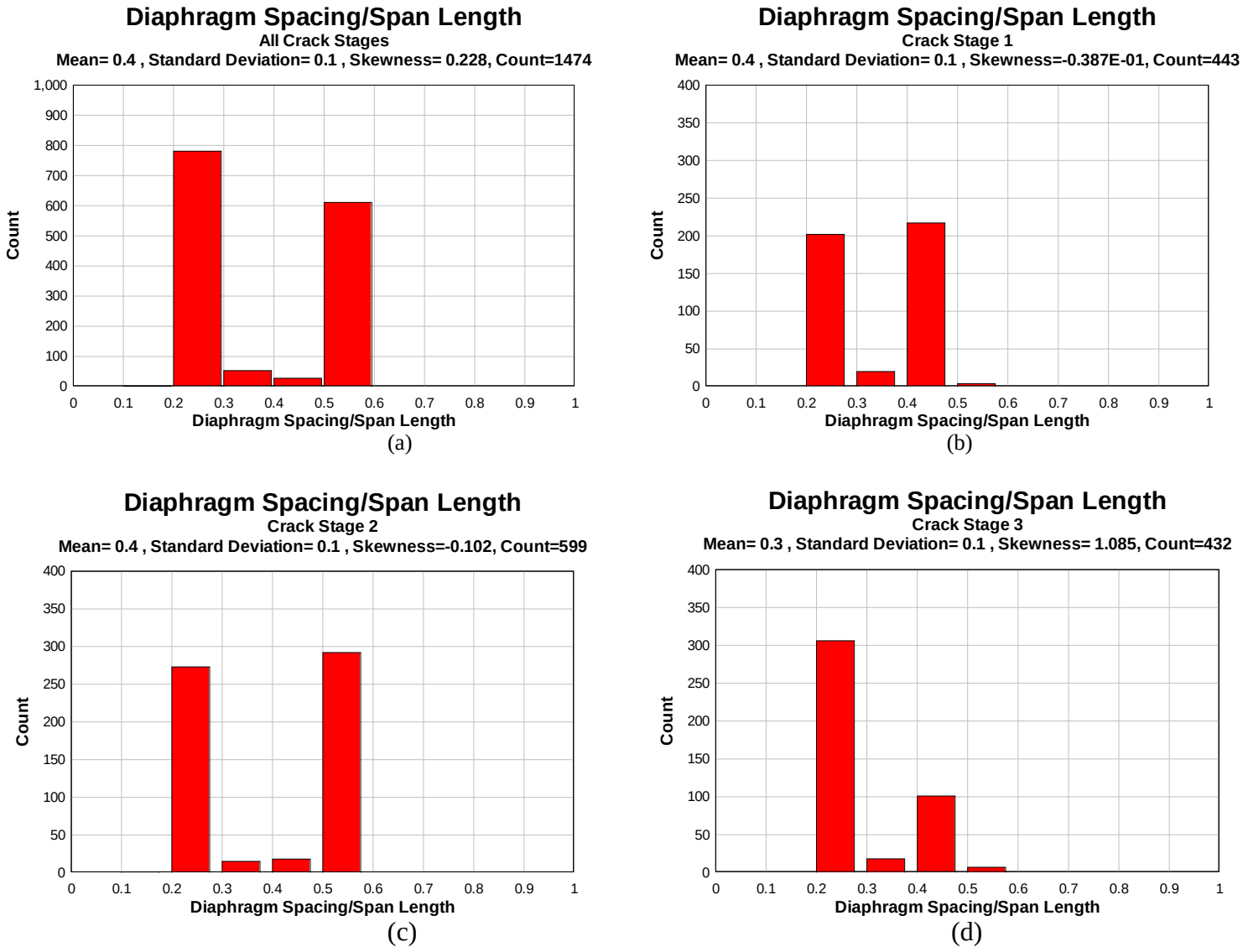

Figure 2.11: Diaphragm spacing/span length – (a) All crack stages; (b) Crack Stage 1; (c) Crack Stage 2; (d) Crack Stage 3

2.10 NUMBER OF DIAPHRAGMS

For each span, the number of diaphragms was determined from the plan view of the overall bridge drawing. For spans with diaphragms, about 53% had 3 diaphragms per span and 43% had 1 diaphragm, nearly an even split, as shown in Figure 2.12a. When the data set was grouped by crack stage and analyzed, the nearly even split between the number of spans with 1 and 3 diaphragms was seen for Crack Stages 1 and 2, but not for Crack Stage 3. The large majority, 71%, of the Crack Stage 3 spans had 3 diaphragms per span. This resulted in a slightly higher average number of diaphragms per span for Crack Stage 3 as compared to Crack Stages 1 and 2, as shown in Figures 2.12b, 2.12c, and 2.12d. This may imply that the additional diaphragms do not provide any considerable increase in load distribution compared with fewer diaphragms.

2.11 DIAPHRAGM WIDTH

The diaphragm web width was obtained from the design drawing details of the diaphragm cross-section. The most common width of diaphragm was observed to be 8 inches, occurring in 52% of the spans, as shown in Figure 2.13a. The most common width of diaphragm remained at 8 inches for every crack stage, as shown in Figures 2.13b, 2.13c, and 2.13d. Diaphragms also tended to be only lightly reinforced.

2.12 DIAPHRAGM HEIGHT

The diaphragm height was also obtained from the design drawing details of the diaphragm cross-section. The three most common ranges of diaphragm height for all crack stages were 40 to 42 inches, 34 to 36 inches, and 46 to 48 inches at rates of 17%, 14%, and 12%, respectively, as shown in Figure 2.14a. The diaphragm heights, when grouped by crack stage and averaged, tended to increase with crack stage as seen in Figures 2.14b, 2.14c, 2.14d, and 2.14e.

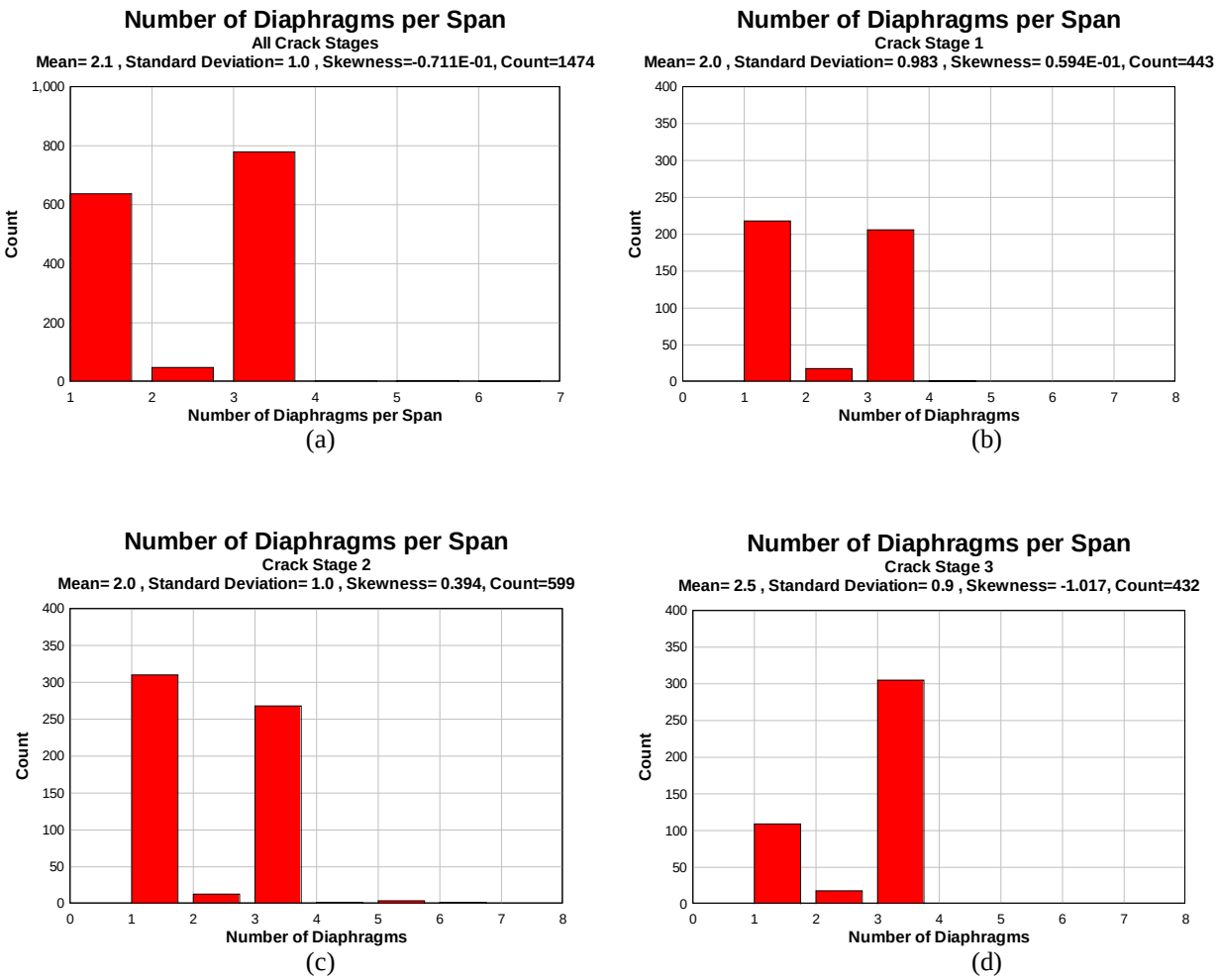

Figure 2.12: Number of diaphragms per span – (a) All crack stages; (b) Crack Stage 1; (c) Crack Stage 2; (d) Crack Stage 3

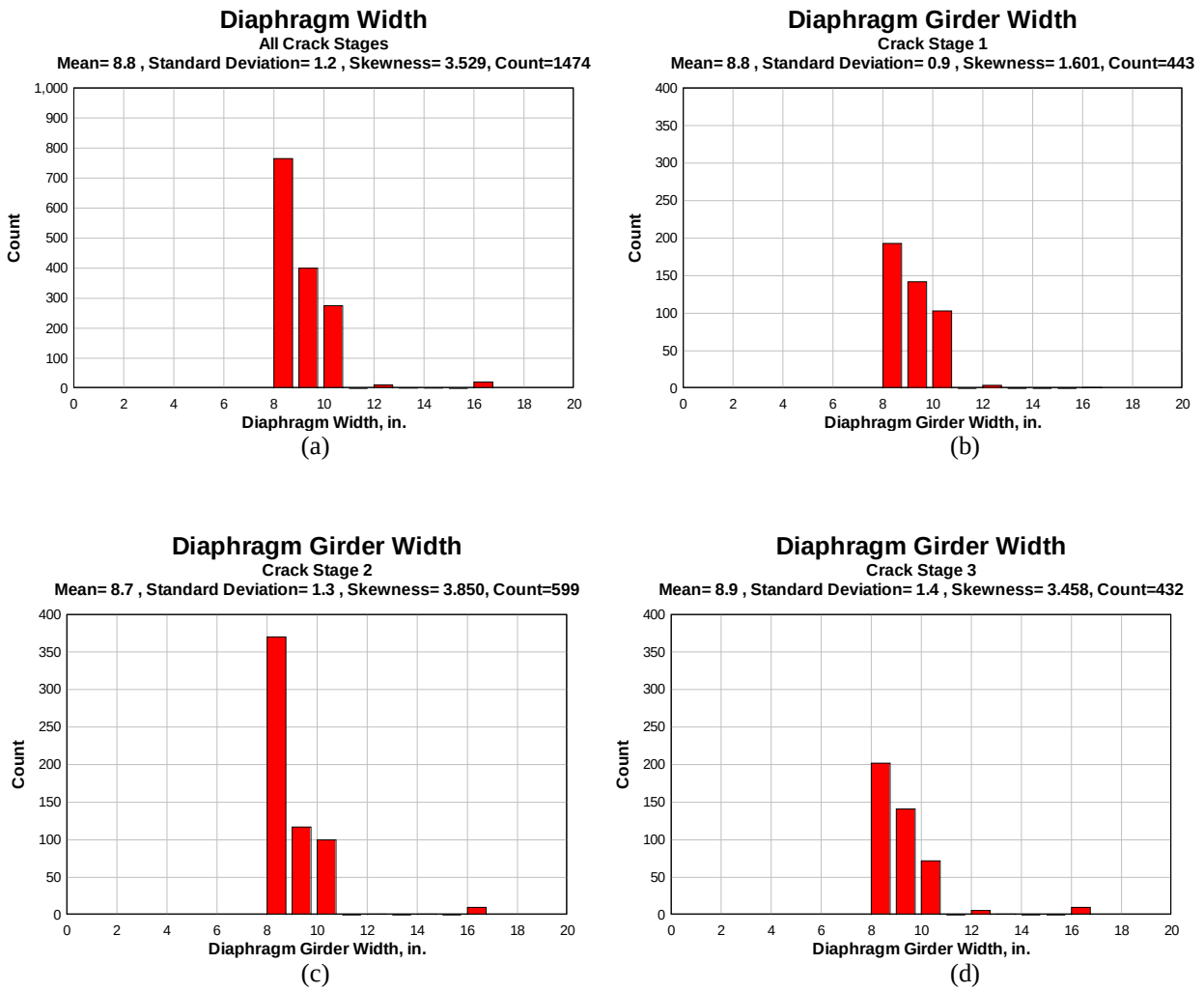

Figure 2.13: Diaphragm girder width – (a) All crack stages; (b) Crack Stage 1; (c) Crack Stage 2; (d) Crack Stage 3

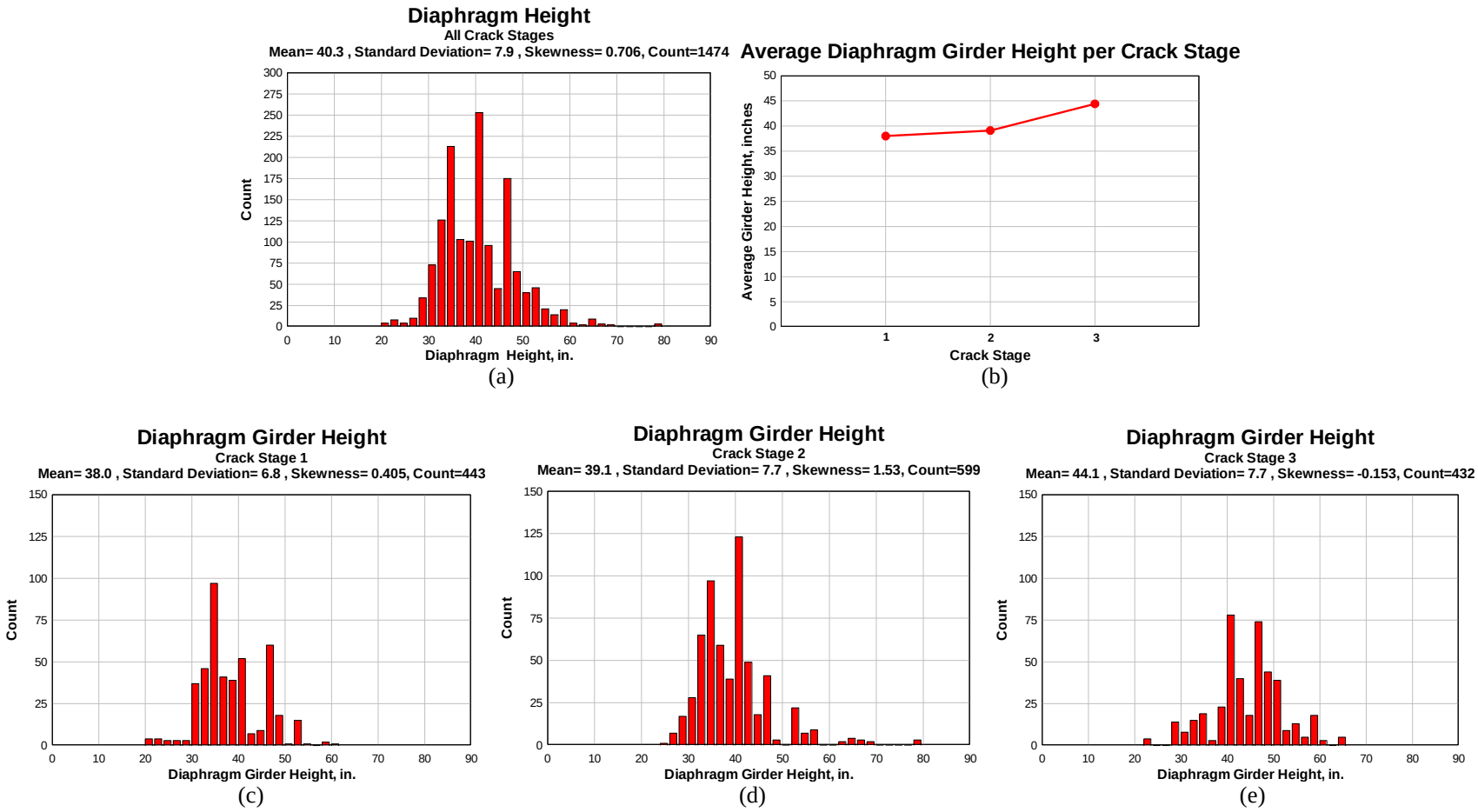

Figure 2.14: Diaphragm height – (a) All crack stages; (b) Average per crack stage; (c) Crack Stage 1; (d) Crack Stage 2; (e) Crack Stage 3

3.0 MATERIALS

The concrete strength and grade of reinforcing steel for each bridge was taken from the general notes normally located on the first page of the bridge design drawings. The specified concrete strength for almost all bridges was 3300 psi (Figure 3.1) and the class was AASHTO Class A. Only two bridges had a specified concrete strength of 3000 psi. In addition, the grade of reinforcing steel for all bridges in the database was found to be intermediate grade, corresponding to ASTM 15-50 for billet-steel bars and ASTM 160-50 for axle-steel bars, both for 1950. Rail steel bars did not have intermediate grade steel. For ASTM 15-50 and ASTM 160-50 intermediate grade deformed bars, the tensile strength requirements were between 70,000 and 90,000 psi. The minimum yield point requirement was 40,000 psi and the minimum percent elongation in an 8 in. gage length was:

$$\%\ elongation = \frac{1{,}100{,}000\,psi}{f_u} \qquad \textbf{(3-1)}$$

where f_u is the ultimate tensile strength in psi and % *elongation* is not less than 12%

The bend test requirements for deformed bars with bar designation number under #6 nominal diameter was 180 degrees, with the diameter of the pin around which the specimen is bent specified to be equivalent to six times the diameter of the specimen. For deformed bars with bar designation number over #6, the bend test requirement was 90 degrees, with the diameter of the pin around which the specimen is bent specified as six times the diameter of the specimen. The minimum requirements for deformations of the deformed steel bars were specified in ASTM A305-50.

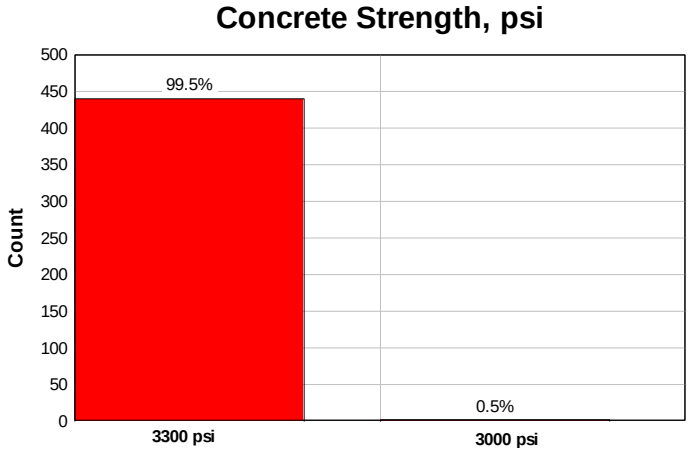

Figure 3.1: Concrete strength

4.0 MEMBER PROPORTIONS

4.1 T-BEAMS

The cross-sectional shape of the bridge girders was determined from the bridge design drawings of the girder cross-sections. Of the total number of spans in the database, 98% were composed of T-beams (Figure 4.1a). The rest of the spans, only about 2%, were composed of girders with bulb-shaped sections (Figure 4.1b).

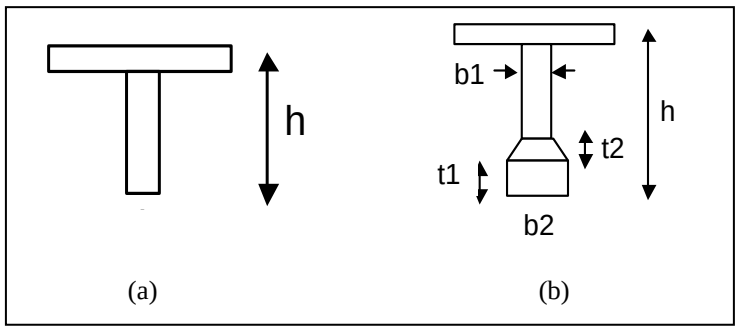

Figure 4.1: Cross-sectional shape – (a) T-beam section; (b) Bulb shape beam section

4.2 WEB WIDTH AT MIDSPAN AND SPAN ENDS

The girder web width was determined based on design drawing details of the bridge cross-section. The girder width often increased at support locations due to tapering. Therefore, girder width was analyzed separately at midspan and at support locations. Girder width at midspan ranged between 9 in. and 23.5 in., and at support locations ranged between 9 in. and 33 in. The most common girder width at both midspan and support locations was 13 in., as shown in Figures 4.2a and 4.2b, and did not change with crack stage. However, variations did occur between crack stages in the distribution of girder widths for both midspan and support locations, resulting in variation of the average girder width per crack stage, as shown in Figures 4.2c and 4.2d. Data indicated that larger girder widths tended to be at a higher crack stage. This was observed for girder widths at both the midspan and support locations, as illustrated in Figures 4.2e through 4.2j.

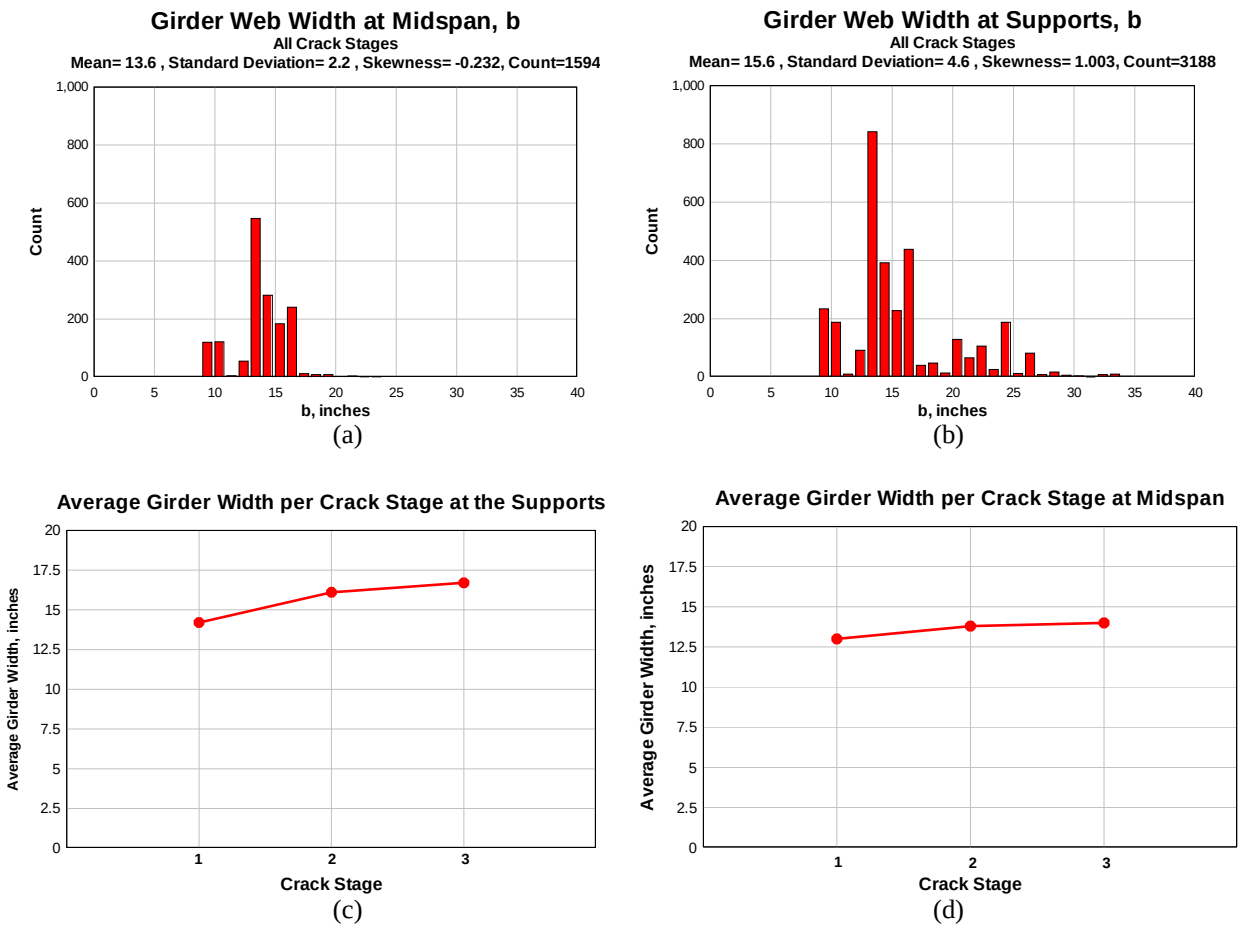

Figure 4.2: Girder width – (a) All crack stages, midspan; (b) All crack stages, supports; (c) Average per crack stage, midspan; (d) Average per crack stage, supports

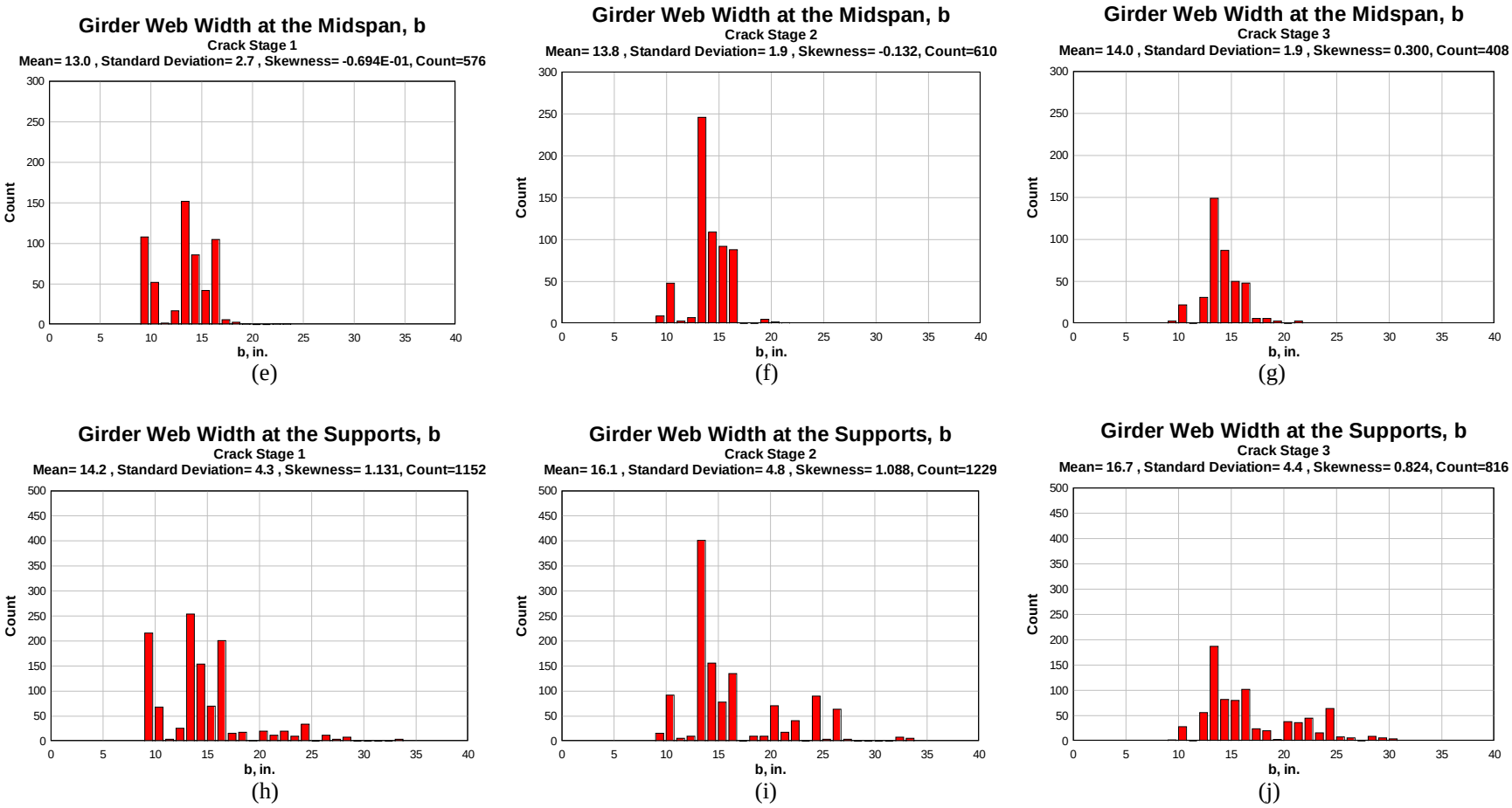

Figure 4.2 (continued): Girder width – (e) Crack Stage 1, midspan; (f) Crack Stage 2, midspan; (g) Crack Stage 3, midspan; (h) Crack Stage 1, supports; (i) Crack Stage 2, supports; (j) Crack Stage 3, supports

4.3 OVERALL GIRDER HEIGHT AT MIDSPAN AND SPAN ENDS

Girder height was determined based on design drawing details of the bridge cross-section. Frequently the girder height increased at support locations due to a haunch. As a result, data for girder height was independently analyzed at support locations and at midspan. The girder height at midspan ranged between 22 in. and 78 in., and at support locations ranged between 22 in. and 120.5 in.

There were three peak ranges of girder heights that occurred with approximately the same frequency. These ranges were the same for both midspan and support locations and were 36 to 38 inches, 42 to 44 inches, and 48 to 50 inches as shown in Figures 4.3a and 4.3b. At midspan, these occurred at rates of 15%, 16%, and 12%, respectively. At support locations, these occurred at rates of 12%, 11%, and 13%, respectively. Comparison of girder heights at midspan and support locations between different crack stages suggested that bridges with larger girder heights tended to be at a higher crack stage, as shown in Figures 4.3c through 4.3j.

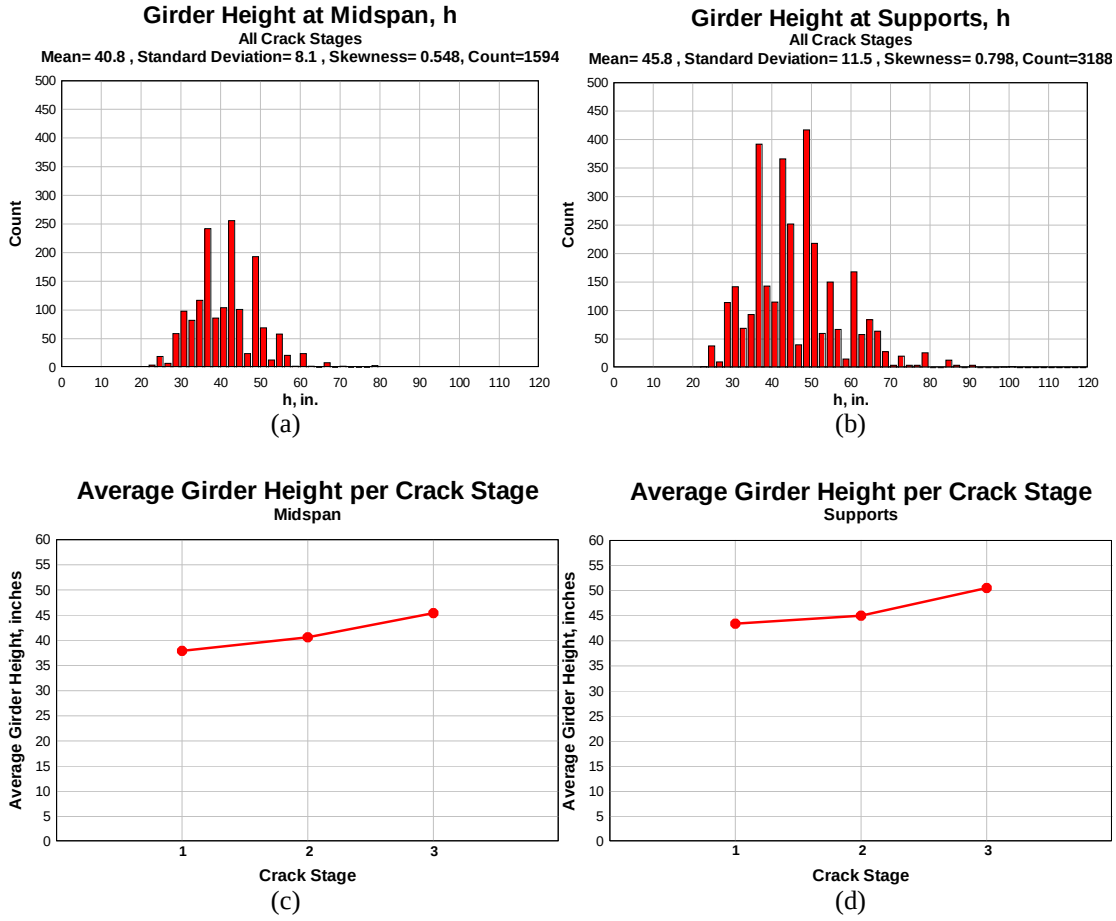

Figure 4.3: Girder height – (a) All crack stages, midspan; (b) All crack stages, supports; (c) Average per crack stage, midspan; (d) Average per crack stage, supports

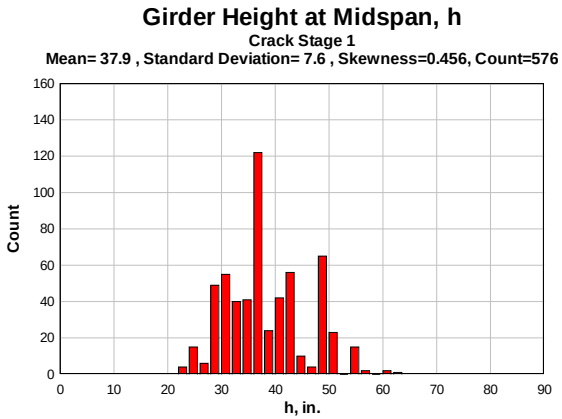

(e)

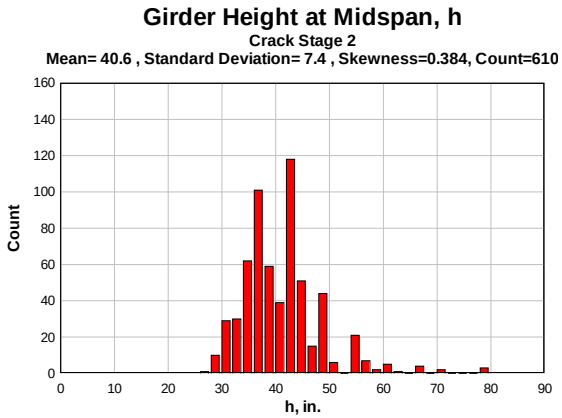

(f)

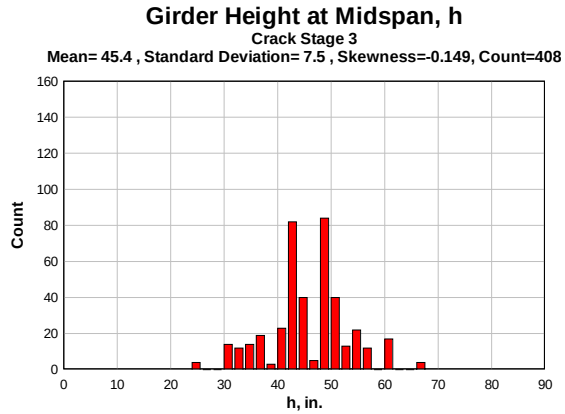

(g)

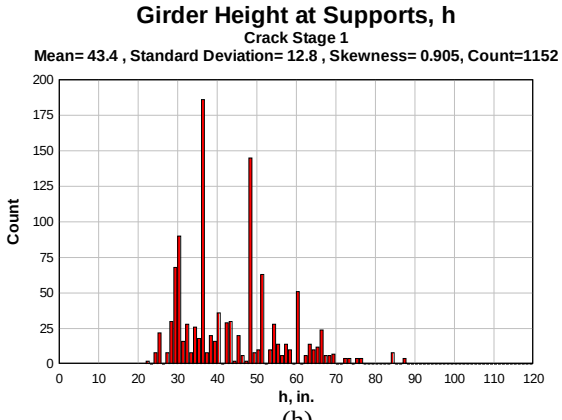

(h)

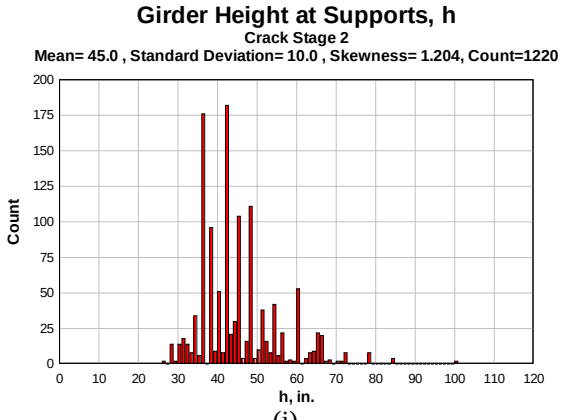

(i)

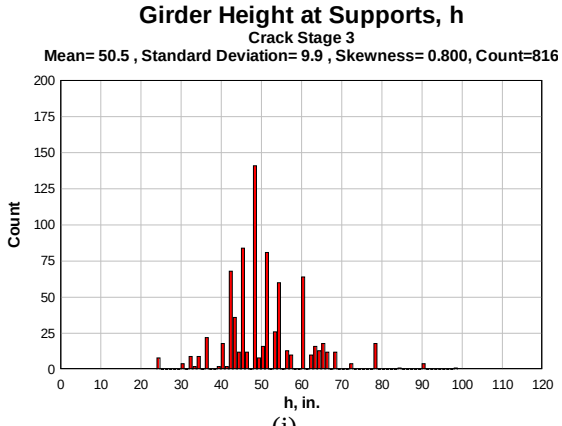

(j)

Figure 4.3 (continued): Girder height – (e) Crack Stage 1, midspan; (f) Crack Stage 2, midspan; (g) Crack Stage 3, midspan; (h) Crack Stage 1, supports; (i) Crack Stage 2, supports; (j) Crack stage 3, supports

4.4 CROSS-CORRELATION OF WEB WIDTH AND GIRDER HEIGHT AT MIDSPAN AND SPAN ENDS

Girder height and girder width were compared at midspan and at support locations to identify correlations between the variables. While the data points are dispersed, there was a slight tendency for the girder height to increase with girder width (Figure 4.4a). At support locations, girder width can increase independently due to tapering, girder height can increase independently due to a haunch, and girder height and width can increase simultaneously where both tapers and haunches are used, as demonstrated in Figure 4.4b.

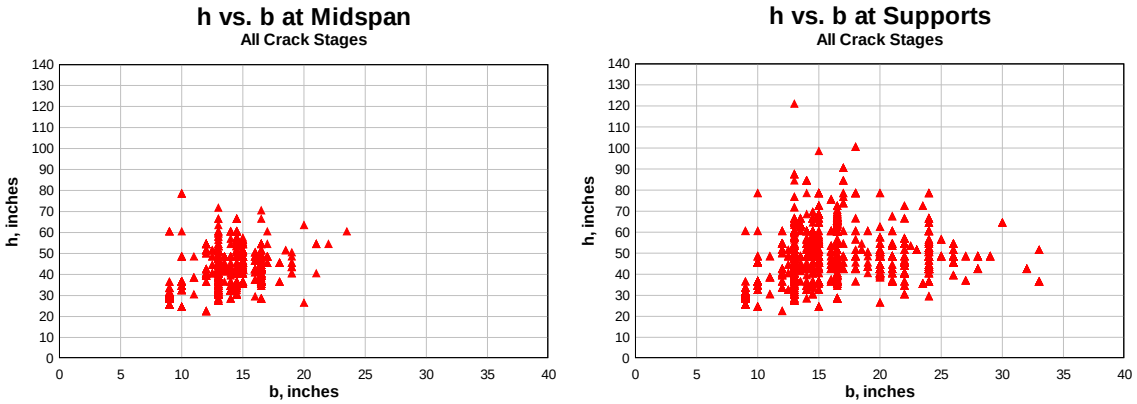

(a) (b)

Figure 4.4: Girder height versus girder width at (a) midspan and (b) supports

4.5 H/B AT MIDSPAN AND SPAN ENDS

The ratio of girder height to width at both midspan and support locations was most frequently 2.75 occurring at a level of 19% and 12%, respectively, as shown in Figures 4.5a and 4.5b. The girder height to width ratio at midspan for Crack Stage 3 bridges was on average 3.3, a slightly higher value than the 3.0 averages for both Crack Stage 1 and 2 bridges, as shown in Figures 4.5c, 4.5d, and 4.5e. The average girder height to width ratio at support locations for Crack Stage 1 was 3.2, for Crack Stage 2 was 3.0, and for Crack Stage 3 was 3.2, as shown in Figures 4.5f, 4.5g, and 4.5h.

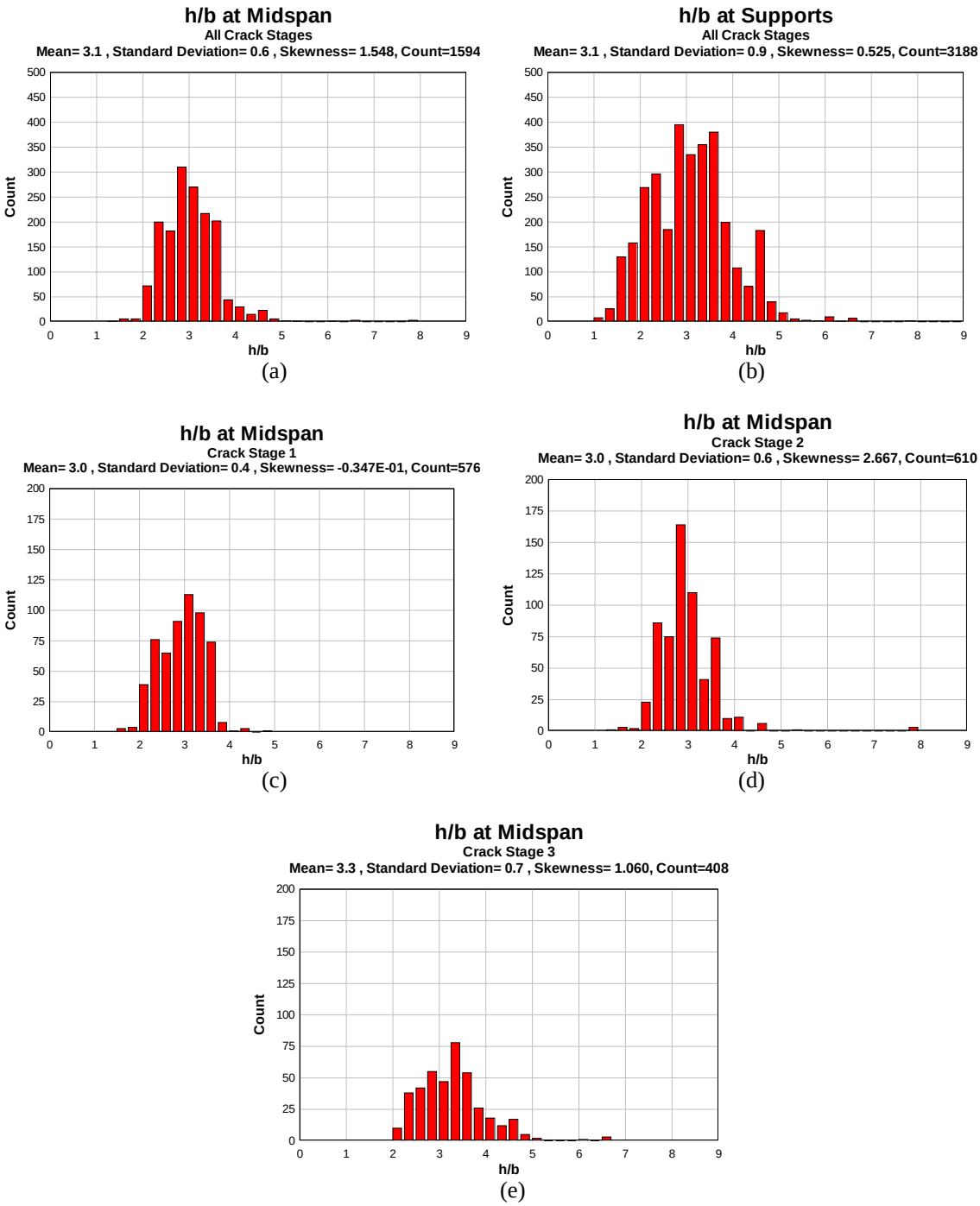

Figure 4.5: Girder height to width ratio – (a) All crack stages, midspan; (b) All crack stages, supports; (c) Crack Stage 1, midspan; (d) Crack Stage 2, midspan; (e) Crack Stage 3, midspan

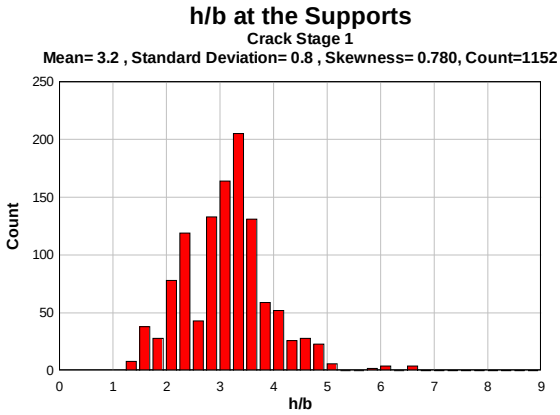

(f)

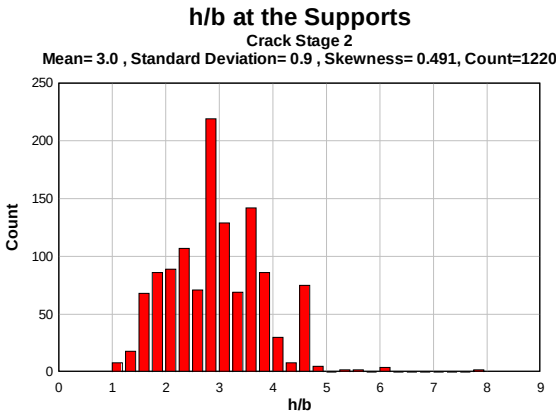

(g)

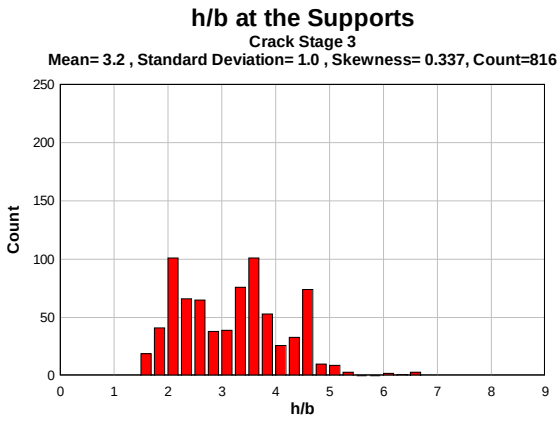

(h)

Figure 4.5 (continued): Girder height to width ratio – (f) Crack Stage 1, supports; (g) Crack Stage 2, supports; (h) Crack Stage 3, supports

4.6 H vs. L AT MIDSPAN AND SPAN ENDS

Girder height was compared to the span length to determine any correlation between the two parameters. Girder heights at the support and at midspan tended to increase with span length as shown in Figures 4.6a and 4.6b.

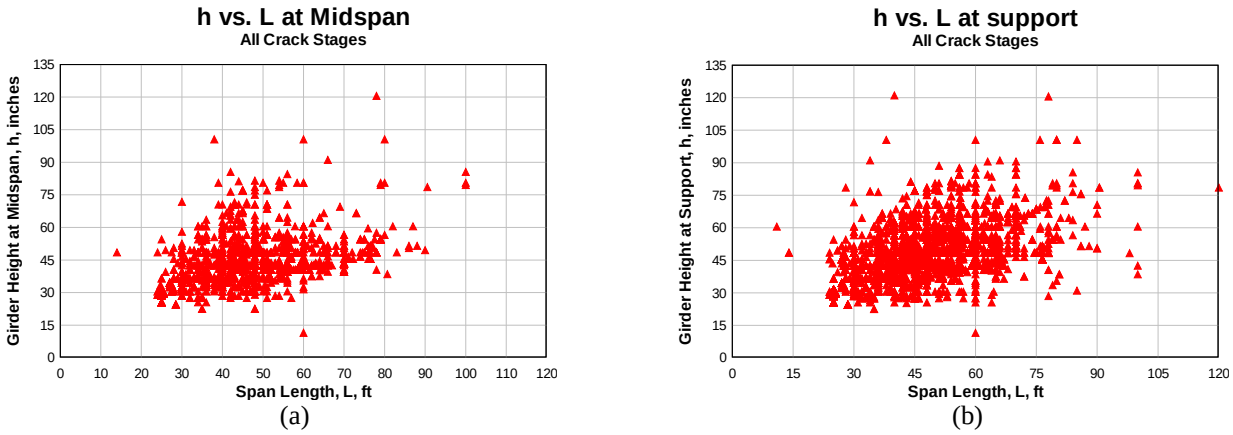

Figure 4.6: Girder height versus span length at (a) midspan and (b) supports

4.7 TAPERS AND HAUNCHES

Tapers and haunches were determined based on the bridge girder plan and elevation design drawings. The length of taper and/or haunch, and the end dimensions of the girder were recorded. Haunch was determined as the girder height at the support and taper was determined as the girder width at the support. If the span had both a taper and a haunch, then both dimensions, height and width at the support, were recorded. The majority of the T-beams, about 52%, did not have tapers or haunches, as illustrated in Figure 4.7. Approximately 24% of the span ends were haunched only, about 21% were tapered only, and the final 4% were both haunched and tapered.

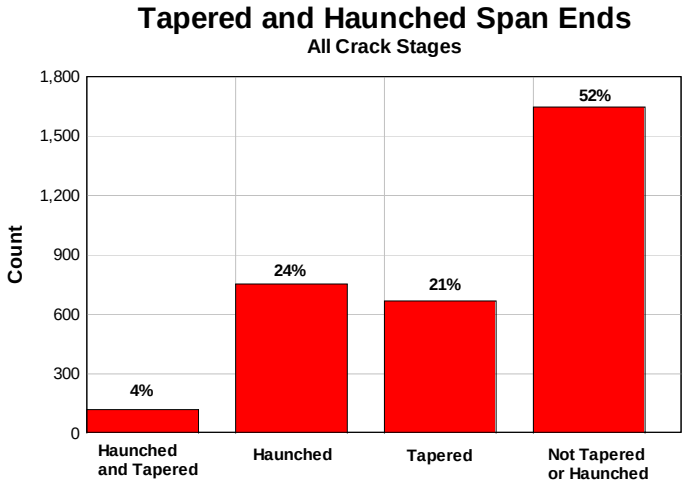

Figure 4.7: Tapered and haunched span ends

4.8 STIRRUP SPACING RANGE AND STIRRUP BAR SIZE

Stirrup spacing was determined from the girder elevation drawings. The design drawings contained stirrup spacing, number of stirrups, and the stirrup bar sizes. The minimum stirrup spacing per span was most frequently 6 inches, occurring in 32% of the spans, while the maximum was most frequently 18 inches, occurring in 32% of the spans, as can be seen in Figures 4.8a and 4.8b. The bar designation number of stirrups ranged between #3 and #5, but were predominantly #4 bars, occurring in about 79% of the spans.

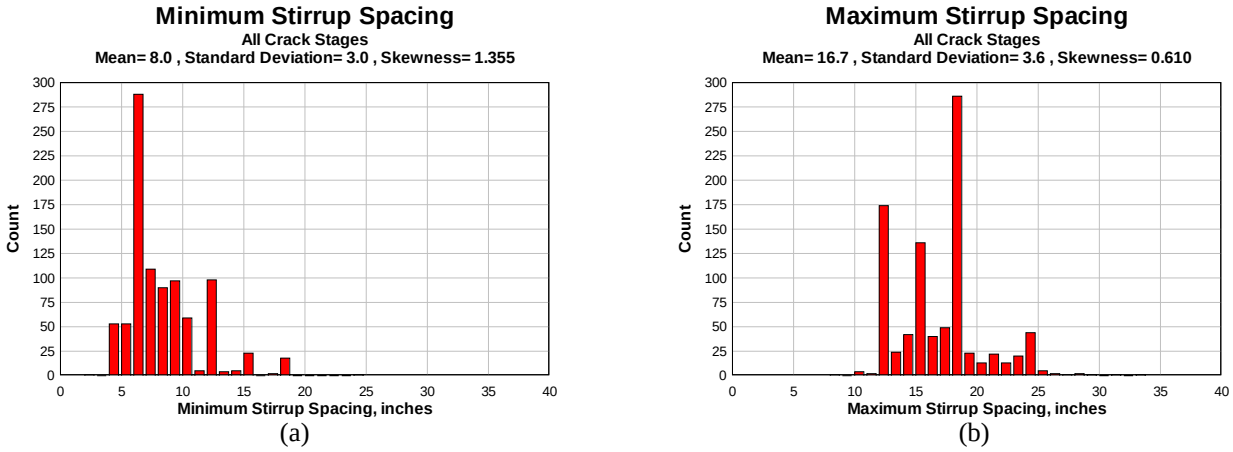

Figure 4.8: Stirrup spacing – (a) minimum; (b) maximum

4.9 AREA OF REINFORCING STEEL

Reinforcing steel details such as bar size, number of bars, number of layers, and cutoff locations along the span, were taken from the girder elevation and girder cross-sectional details in the bridge design drawings. Using this information, the area of reinforcing steel was found at points along the beam, namely the quarter and midpoints along the span, as well as the area of reinforcing steel at the top of girders over continuous supports.

The area of reinforcing steel at the quarter span location of the girders ranged between 2.0 and 26.0 in^2. The average area of reinforcing steel at the quarter points was 8.8 in^2, and the most commonly occurring area was between 6.0 and 7.0 in^2, accounting for approximately 24% of the spans, as shown in Figure 4.9a. The area of 6.0 to 7.0 in^2 was the most frequently occurring for Crack Stage 1, at a rate of 32%, as shown in Figure 4.9b. Crack Stage 3 spans most frequently had an area between 9.0 and 10.0 in^2, at a rate of 16%, as shown in Figure 4.9c.

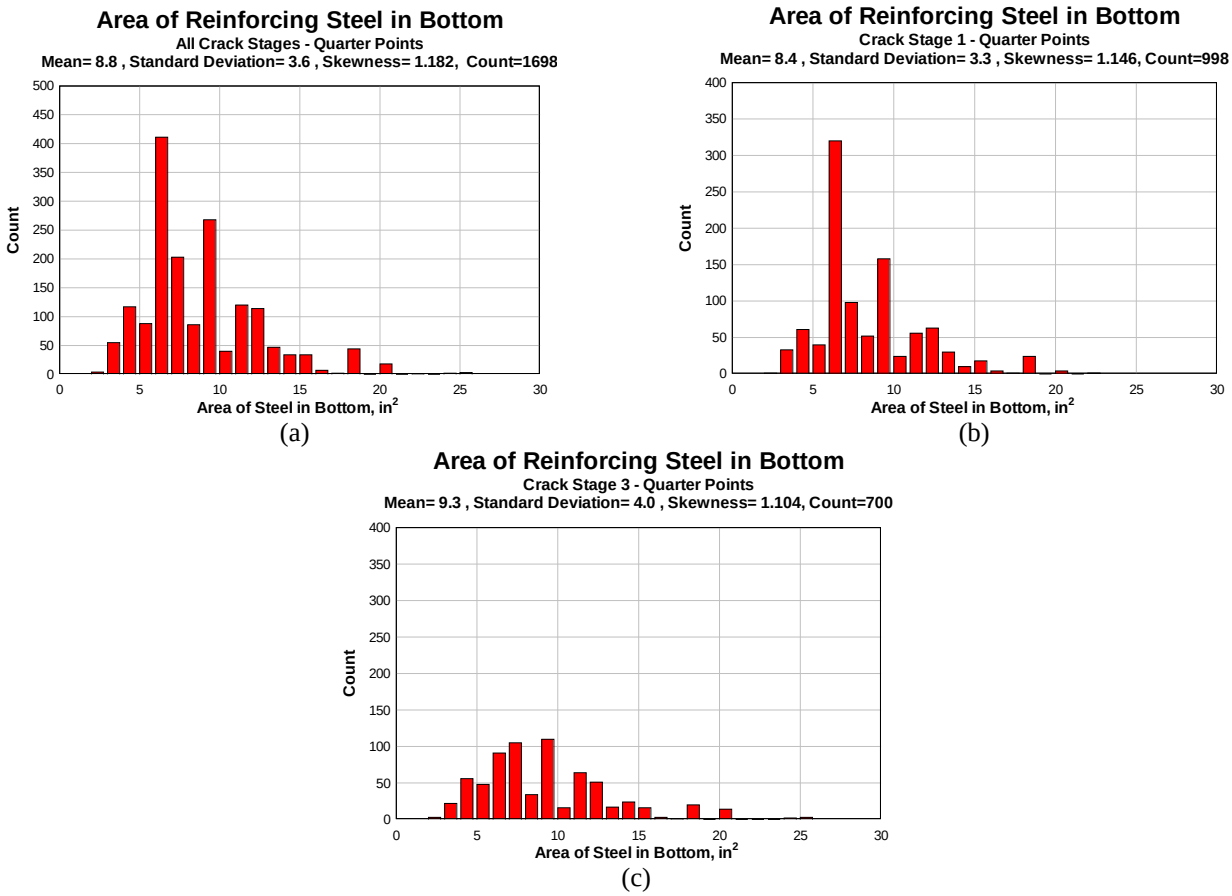

Figure 4.9: Area of bottom reinforcing steel at quarter points of span length – (a) All crack stages; (b) Crack Stage 1; (c) Crack Stage 3

The area of bottom reinforcing steel at midspan of the girders ranged between 3.0 and 27.0 in^2, with an average of 10.2 in^2. The most commonly occurring area was between 6.0 and 7.0 in^2, accounting for approximately 20% of the spans, as shown in Figure 4.10a. For Crack Stage 1, the area of 6.0 to 7.0 in^2 was the most frequently occurring, at a rate of 30%, as shown in Figure 4.10b. The most common area of reinforcing steel at midspan for Crack Stage 3 spans was split between 9.0 to 10.0 in^2, and 12.0 to 13.0 in^2, both at rates of 12%, as shown in Figure 4.10c.

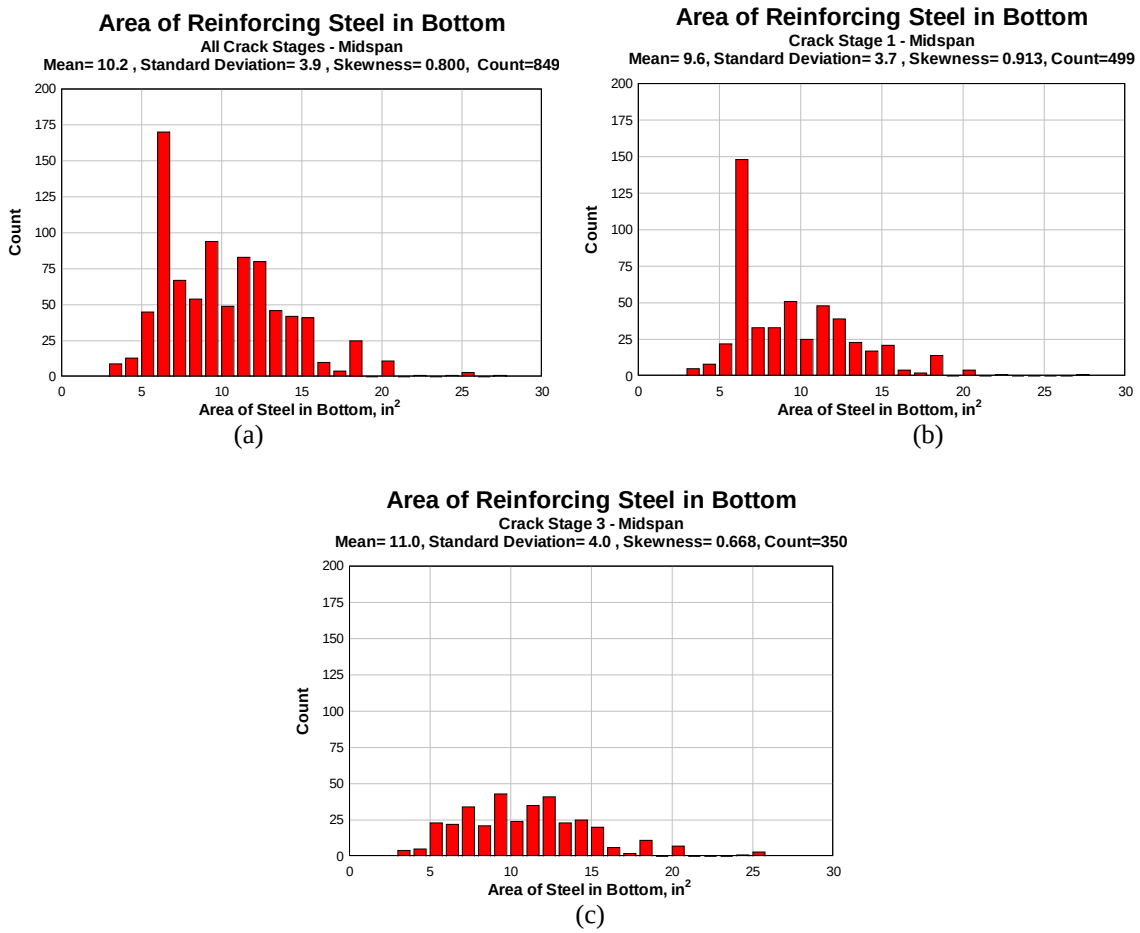

Figure 4.10: Area of bottom reinforcing steel at midspan – (a) All crack stages; (b) Crack Stage 1; (c) Crack Stage 3

The area of reinforcing steel at the top of the continuous supports ranged between 2.0 and 26.0 in^2, with an average of about 12.4 in^2. The most frequently occurring range of reinforcing steel area was between 10.0 and 11.0 in^2 at a rate of 12%, as shown in Figure 4.11a. For Crack Stage 3, the most common range of reinforcing steel area was between 12.0 and 13.0 in^2, while for Crack Stage 1 the most common range was between 10.0 and 11.0 in^2, occurring at rates of 12% and 15%, respectively, as shown in Figures 4.11b and 4.11c.

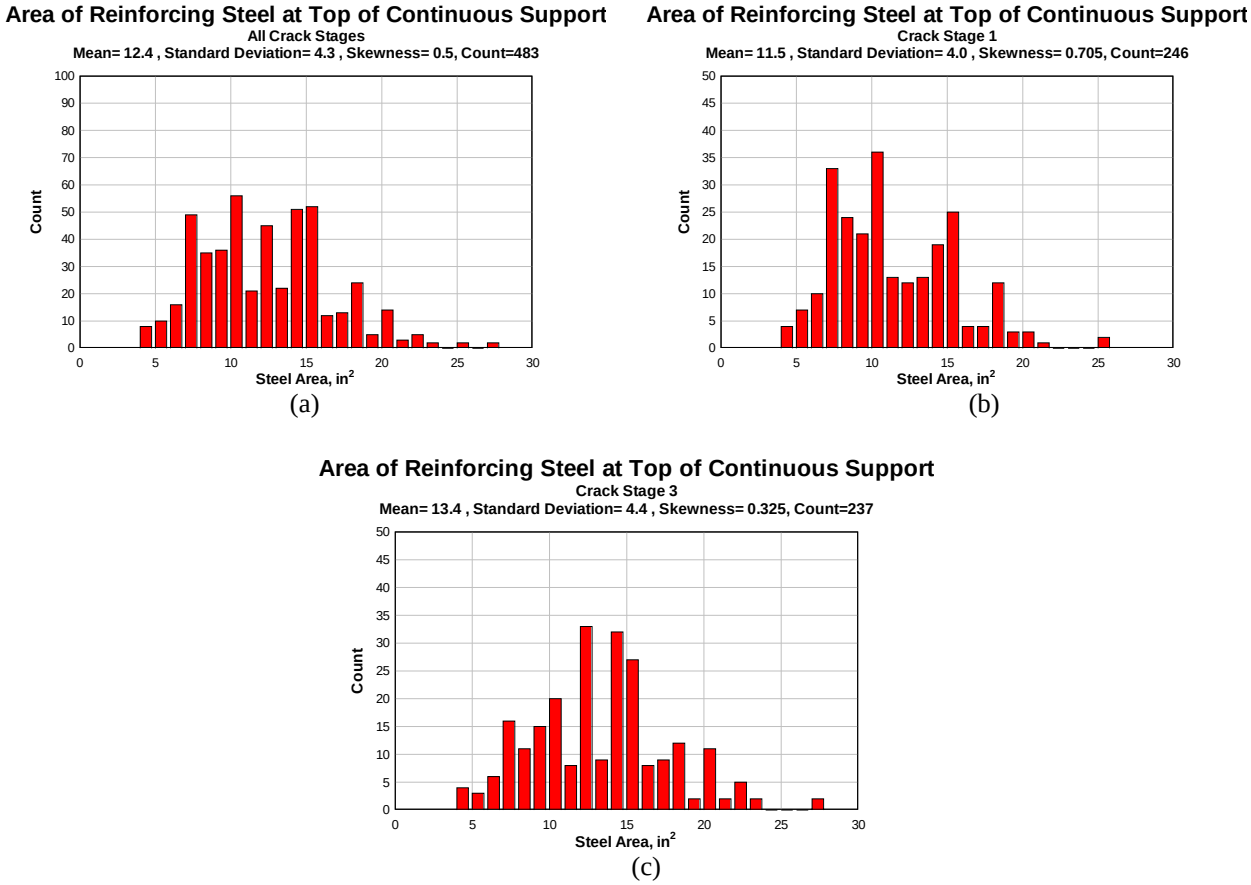

Figure 4.11: Area of top reinforcing steel over continuous support – (a) All crack stages; (b) Crack Stage 1; (c) Crack Stage 3

5.0 APPLICATION OF DATABASE FOR STRUCTURAL ANALYSIS

5.1 DEAD LOAD

Dead load was calculated as a uniform load (kips/ft) along a single girder using database geometry information on the bridge and member properties. The dead load was computed as:

$$DL = \frac{V_{concrete} * W_{concrete} + V_{asphalt} * W_{asphalt}}{L * n} + \frac{W_{parapet}}{n} \quad \textbf{(5-1)}$$

where L is the span length measured from center-to-center of supports, $W_{concrete}$ is the weight of reinforced concrete taken as 150 lb/ft^3, $W_{asphalt}$ is the weight of asphalt taken as 140 lb/ft^3 (pg. 3-13 of 1999 AASHTO LRFD Bridge Design Specifications) at a thickness of 2 in., and n is the number of girder lines supporting the bridge.

Based on parapet designs for 4 different bridges, the weight of the parapet was taken as 250 lb/ft and applied over all the girders. The total concrete volume was calculated by summing the volume of the slab, girder stems and diaphragm stems.

The range of highest frequency for dead load was between 1.5 and 1.75 kips/ft per girder in approximately 30% of the spans, as shown in Figure 5.1a. The second highest frequency was for dead load that was between 1.25 and 1.5 kips/ft per girder, occurring at a rate of 25%. Finally, 17% of the spans had dead load between 1.75 and 2 kips/ft per girder. Higher crack stage bridges tended to have higher dead loads as shown in Figures 5.1b through 5.1e.

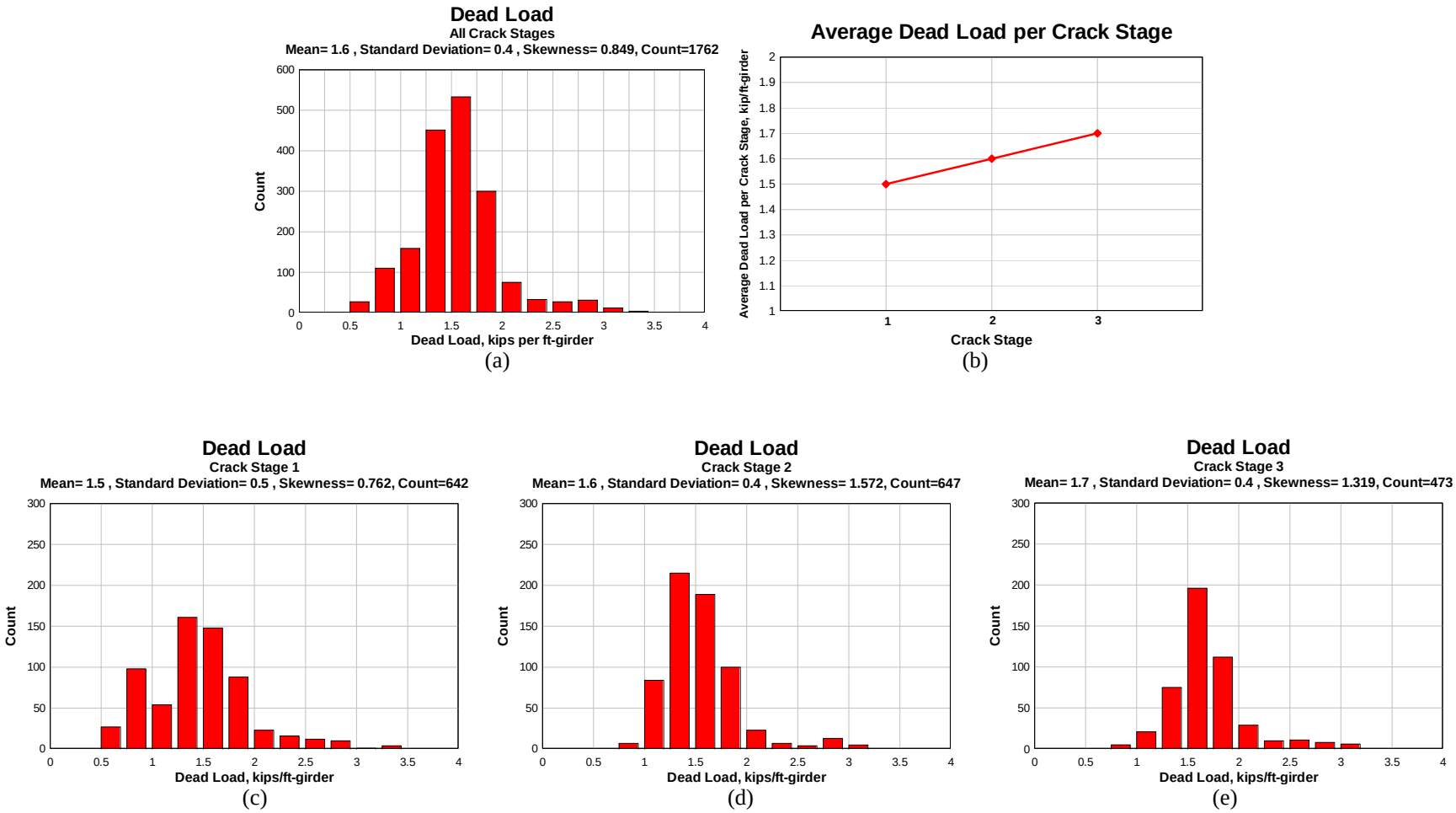

Figure 5.1: Dead load – (a) All crack stages; (b) Average per crack stage; (c) Crack Stage 1; (d) Crack Stage 2; (e) Crack Stage 3

5.2 SHEAR CAPACITY

Using the geometry and reinforcing steel arrangements of each bridge span, the nominal shear capacity, V_n, was computed as:

$$V_n = V_c + V_s \quad \textbf{(5-2)}$$

where V_c is the nominal concrete shear capacity determined as:

$$V_c = 2\sqrt{f'_c}bd \quad \textbf{(5-3)}$$

and V_s is the nominal shear strength provided by shear reinforcement determined as:

$$V_s = \frac{A_v f_y d}{s} \quad \textbf{(5-4)}$$

The effective depth of girder d was approximated using

$$d = h - 2.5 \quad \textbf{(5-5)}$$

where h is the height of the girder (in.) and 2.5 approximately accounts for cover concrete and the centroidal location of the flexural steel.

The compressive strength of the concrete, f'_c, was taken to be 3300 psi and the yield strength of the reinforcing steel, f_y was taken as 40 ksi. The nominal shear capacity was computed at support locations and at midspan for the two most common types of indeterminacy: simple spans and 3-span continuous bridges.

The range of nominal shear capacity at the span ends of 3-span continuous bridges was found to be between approximately 45 and 300 kips per girder and had an average of 130 kips per girder. The most frequently occurring range of nominal shear capacity was between 80 and 100 kips per girder, for approximately 24% of the spans, as shown in Figure 5.2a. The average nominal shear capacity for Crack Stage 3 span ends was 143 kips per girder whereas the average nominal shear capacity for Crack Stage 1 span ends was 121 kips per girder, as shown in Figures 5.2b and 5.2c. Crack Stage 3 span ends had a higher incidence of shear capacity between 100 and 120 kips, accounting for approximately 22% of the spans ends. The most common range of shear capacity for Crack Stage 1 accounted for approximately 30% of the span ends and ranged between 80 and 100 kips.

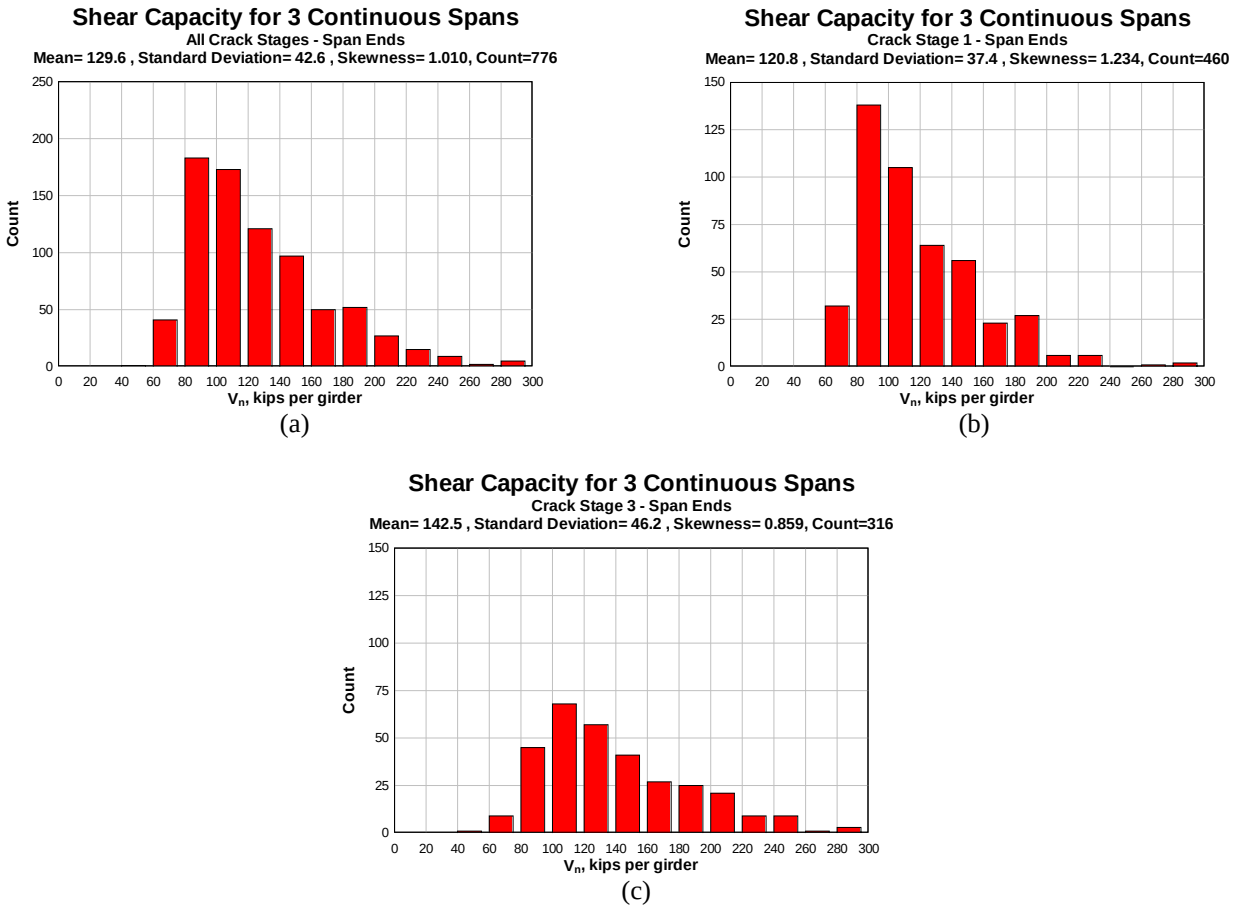

Figure 5.2: Shear capacity at span-ends of 3 continuous spans – (a) All crack stages; (b) Crack Stage 1; (c) Crack Stage 3

The range of nominal shear capacity at midspan of the 3-span continuous bridges was found to be between approximately 60 and 207 kips per girder and had an average of 109 kips per girder. The most common range of nominal shear capacity at midspan of the group of 3-span continuous bridges was between 100 and 120 kips per girder and accounted for 38% of the spans, as shown in Figure 5.3a. This range of nominal shear capacity was also the most common within the Crack Stage 3 spans, accounting for approximately 38% of the spans, as shown in Figure 5.3c. The Crack Stage 1 spans had an approximate even break between those in the range of 80 to 100 kips per girder and those in the range of 100 to 120 kips per girder, accounting for 38% and 37% of the spans, respectively, as shown in Figure 5.3b.

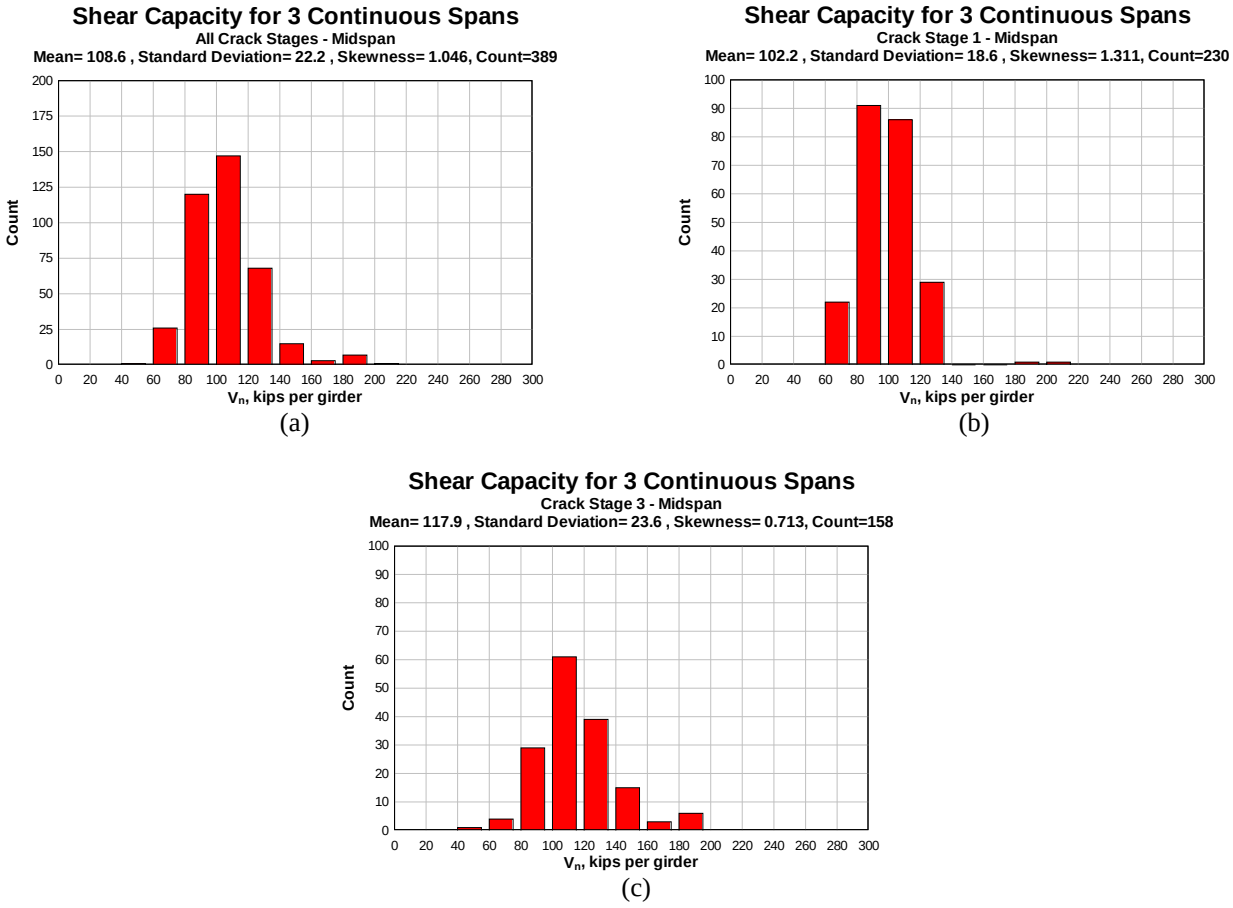

Figure 5.3: Shear capacity at midspan of 3 continuous spans – (a) All crack stages; (b) Crack Stage 1; (c) Crack Stage 3

The range of nominal shear capacity at span ends for simple spans was between 47 and 270 kips per girder, with an average of approximately 107 kips per girder. The most frequently occurring range of nominal shear capacity at midspan of the simple spans was between 80 and 100 kips per girder and accounted for approximately 36% of the simple span ends, as shown in Figure 5.4a. The average nominal shear capacity for the span ends of the simple spans for Crack Stage 3 was 144 kips per girder, while for Crack Stage 1 the average was about 97 kips per girder, as shown in Figures 5.4b and 5.4c. For Crack Stage 3 simple span ends, the most frequently occurring range of shear capacity was between 120 and 140 kips per girder, accounting for 26% of the Crack Stage 3 spans. For Crack Stage 1 simple span ends, the most frequently occurring range of shear capacity was between 80 and 100 kips per girder, accounting for 43% of the Crack Stage 1 spans.

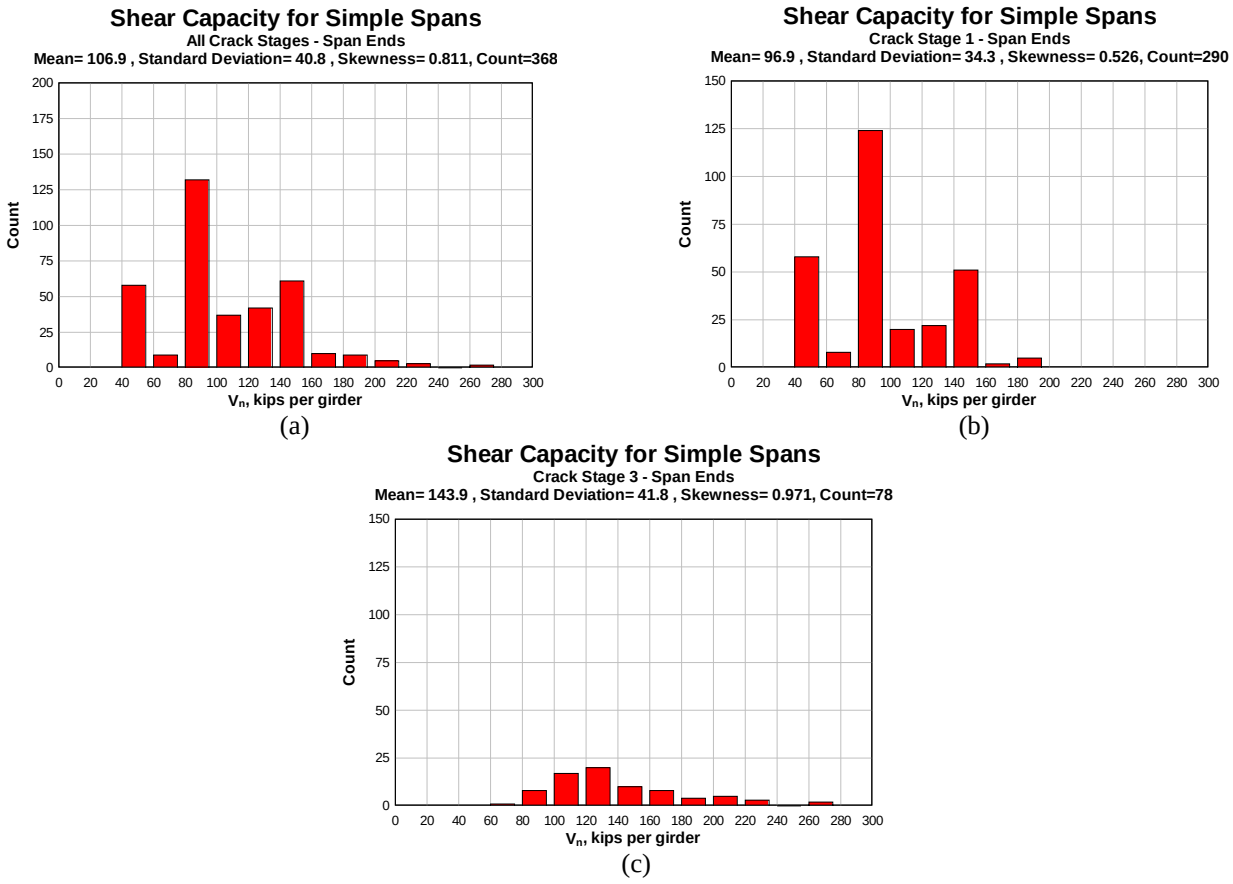

Figure 5.4: Shear capacity at span-ends of simple spans – (a) All crack stages; (b) Crack Stage 1; (c) Crack Stage 3

The range of nominal shear capacity for midspan locations of the simple spans was between 52 and 205 kips per girder, with an average of about 93 kips per girder. The most frequently occurring range of nominal shear capacity at midspan of the simple spans was between 80 and 100 kips per girder and accounted for approximately 24% of the simple spans, as shown in Figure 5.5a. For Crack Stage 3 simple spans, the average nominal shear capacity was 126 kips

per girder, while for Crack Stage 1 spans, the average nominal shear capacity was 84 kips per girder, as shown in Figures 5.5b and 5.5c. The most frequently occurring range of shear capacity for Crack Stage 3 simple spans was between 120 and 140 kips per girder, accounting for 46% of the spans. The most frequently occurring range of shear capacity for the Crack Stage 1 simple spans was between 80 and 100 kips per girder, accounting for 30% of the spans.

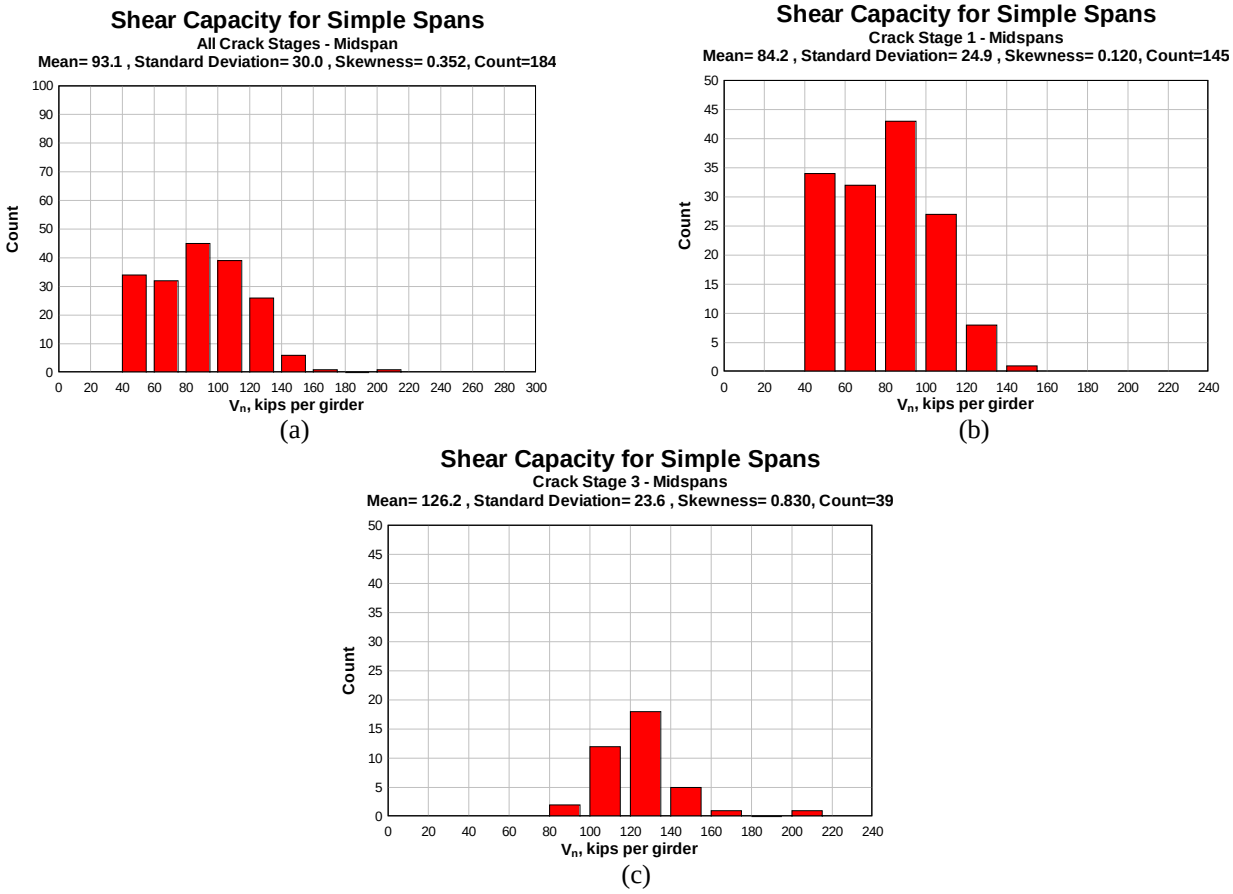

Figure 5.5: Nominal shear capacity at midspans of simple spans – (a) All crack stages; (b) Crack Stage 1; (c) Crack Stage 3

5.3 SHEAR CAPACITY FOR LIVE LOAD

For the two most frequently occurring types of structural indeterminacy, (simple spans and 3-span continuous bridges) the factored dead load shear was subtracted from the factored shear capacity at points along each span to find the remaining capacity for service level live load shear forces in the span. This was computed as:

$$V_{LL} = \frac{\varphi_v V_n - \gamma_{DL} V_{DL}}{\gamma_{LL}} \qquad \textbf{(5-6)}$$

where V_{DL} is the service level dead load shear, V_n is the shear capacity, ϕ_v is 0.9, γ_{DL} is 1.25, and γ_{LL} is 1.35 according to the 1998 AASHTO LRFD Bridge Design Specifications (Strength II).

The service level dead load shear, $V_{DL,}$ was computed using the slope deflection method for a uniform dead load in kips/ft along a single girder. The uniform dead load was calculated using Equation 5-1. The data for V_{LL} was analyzed at support and midspan locations for each of the simple span and 3-span continuous bridges.

For the span ends of the 3-span continuous bridges, the range of shear capacity for live load was between 27 and 174 kips per girder. The average shear capacity for live load was about 79 kips per girder, with the most common range between 60 and 80 kips per girder, accounting for about 36% of the spans, as shown in Figure 5.6a. For Crack Stage 3, the average shear capacity for live load was 84 kips per girder while the average for Crack Stage 1 was 76 kips per girder. The most frequently occurring range for both Crack Stages 1 and 3 spans was between 60 and 80 kips per girder at a rate of 38% and 33%, respectively, as shown in Figures 5.6b and 5.6c.

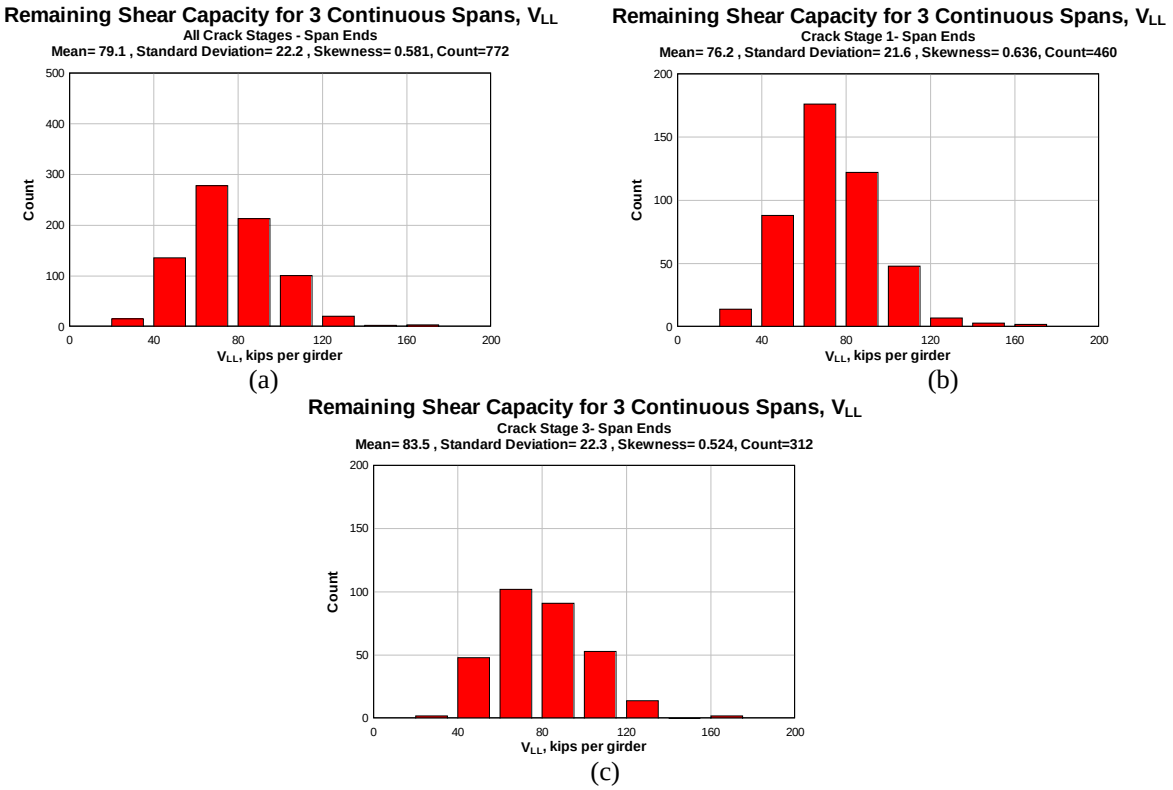

Figure 5.6: Shear capacity for service level live load at span ends of 3 span continuous bridges – (a) All crack stages; (b) Crack Stage 1; (c) Crack Stage 3

For midspan locations of the 3-span continuous bridges, the range of shear capacity for live load was between 27 and 129 kips per girder. The average shear capacity for live load was about 57

kips per girder, with the most frequent range being between 40 and 60 kips per girder, accounting for about 65% of the spans, as shown in Figure 5.7a. For Crack Stage 3, the average shear capacity for live load at the midspan was 61 kips per girder while the average for Crack Stage 1 was 54 kips per girder. Spans of Crack Stage 1 and 3 had shear capacity for live load that were predominantly 40 to 60 kips per girder at rates of 74% and 51%, respectively, as shown in Figures 5.7b and 5.7c.

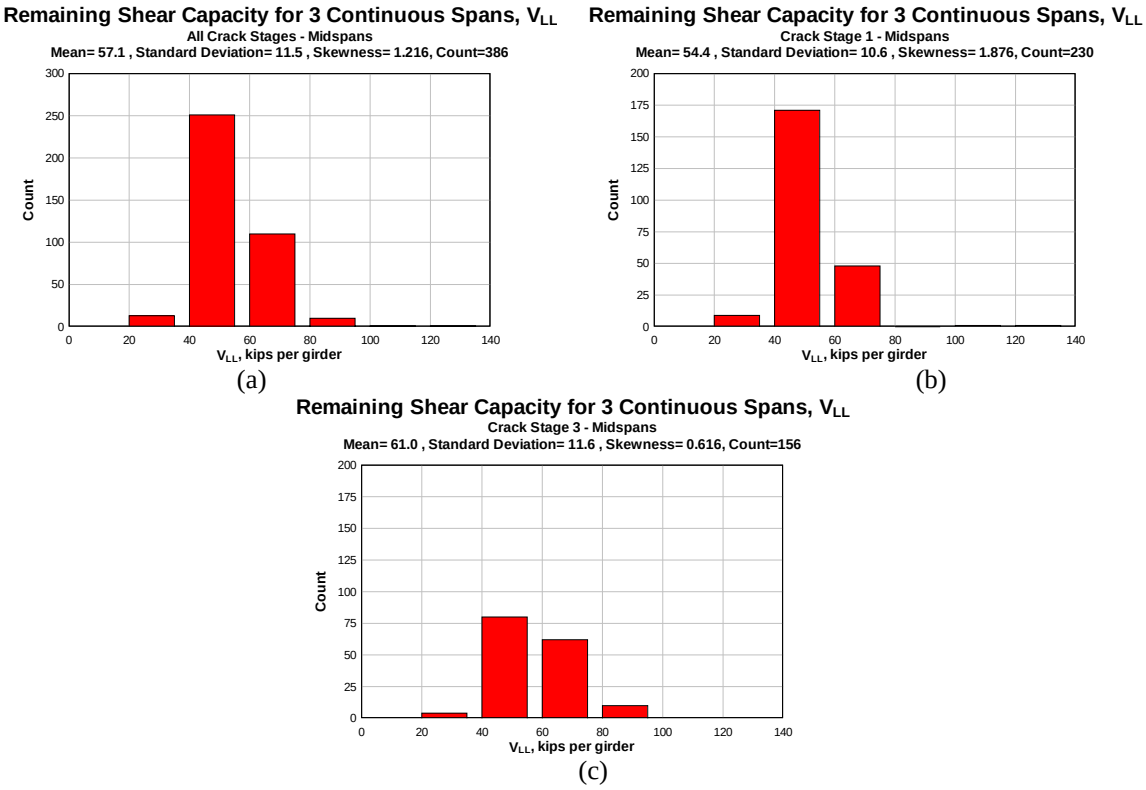

Figure 5.7: Shear capacity for service level live load at midspans of 3 span continuous bridges – (a) All crack stages; (b) Crack Stage 1; (c) Crack Stage 3

For span ends of the simple span bridges, the range of shear capacity for live load was between 27 and 264 kips per girder. The average shear capacity for live load was about 83 kips per girder, with the most common range being between 60 and 80 kips per girder, accounting for about 31% of the spans as shown in Figure 5.8a. This range of values remained as the most frequently occurring range for Crack Stages 1 and 3, where the frequency of shear capacity for live load between 60 and 80 kips per girder occurred at rates of 32% and 27%, respectively, as shown in Figures 5.8b and 5.8c. For Crack Stage 3, the average shear capacity for live load was 106 kips per girder while the average for Crack Stage 1 was 77 kips per girder. The difference in mean values of the shear capacity for live load between the crack stages was due to the difference in statistical distributions. For Crack Stage 3 spans, approximately 67% were 80 kips per girder and above, while for Crack Stage 1, the percentage of values above 80 kips per girder was lower at 40%.

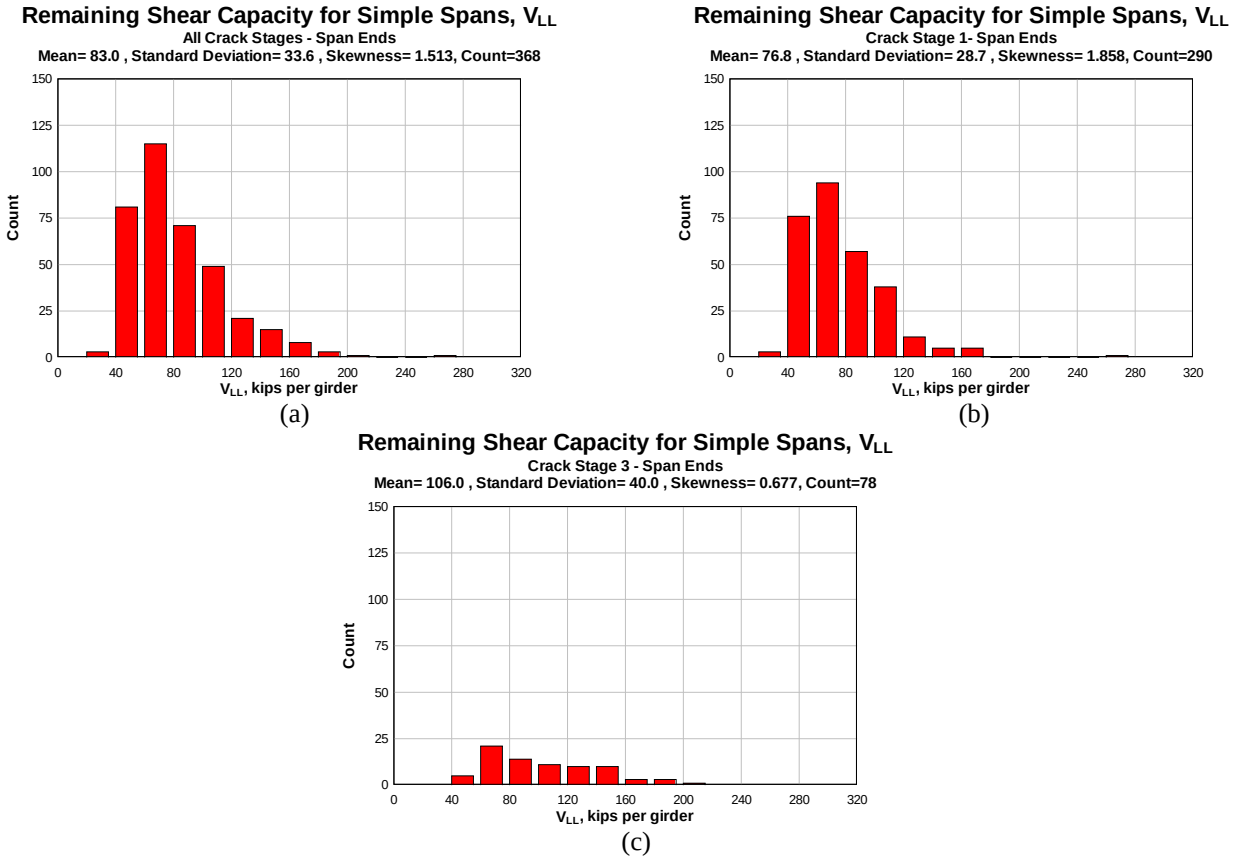

Figure 5.8: Shear capacity for service level live load at span ends of simple spans – (a) All crack stages; (b) Crack Stage 1; (c) Crack Stage 3

For midspan locations of simple span bridges, the range of shear capacity for live load was between 29 and 99 kips per girder. The average shear capacity for live load was about 51 kips per girder, with the data well distributed between 20 and 80 kips per girder, as shown in Figure 5.9a. The range of 20 to 40 kips per girder accounted for 32% of the spans, 40 to 60 kips per girder accounted for 34%, and 60 to 80 kips per girder accounted for 33% of the spans. The rest of the spans (2%) ranged between 80 and 100 kips per girder of shear capacity for live load.

The average shear capacity for live load for Crack Stage 1 and 3 spans were 48 and 64 kips per girder, respectively. For Crack Stage 1 spans, the most frequently occurring range of values for shear capacity for live load was between 20 and 40 kips per girder at a rate of 40%. Next, the range of 40 to 60 kips per girder accounted for 31% and the range of 60 to 80 kips accounted for the rest of the spans (28%), as shown in Figure 5.9b. The most frequently occurring range of values for Crack Stage 3 spans was between 60 and 80 kips per girder at a rate of 49%. The range of 40 to 60 kips per girder accounted for 41%. The two ranges of 20 to 40 kips and 80 to 100 together accounted for the rest of the spans, only about 10%, as shown in Figure 5.9c.

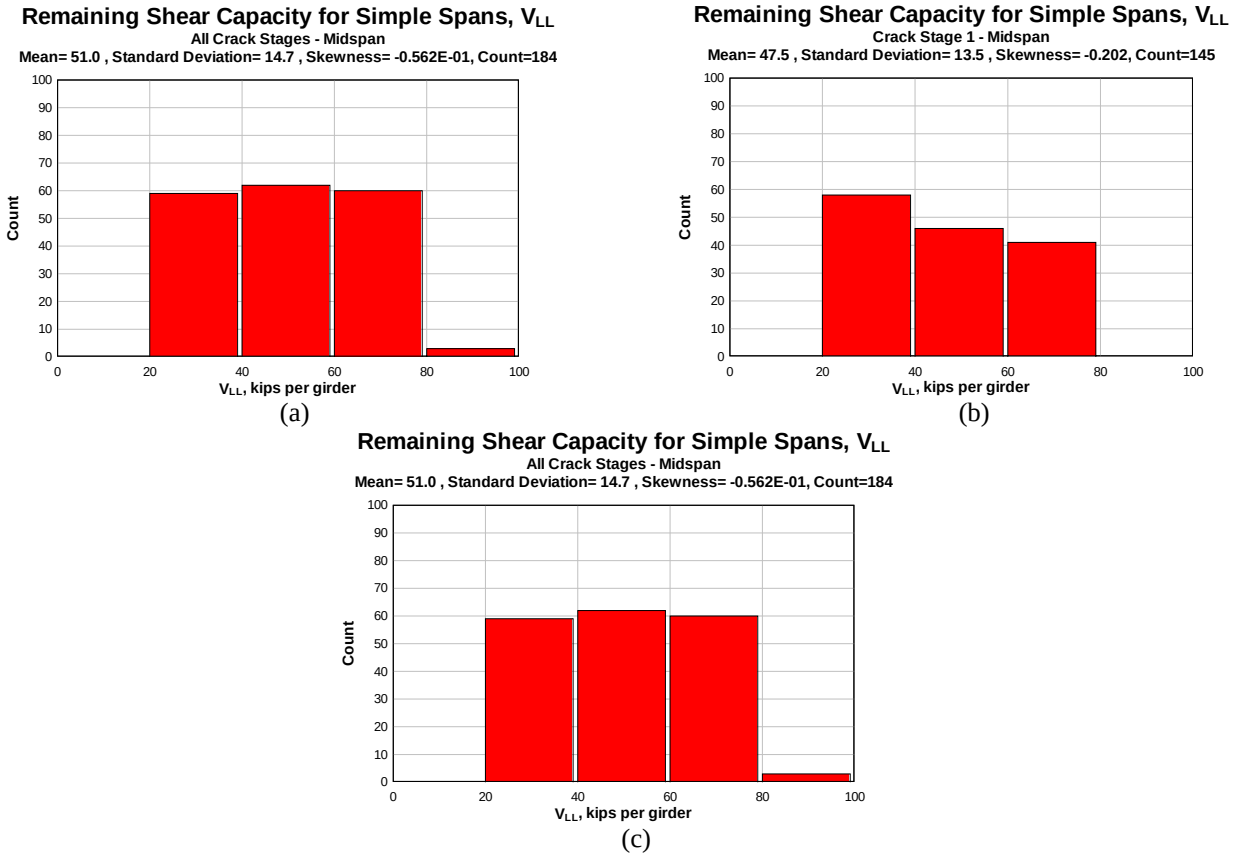

Figure 5.9: Shear capacity for service level live load at midspan of simple spans – (a) All crack stages; (b) Crack Stage 1; (c) Crack Stage 3

6.0 APPLICATION OF DATABASE FOR RESEARCH PLAN

Using information extracted from the population of cracked RCDG bridges contained in the database, laboratory specimens were dimensioned and bridges for field investigation were identified. Laboratory specimens were designed to reflect the vintage details and materials of the population of cracked bridge girders in the inventory and provide specimens that perform as intended to reflect field damage states. Other constraints included effective width of flanges, overall specimen length and weight, as well as force and stroke capacities of laboratory testing equipment.

The laboratory specimens were selected to have a girder web width of 14 in. and height of 48 in. These correspond to the most frequently occurring girder web width and girder height at support locations for all bridges, which is 13 in. and the range between 48 and 50 in, respectively. The stirrups were of bar size #4 as this size accounted for approximately 79% of stirrup sizes for the spans. Stirrup spacing for the laboratory specimens ranged between 6 in. and 18 in., corresponding to the largest distributions of stirrup spacing found in the database.

The area of positive-moment flexural reinforcing steel was 9.4 in^2, corresponding to the average area of bottom reinforcing steel for all bridges found at the midspan to be 10.2 in^2. The area of negative-moment reinforcing steel was also 9.4 in^2, while the corresponding average area of negative-moment steel at continuous supports was 12.4 in^2. The specimens contained flexural steel corresponding to ASTM A-615 Grade 60 reinforcing steel, given that grade 40 steel is not available for large reinforcing bar sizes.

Stirrup reinforcing bars were ASTM A-615 Grade 40 with an actual yield stress of 51 ksi. This corresponds reasonably well with intermediate grade steel specified in the 1950's. The specified 28-day strength of concrete for the laboratory specimens was 3300 psi, as this was found to be the predominant value in the database. Actual concrete strengths achieved for specimens were approximately 4000 psi, a reasonable value for in-situ concrete of this age and quality.

The bridges chosen for the field investigation were Spores Bridge, Jasper Bridge, and Willamette River Bridge. These bridges had geometries and member proportions that were representative of the population of cracked RCDG bridges in Oregon. These attributes included indeterminacy, span length, and member proportions. All three bridges contained simple spans and two of them also had 3-span continuous portions. These were the two predominant types of indeterminacy found in the database. The span lengths of these bridges ranged between 48 and 60 ft, corresponding to frequently occurring span lengths in the database.

All bridges contained girders with widths between 13 and 14.5 in., the most frequently occurring girder widths found in the database. Girder heights for the chosen field study bridges were between 42 in. and 53 in., again heights frequently observed in the database. The girders in these bridges included tapers (Spores Bridge), haunches (Jasper Bridge), and uniform prismatic girders (Willamette River Bridge) to cover the full range encountered in the database population of

bridges. In general, the bridges fully reflected typical conditions and configurations of the cracked RCDG bridge population in the state.

7.0 CONCLUSION

Although there were several parameters and relationships that showed some trend related to the level of damage for bridges in the field, on the whole, none of the parameters were prominent and most of the trends were subtle.

One of the trends observed from the database research was that, in general, bridges at a higher crack stage tended to have larger girders and longer span lengths. This is likely due to the design practice at the time. When more capacity was needed and the addition of reinforcing steel was not possible due to constructability (minimum stirrup spacing is about 4 to 6 in.), a designer would increase the girder size to obtain more contribution from the concrete. As a result, girders of larger dimensions would have proportionally less steel reinforcement than corresponding girders of smaller dimensions. This is further compounded by a higher concrete stress for design than would be permissible today.

This may help to explain the higher number of larger girders and longer spans within the population at the Crack Stage 3 level. Given that there were no strong or predominant trends within parameters or inter-relationships found within the database, assessment of shear-cracked RCDG bridges in Oregon may not permit a uniform or standard approach, but will likely require assessment of individual bridges and member proportion details.

PART II: FIELD STUDY AND ANALYSIS

8.0 INTRODUCTION AND BACKGROUND

There are large numbers of conventionally reinforced concrete (CRC) bridges remaining in the national inventory that are lightly reinforced for shear. One of the most common types is the slab-girder bridge that was widely used during the highway expansion of the late 1940's through the early 1960's. Bridges of this type have girders cast integrally with the slab and may be single span or continuous over multiple supports.

Early AASHTO provisions for shear design of CRC bridges used allowable stress design and relied on the concrete to carry a prescribed working stress at service load levels (*AASHO 1944, 1949, 1953, 1957, 1961, 1965*). The magnitude of working stress permitted for the concrete in shear was $0.02f'_c$ for unanchored longitudinal bars and $0.03f'_c$ for anchored longitudinal bars. Reinforcing steel was used to provide supplemental resistance when required and the permissible stirrup stress increased to 20 ksi in 1953 from 16 ksi in 1949. Salient shear related provisions in the AASHTO code during this time period are summarized in Table 8.1.

Shear design provisions for CRC bridges have evolved to reflect the latest experimental research, behavior theories, analysis methods, and service performance. Following the collapse of two separate warehouses at Air Force bases in Ohio and Georgia in 1955 and 1956, significant experimental research work was undertaken to improve the understanding of shear behavior. This research indicated that previous design provisions overestimated the concrete contribution to shear capacity; consequently, permissible concrete stresses were reduced in the early 1960's to $1.1\sqrt{f'_c}$ (*ACI 1963*). As seen in Table 8.1, designers in the 40's, 50's, and 60's relied on a larger allowable concrete stress than would be permitted today. As a result, these early designs would require smaller sized stirrups or more widely spaced shear reinforcement.

During this same time period, the service level truck load model H20-S16-44 did not change and remains the current HS20-44 truck used in the 17th Edition of the Standard Specification as shown in Figure 8.1(*AASHTO 2002*). While the load model has not changed, it is clear that actual truck load magnitudes and the volume of truck traffic have increased over time.

Table 8.1: Changes in AASHTO Standard Specifications (3rd – 12th editions)

	Year (edition)									
	1941(3rd)	1944(4th)	1949(5th)	1953(6th)	1957(7th)	1961(8th)	1965(9th)	1969(10th)	1973(11th)	1977(12th)
Reinforced Concrete Design										
- Effective flange width (minimum of)	1/4 of the span length of the beam, in. Girder spacing (center to center), in. 12 t_{slab} + b_w									
	6 b_w	N/A	N/A	N/A	N/A	N/A	N/A	N/A	N/A	
- Diaphragm for L > 40'	At the middle or at the third points									
Loads:										
Impact formula	I = 50/(L+125)									
Lateral distribution to interior concrete stringers										
- Multiple traffic lanes on concrete floor	S/5	S/5	S/5	S/5	S/5	S/5	S/6	S/6	S/6	
Concrete:										ACI specification format
Allowable Stresses										
Flexural (extreme fiber)										
- Compression	0.33f'c	0.33f'c	0.33f'c	0.40f'c	0.40f'c	0.40f'c	0.40f'c	0.40f'c	0.40f'c	
- Tension (plain) for footings	0.025f'c	0.025f'c	0.030f'c	0.030f'c	0.030f'c	0.030f'c	0.030f'c	0.030f'c	0.030f'c	
Shear										
Beam w/o web reinforcement										
- Long. bars not anchored	0.02f'c	0.02f'c	0.02f'c	0.02f'c	0.02f'c	0.02f'c	0.02f'c	0.02f'c	0.02f'c	
- Long. bars anchored	0.03f'c	0.03f'c	0.03f'c	0.03f'c	0.03f'c	0.03f'c	0.03f'c	0.03f'c	0.03f'c	
Beam w/ web reinforcement										
- Long. bars not anchored	0.046f'c	0.046f'c	0.046f'c	0.075f'c	0.075f'c	0.075f'c	0.075f'c	0.075f'c	0.075f'c	
- Long. bars anchored	0.060f'c	0.060f'c	0.060f'c							
Horizontal shear	N/A	N/A	N/A	0.10f'c	0.15f'c	0.15f'c	0.15f'c	0.15f'c	0.15f'c	
Bond										
- Not anchored	0.033f'c	0.033f'c	0.050f'c	N/A						
- Anchored	0.050f'c	0.050f'c	0.075f'c	N/A						
For deformed bars:										
- Top bars	N/A			0.06f'c	0.06f'c	0.06f'c	0.06f'c	0.06f'c	N/A	
- Straight or hooked ends	N/A			0.10f'c	0.10f'c	0.10f'c	0.10f'c	0.10f'c	N/A	

Table 8.1 (continued): Changes in AASHTO Standard Specifications (3rd – 12th editions)

	Year (edition)									
	1941(3rd)	1944(4th)	1949(5th)	1953(6th)	1957(7th)	1961(8th)	1965(9th)	1969(10th)	1973(11th)	1977(12th)
- Size #3 - #11 top bars	N/A								$(3.4\ f'c^{1/2})/D$	ACI specification format
- Bars other than top bars	N/A								$(4.8\ f'c^{1/2})/D$	
- Size #14 and #18 top bars	N/A								$(2.1\ f'c^{1/2})$	
- Bars other than top bars	N/A								$(3.0\ f'c^{1/2})$	
- All deformed compression bars	N/A								$(6.5\ f'c^{1/2})$	
Reinforcement:										
Allowable Stresses (Intermediate Grade)										
Tension										
- Flexural (ksi)	18*	20	20	20	20	20	20	20	Grade 40 or 60	
- Stirrup (ksi)	16*	18	16	20	20	20	20	20		
Compression (ksi)	nf_c	nf_c	nf_c	nf_c	16	16	16	20		
Details										
Minimum stirrup spacing	< 3/4d	< 3/4d	< 3/4d	< 3/4d	<1/2h (web reinforcement required) or < 3/4h (noweb)					
1st stirrup location (from the face of the support)	<1/4d	<1/4d	<1/4d	<1/4d	<1/4d					
Extension of flexural rebars beyond the not needed point (min.)	45D	15D								
Flexural rebar spacing (in.)	Min. of 2.5D of round bars (c. to c.) or 3 times the side dimensions of square bars (c. to c.), but > 1.5 times max. agg. size (clear) for all cases						> 1.0D (clear) excluding multilayer rebars, > 1.33 times max. agg. size (clear), or > 1 in.		< 18 in., > 1.5D, > 1.5 times max. agg., or > 1.5 in.	
General covering (in.)	2 in. clear						2 in. clear, 1.5 in. for stirrups			
- Slab	1 in. clear						1.5 in. at top, 1 in. at bottom			
- Footing	3 in. clear									
- Work eposed to sea water	4 in. clear									
Max. rebar size	1.5 in square or equivalent									
Concrete Material										
Class A concrete mixtures:										
Max. net water content per bag of cement (gallons), Method A	6	6	6	N/A	N/A	N/A	N/A	N/A	N/A	

Table 8.1 (continued): Changes in AASHTO Standard Specifications (3rd – 12th editions)

	Year (edition)									
	1941(3rd)	1944(4th)	1949(5th)	1953(6th)	1957(7th)	1961(8th)	1965(9th)	1969(10th)	1973(11th)	1977(12th)
Cement content (sacks per cu.yd.)	N/A	N/A	N/A	6	6	6	6	6	6	
Maximum aggregate size (in.)										
- Round Mesh	1.25	N/A	N/A	N/A	N/A	N/A	N/A	N/A	N/A	
- Square mesh	1.00	1in. - No.4								
Minimum concrete strength (psi)	3000									
Major Changes (related to reinforced concrete design)	H-S truck loadings were added.	Modifications for H-S truck axle spacing and lane loadings were made.	Clarification of live load applications and distribution of loads were made.	Revisions are made in the provisions for rein. steel and concrete design stresses to conform to the new deformed bar.	AASHO adopted Standard Specification for Highway Materials and Methods of Sampling and Testing	Prestressed concrete sections were revised.	Fatigue stress section was added.	None	Load factor design concepts were included.	

* No distinction between structural and intermediate grade rebars

Notation

b_w = the width of the beam, in.

d = effective depth, in.

D = rebar diameter, in.

f_c = compressive stress in concrete, ksi

f'_c = concrete strength, psi

h = total height (top of the slab to the bottom of the beam), in.

I = impact factor

L = span length, ft.

n = ratio of modulus of elasticity of steel to that of concrete

S = average spacing of stringers, ft.

t_{slab} = slab thickness, in.

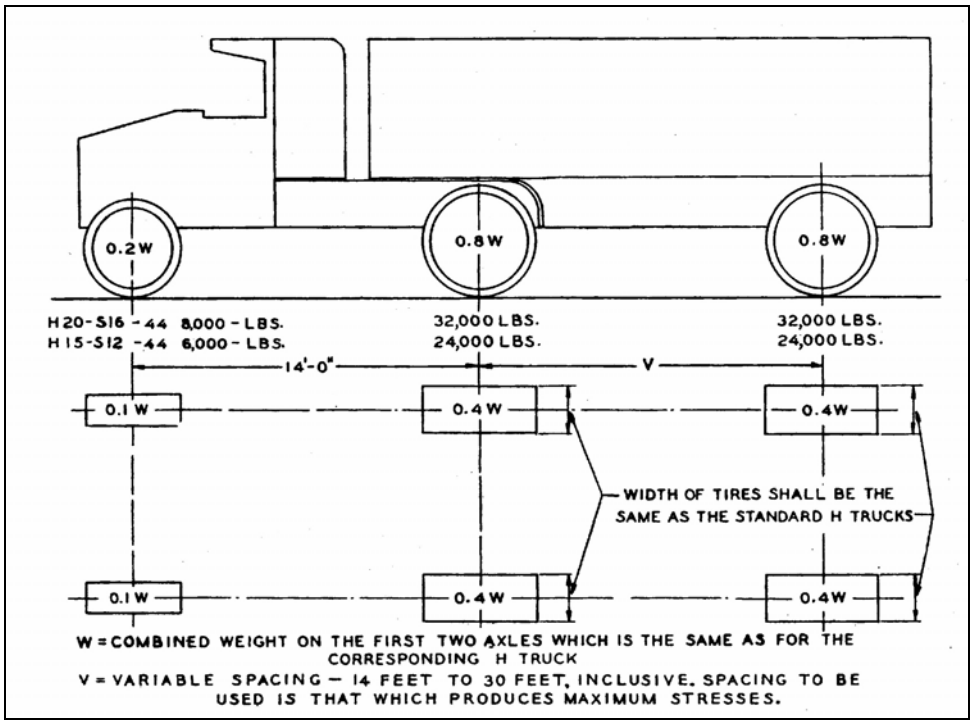

(a)

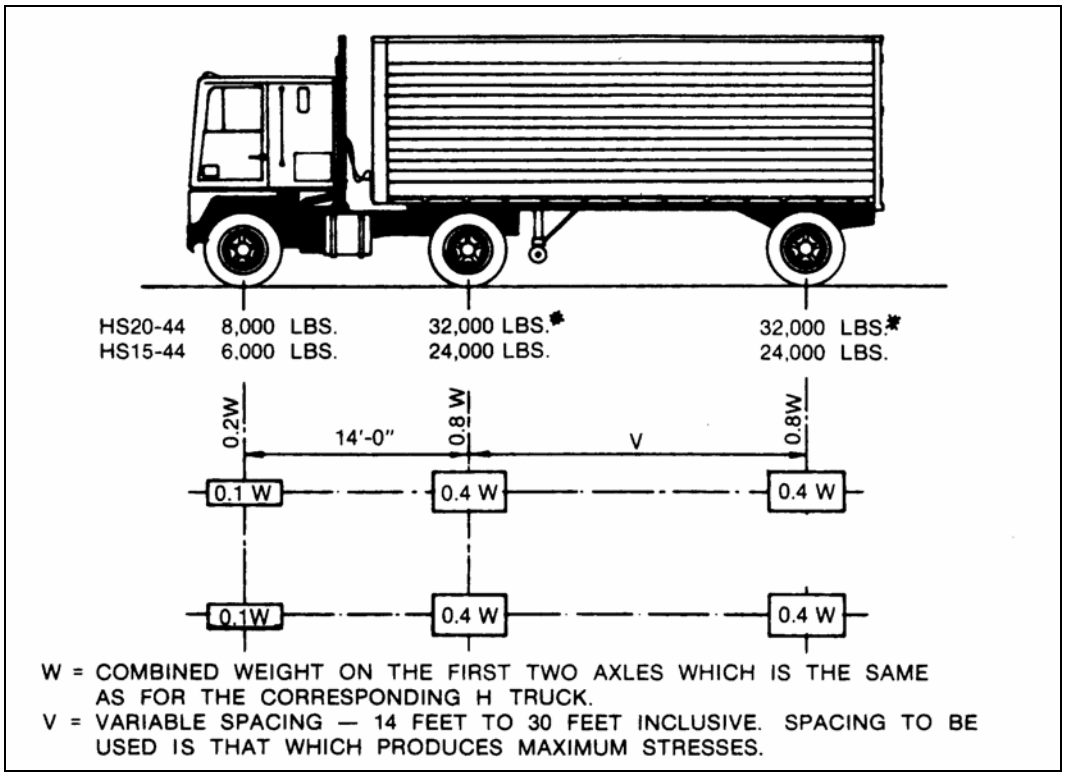

(b)

Figure 8.1: AASHTO Standard Specification design truck – (a) 4th Edition (*AASHTO 1944*); (b) 17th Edition (*AASHTO 2002*)

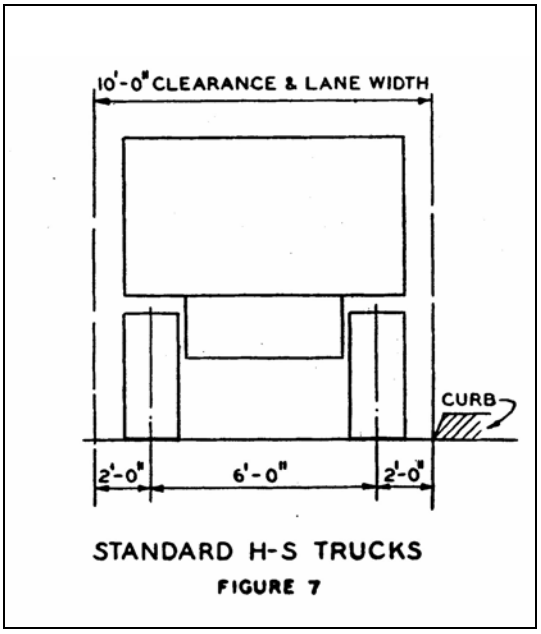

(c)

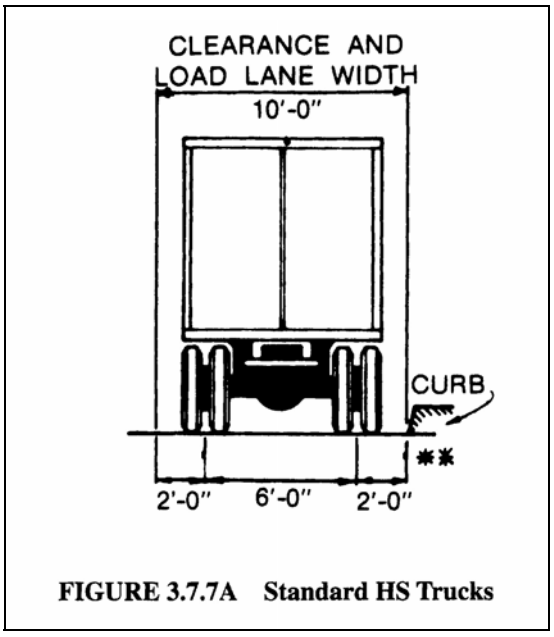

(d)

Figure 8.1(continued): AASHTO Standard Specification design truck – (c) 4th Edition (*AASHTO 1944*); (d) 17th Edition (*AASHTO 2002*)

Many CRC slab-girder bridges are reaching the end of their originally intended design life. The combined effects of over-estimation of the concrete contribution to shear resistance at design, increasing service load magnitudes and volume, as well as shrinkage and temperature effects, may contribute to diagonal tension cracking in these bridges.

Due to the relatively light shear reinforcement, diagonal cracks may not be well constrained and therefore become quite wide. Inspections of approximately 1,800 vintage CRC slab-girder bridges in Oregon revealed over 500 with varying levels of diagonal tension cracking as shown in Figure 8.2. Crack widths over 0.1 inches were observed. These findings resulted in load postings, monitoring, emergency shoring, repairs, and bridge replacements.

Due to the large numbers of bridges involved and their distribution across the state, a research study was undertaken to investigate the remaining capacity and life of diagonally cracked CRC slab-girder bridges. This study includes field testing, laboratory testing, and analysis components. This part of the report describes findings of the field studies with corresponding analysis results of an in-service 1950's vintage CRC slab-girder bridge with diagonal tension cracks.

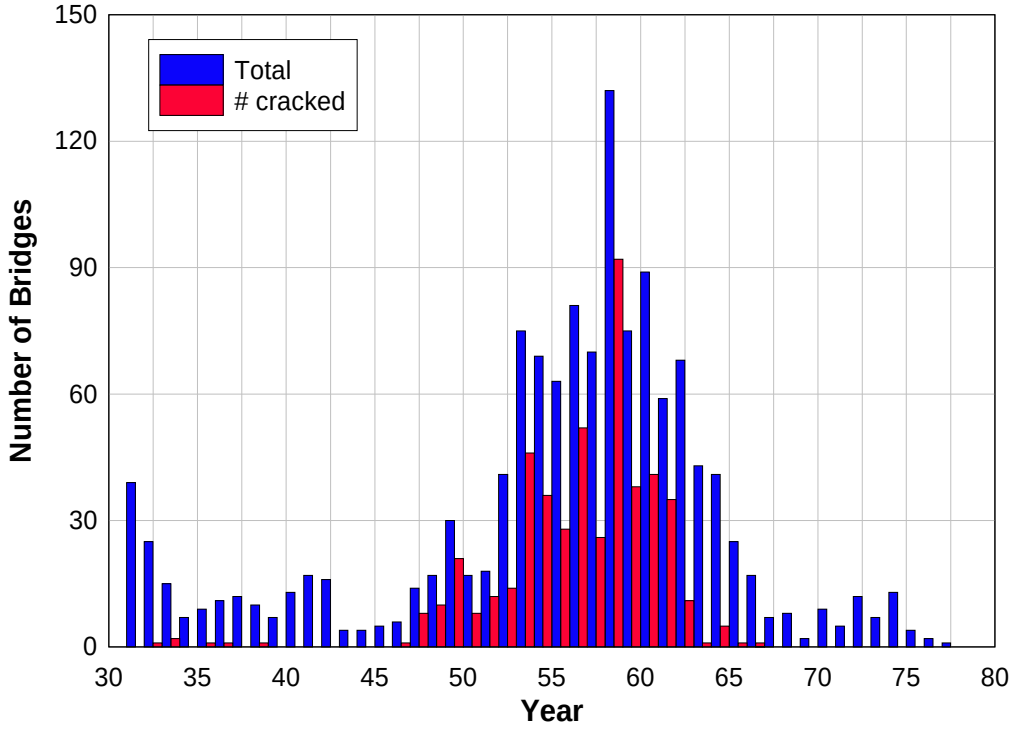

Figure 8.2: Distribution of total number of concrete bridges constructed each year and those identified with diagonal tension cracks

8.1 FIELD STUDY BRIDGE

The Willamette River Bridge on Oregon Highway 219, located near Newburg, Oregon was selected for field investigation. The slab-girder bridge was designed in 1954 and built in 1956. The bridge consists of ten spans: four steel plate girder spans over water and three conventionally reinforced concrete approach spans at each end. Concrete approach spans exhibited significant diagonal cracks and were scheduled for repair using externally bonded fiber-reinforced polymer materials. The bridge has a regular layout with rectangular prismatic girders as shown in Figure 8.3, which simplify analyses and component tests for further investigation.

The south approach spans as shown in Figure 8.4 were selected for instrumentation due to their accessibility. The approach spans have three equal span lengths, 16764 mm (55 ft) each, and have a total width of 10668 mm (35 ft). The spans comprise one simple span (Span 10) having five girders (368 × 1346 mm) and two continuous spans (Spans 8 and 9) having four girders (330 × 1346 mm). Reinforced concrete diaphragms (229 × 1219 mm) are located at quarter points of each span. The approach spans have three simple supports (at Bent 5, 6, and Pier 5) and one fixed support at Bent 4 with a transverse beam (419 × 1803 mm) supported by two columns.

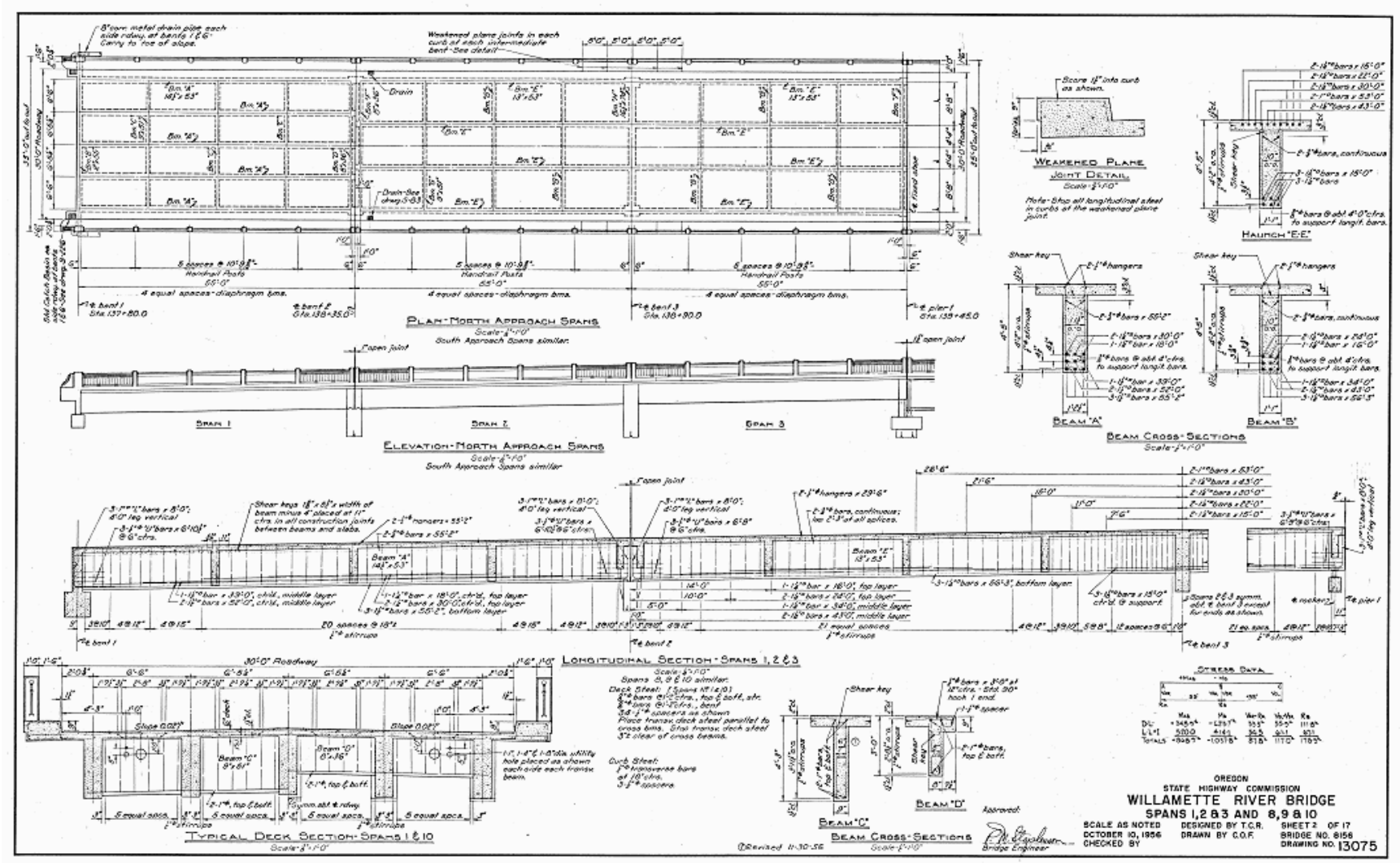

Figure 8.3a: Plan view of Willamette River Bridge on OR 219

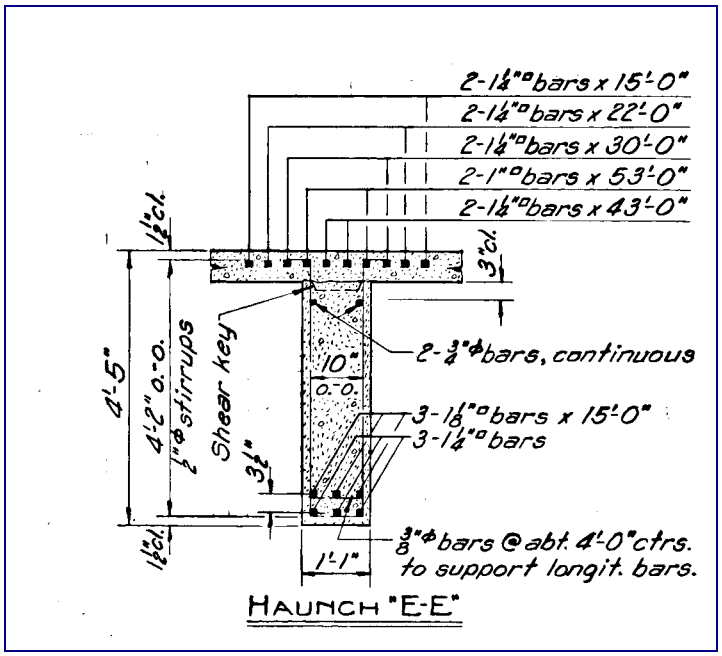

Figure 8.3b: Elevation view of typical girder

Figure 8.4: South approach spans of Willamette River Bridge on OR 219

9.0 INSPECTION AND INSTRUMENTATION

The bridge was inspected and cracks were marked to identify crack locations and orientations on the girders. A reference grid was marked on the girder faces to facilitate inspection and referencing of crack locations relative to support locations. Cracks having widths above a threshold of 0.3 mm (0.013 in.) were recorded. Several crack width measurements were taken along the crack length for each crack. A rebar locator, Proceq Profometer 3, was used to locate reinforcing steel stirrups in the girders. CAD drawings were developed to record the cracks and stirrup locations for the girders as shown in Appendix A.

Example diagonal cracks in the girders are shown in Figure 9.1. Distributed diagonal cracks were identified throughout the interior and exterior girders. Crack widths were widest near the girder midheight and tapered to very fine or zero at the beam soffit and zero in the compression zone. The widest crack observed was 1.25mm (0.05 in.) near the interior support of the exterior girder. Exterior girders generally exhibited more cracks than the interior girders, and crack widths tended to be wider for exterior girders. Diagonal cracks were more frequent and more closely spaced near support locations.

Eight diagonal cracks were selected for instrumentation to monitor crack motions and strains in steel stirrups. The selected diagonal crack locations are shown in Appendix A. All instrumented diagonal crack locations were in the northbound lane and on the bridge girders except for Location #1 which was on the transverse beam at Bent 4. Two diagonal cracks – Locations #2 and #3, were in the simple span, and six diagonal cracks – Locations #1 and #4 - #8, were in the continuous spans. At two locations, Locations #2 - #3 and #6 - #7, instruments were placed on both interior and exterior girders to help assess load distribution. Table 9.1 shows the location and details of the eight instrumented diagonal cracks.

Table 9.1: Details of instrumented locations

Location No.	Horizontal Position in mm (in)†	Vertical Position in mm (in)††	Largest crack width in mm (in)
1†††	33528 (1320)	775 (30.5)	0.9 (0.035)
2	972 (38.25)	559 (22)	0.9 (0.035)
3	2254 (88.75)	451 (17.75)	0.7 (0.028)
4	18898 (744)	711 (28)	0.6 (0.024)
5	29782 (1172.5)	648 (25.5)	1.25 (0.050)
6	36722 (1445.75)	470 (18.5)	1.0 (0.040)
7	36398 (1433)	318 (12.5)	0.4 (0.016)
8	49086 (1932.5)	641 (25.25)	0.6 (0.024)

† distance to Bent 6

†† distance to the bottom of the girders

††† gages located on the transverse beam

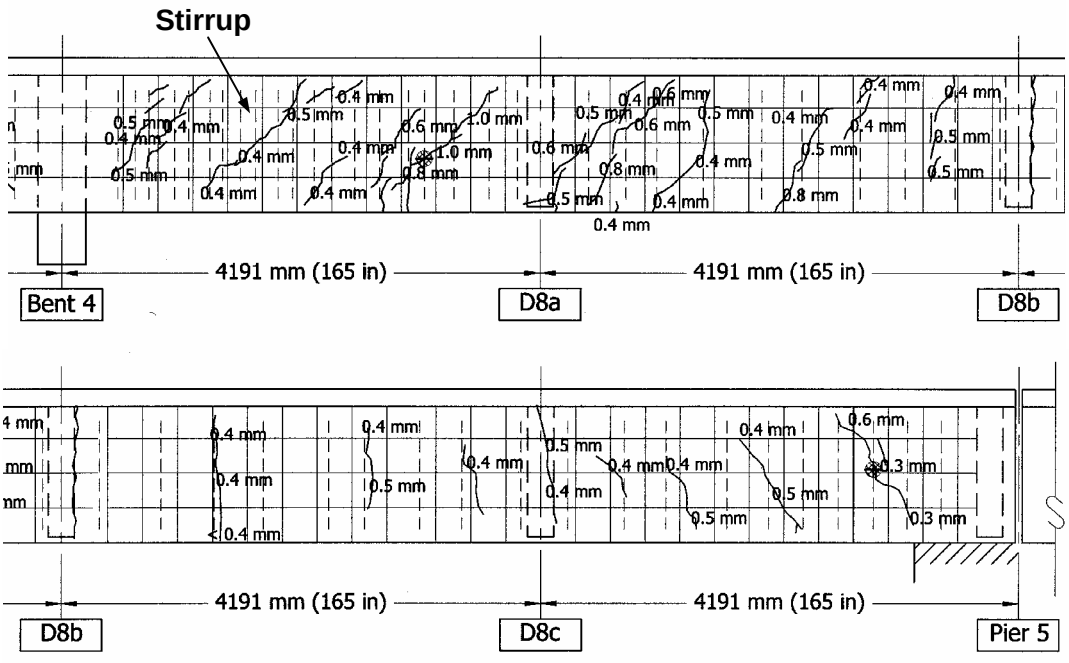

Figure 9.1: Example diagonal cracks and crack and stirrup mapping

Strain gages (6.4mm (0.25 in.) gage length) were placed on the steel stirrups at locations where stirrups crossed a diagonal crack. Concrete cover was removed and the stirrup surface was prepared before applying the strain gage. A spring return linear position sensor was installed near the strain gage to measure associated crack displacements. A typical instrumented location is shown in Figure 9.2.

Figure 9.2: Example instrumented location of stirrup crossing diagonal crack

The strain gages and displacement sensors were connected to a data acquisition system controlled by a personal computer. Data from all sensors were acquired at a rate of 50 Hz. Higher rates were also evaluated but the selected rate was adequate to capture the dynamic and impact responses of the structure. The data acquisition system was placed in an enclosure and anchored to the pier as shown in Figure 9.3, for long-term monitoring of ambient traffic load effects.

Figure 9.3: Instrumentation enclosure on pier

10.0 FIELD DATA

Two types of live load data were collected: response under ambient traffic and response under controlled truck loading. Stirrup stresses and crack displacements generated by ambient traffic were recorded from October 21 to October 30, 2001.

10.1 AMBIENT TRAFFIC INDUCED STRESSES

Ambient traffic induced stresses in stirrups at crack locations were monitored for a period of over 7 days. Continuous time-histories of stirrup strains were recorded for each instrumented location. The time-histories were saved in 10 minute intervals as illustrated in Figure 10.1a. An expanded view of an individual event is shown in Figure 10.1b.

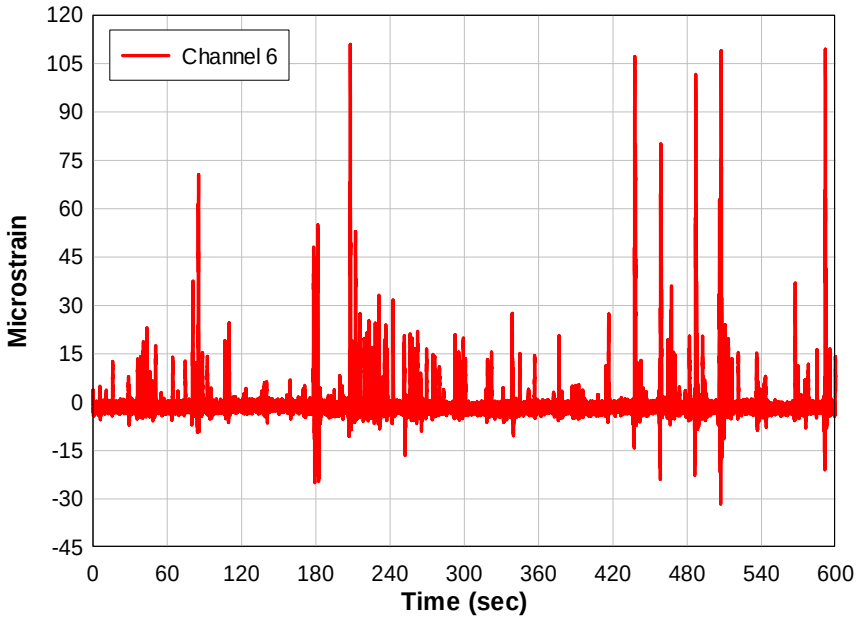

Figure 10.1a: Ten minute time history for stirrup strain at Location #6

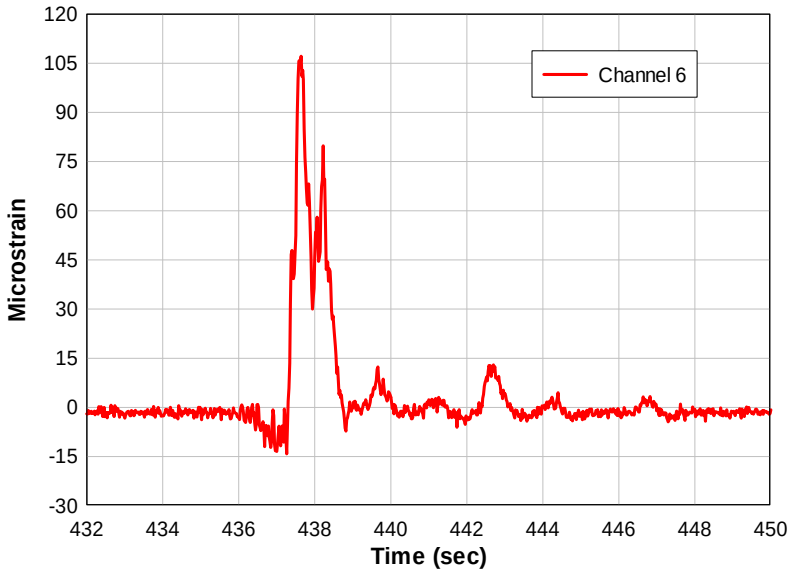

Figure 10.1b: Expanded view of time history for stirrup strain at Location #6

Strain-ranges and numbers of cycles during each of the 10 minute histories were computed using a rainflow counting technique (*Downing and Socie 1982*). Strains below 10 με were disregarded and the bin size was 10 με. Strains were converted to stress by multiplying by the modulus of elasticity for steel. Stress-ranges and numbers of cycles recorded are shown in Figure 10.2 for each of the instrumented locations.

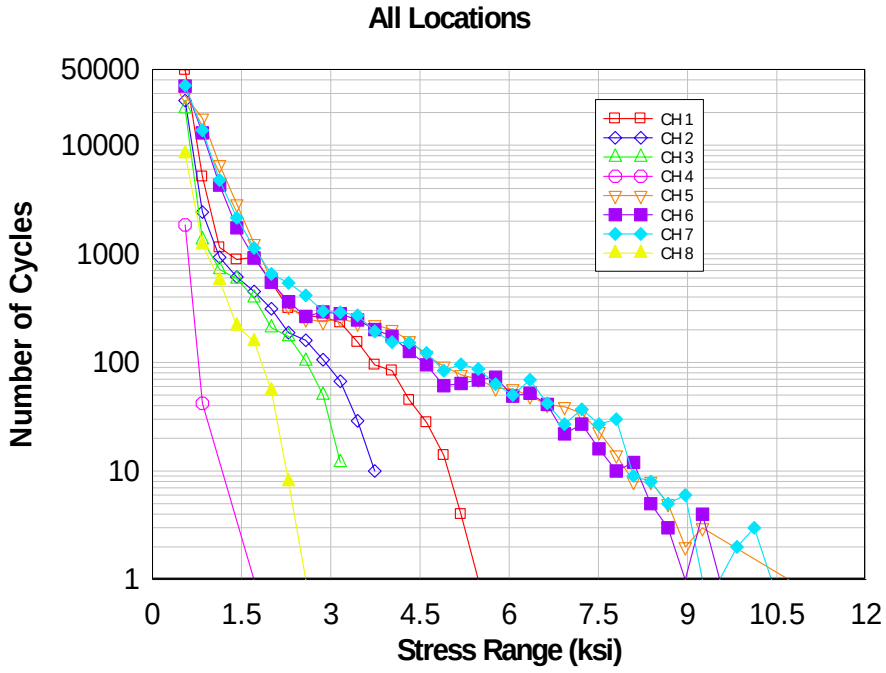

Figure 10.2: S-N Curve for all locations

The stress-ranges and numbers of cycles recorded for each day at Location #1 are shown in Figure 10.3. The numbers of cycles at each stress-range were consistent for each day except the sixth day, which corresponded to Sunday.

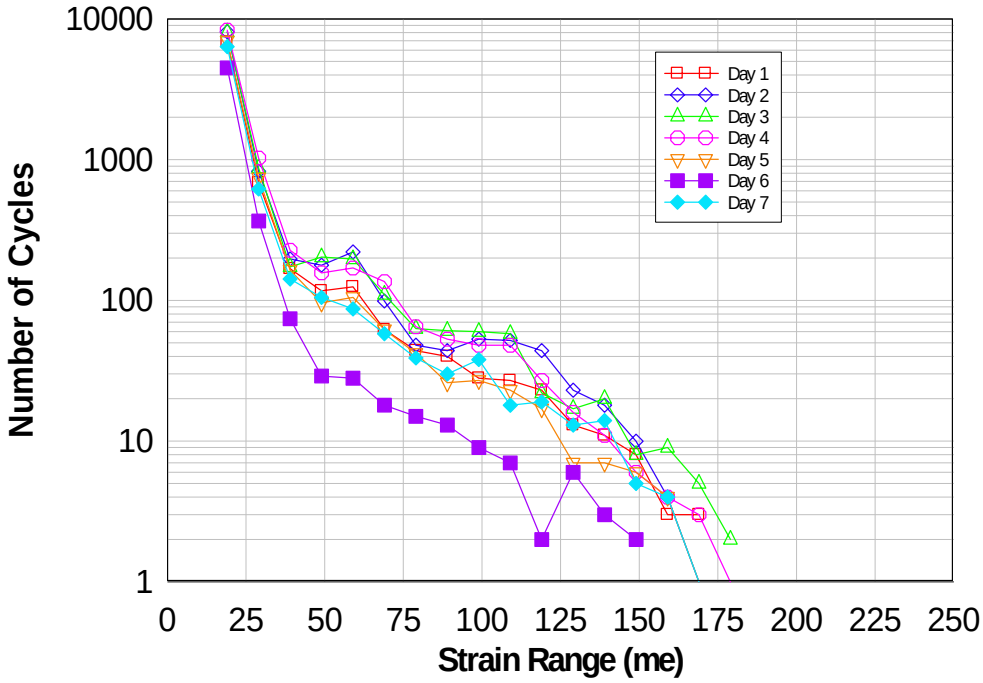

Figure 10.3: Numbers of cycles and strain-ranges on each day for Location #1

Example cycle counts for stress ranges of 0.5, 2, and 5 ksi at Location #7 (shown in Figure 10.4) indicate that smaller stress ranges typically occur during the day, but the larger stresses may occur at any time. The single largest stress-range measured at any location was 10.6 ksi at Location #5.

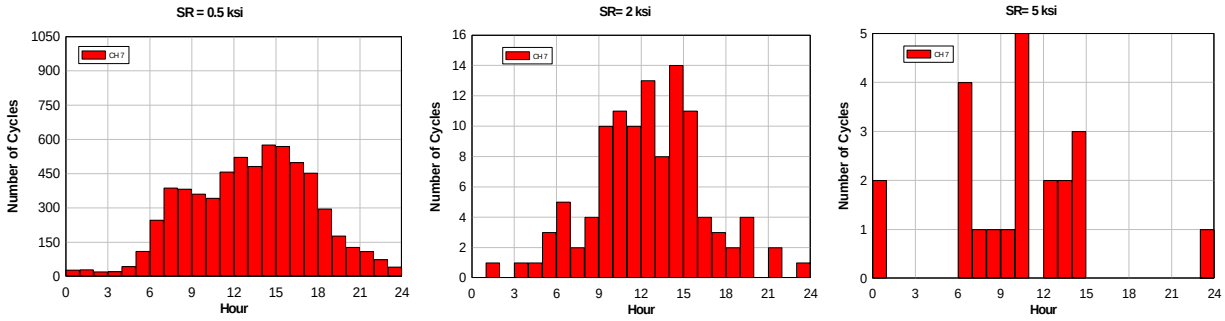

(a) 0.5 ksi (b) 2 ksi (c) 5 ksi

Figure 10.4: Cycle count at time of day for Location #7

Using Miner's Rule, the variable amplitude stresses can be described as an equivalent constant amplitude stress-range for each of the instrumented locations (*Miner 1945*):

$$SR_{eqv} = \sqrt[3]{\sum \frac{n_i}{N_{tot}} SR_i^3} \qquad \textbf{(10-1)}$$

where SR_i is the i^{th} stress-range, n_i is the number of cycles observed for the i^{th} stress-range, and N_{tot} is the total number of cycles at all stress ranges.

The equivalent constant amplitude stress-ranges were below 2 ksi for all of the instrumented locations, as seen in Table 10.1. The total numbers of cycles the bridge may have experienced can be conservatively estimated by assuming the vehicular volume and load magnitudes have remained constant during the life of the bridge (and can be described by the data taken in October 2001). For a service life of 50 years, the bridge could experience the numbers of stress ranges shown in Figure 10.5.

Table 10.1: Equivalent constant amplitude stress range for all instrumented strains

Location	Equivalent Constant Amplitude Stress Range (ksi)
1	1.00
2	0.85
3	0.78
4	0.46
5	1.58
6	1.54
7	1.62
8	0.68

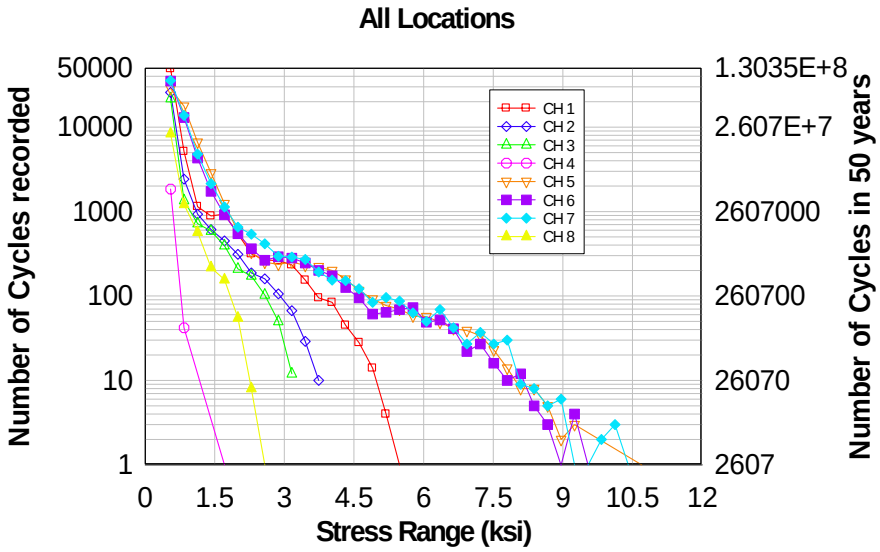

Figure 10.5: Possible number of cycles for a 50 year service life

Previous research on fatigue of rebar indicates that long-life can be achieved if the stress-range is below 10 ksi at bend or tack welds (*MacGregor 1997*). If no significant stress concentrations are found on the rebar, long-life can be achieved if the stress-range is below 20 ksi. Typical fatigue S-N curves for deformed reinforcing bars are shown in Figure 10.6. Given the relatively low equivalent constant amplitude stress-range identified at all instrumented locations, metal fatigue leading to fracture of the embedded stirrups is unlikely. The field data collected on in-situ stirrup stresses will also be used to conduct tests to evaluate deterioration mechanisms for laboratory specimens that are reasonable for operating conditions of in-service CRC slab-girder bridges.

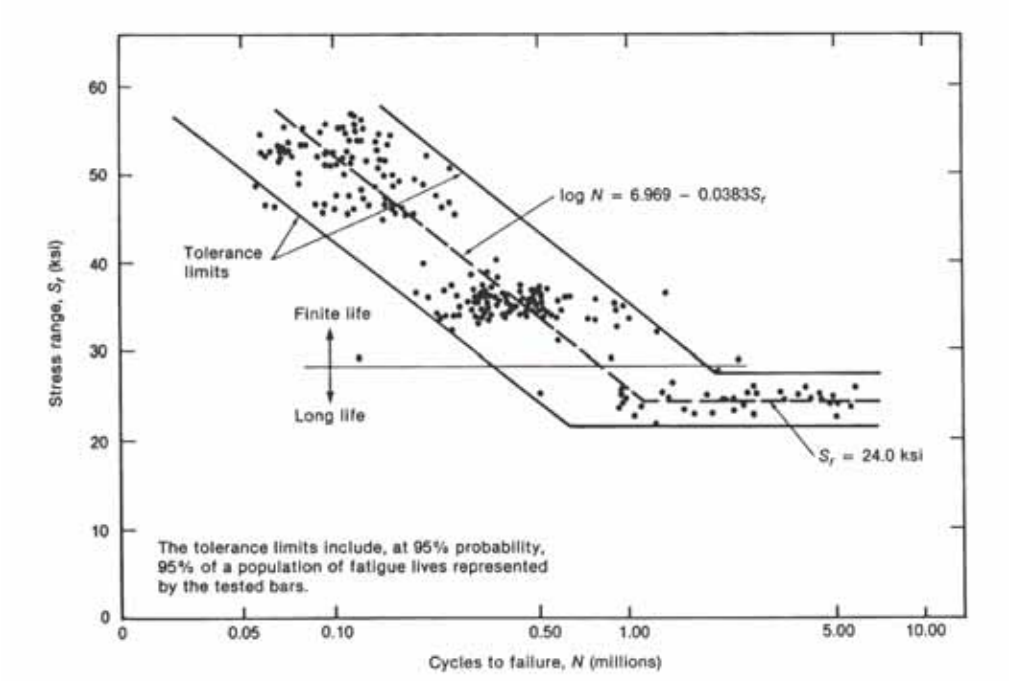

Figure 10.6: Fatigue tests of reinforcing steel (*MacGregor 1997*)

10.2 CONTROL TRUCK TESTING

An ODOT maintenance truck filled with gravel was used to perform controlled truck loading of the bridge. The truck had a gross vehicle weight of 227 kN (51 kip) with axle loads shown in Figure 10.7. ODOT flagging crews prevented other vehicles from being on the bridge simultaneously with the control truck. Eight truck passages were performed, five in the northbound direction and three in the southbound direction. Test truck velocities varied from creep to posted and traveling speeds to capture dynamic and impact effects. Truck speeds were determined from the truck speedometer and reported by the driver.

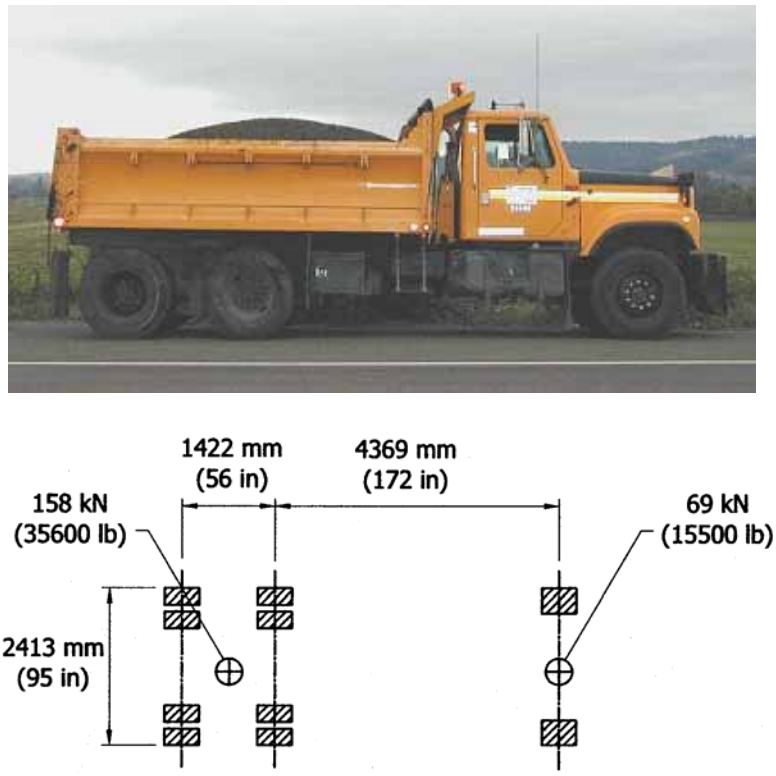

Figure 10.7: Test truck configuration used for controlled loading of bridge

The lane positioning of the different truck passages are shown in Table 10.2. Since the sensors were installed only on the northbound lane, the southbound passages were performed to assess load distribution of the girders across the entire bridge section. For Passage # 2, the passenger-side truck tires were located on the fog line to produce a more direct load transfer to the exterior girder.

Table 10.2: Truck passage configurations

Passage No.	Velocity in km/hr (mph)	Direction	Lane postion
1	8 (5)	North	in lane
2	8 (5)	North	one side on fog line
3	8 (5)	South	in lane
4	80.5 (50)	North	in lane
5	80.5 (50)	South	in lane
6	90 (56)	North	in lane
7	95 (59)	North	in lane
8	103 (64)	South	in lane

Example crack displacements and stirrup strain results are shown in Figure 10.8. Data for all instrumented locations, truck speeds, and directions are contained in Appendix A. Crack opening and closing was observed for the continuous span locations, while only crack opening was observed in the simple span results. Stirrup strains increased with crack opening displacement, but only small compressive strains were observed when crack closing occurred.

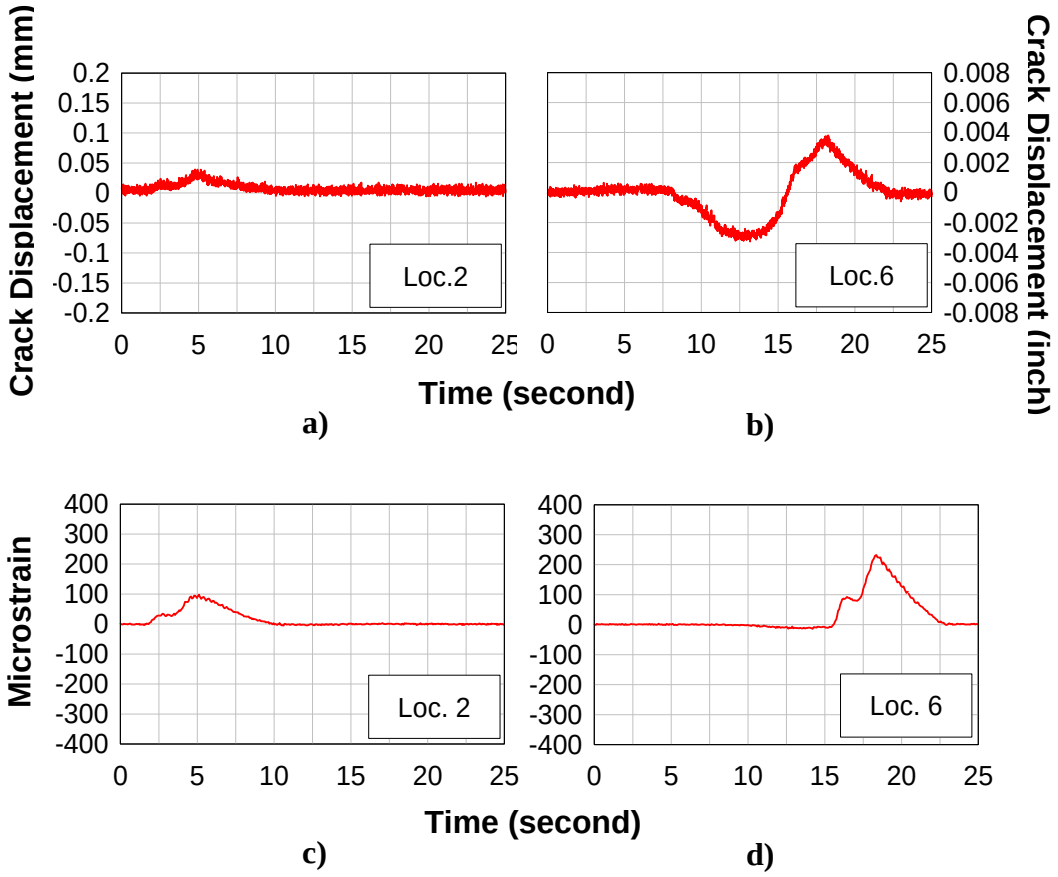

Figure 10.8: Example crack displacement and steel strain results from the northbound passage of the test truck across the bridge with a speed of 8 km/hr: a), c) simple span; b), d) continuous spans

Peak strain values in the continuous spans were higher than those in the simple span due to the fewer number of girders and the role of the structural indeterminacy. As seen in the continuous spans, the truck produced multiple stress reversals that could contribute to metal or bond fatigue between the stirrup and surrounding concrete. The maximum strain range observed was at Location #7 with the truck traveling at a speed of 90 km/hr (56 mph) positioned in the northbound lane. The maximum strain range in the stirrup, from –25 to 358 microstrains, was 383 microstrain.

A linear material response was assumed for the stirrups with the stress range calculated by multiplying the strain range value by the elastic modulus for steel, 200 GPa (29000 ksi). The computed stress range was 76.6 MPa (11.11 ksi). This was larger than any other stress range

observed during the ambient traffic monitoring that was described previously. The AASHTO standard specification provides a method to determine permissible stress range for straight rebar in Section 8.16.8.3 (*AASHTO 2002*). The rebar stress range may not exceed:

$$f_f = 21 - 0.33 f_{min} + 8(r/h) \qquad \text{(AASHTO Equation 8-60)} \quad \textbf{(10-2)}$$

where f_{min} (ksi) is the algebraic minimum stress level with tension being positive and compression being negative and r/h is the ratio of the base radius to height of the rolled transverse deformations.

When the actual value of r/h is not known, it may be taken as 0.3. Using a minimum stress level equal to 5 MPa (0.725 ksi) and r/h ratio assumed to be 0.3, the maximum permissible stress range is 163 MPa (23.64 ksi), which is larger than the maximum stress ranges observed from the field tests.

10.3 DYNAMIC/IMPACT INFLUENCE

Example strain and crack displacement histories are shown in Figure 10.9 for the truck moving at slow and fast speeds across the bridge. The test truck passage at the posted speed of 95 km/h (59 mph) generated a 2.5 second duration loading event as compared to the passage at a creep speed of (5 mph) which generated a 15 second loading event. The maximum values recorded at the higher speed passages were larger than those from the creep speed passages due to dynamic and impact effects. Table 10.3 shows the maximum measured strains at all instrumented locations for four different truck speeds.

The measured strain at each of the higher velocities was divided by the measured strain at the creep velocity to determine an impact factor that reflects an increase in stirrup stresses due to dynamic response and impact of the test truck. On average, for all truck locations, the higher truck speeds produced strain increases of 1.2 times the strains measured at creep speed. The largest strain increase (1.463) occurred at Location #6 when the truck was traveling at 95 km/h (59 mph). At this location, a speed increase of only 15.5 km/h (9 mph) resulted in a 30% increase in strain compared with the 85.5 km/h (50 mph) test.

The AASHTO Standard Specification uses an impact factor of (*AASHTO 2002*):

$$I = \frac{50}{L + 125} \qquad \text{(AASHTO Equation 3-1)} \quad \textbf{(10-3)}$$

where L is the length (ft) of the span loaded to produce the maximum load effect.

The maximum impact fraction is 30% (*AASHTO 2002*). This is the same impact factor used in previous editions of the Specification as shown in Table 10.3. For this bridge (span length of 16764 mm (55 ft)), the calculated impact fraction was 28%. The AASHTO LRFD Specification uses an impact factor of 15% for the fatigue load combination and 33% for factored load

combinations (*AASHTO LRFD 1998*). The average field measured impact factions were less than those recommended by either AASHTO provision. However, individual tests at higher speeds did produce larger impact fractions, particularly at Location #6, which was significantly larger.

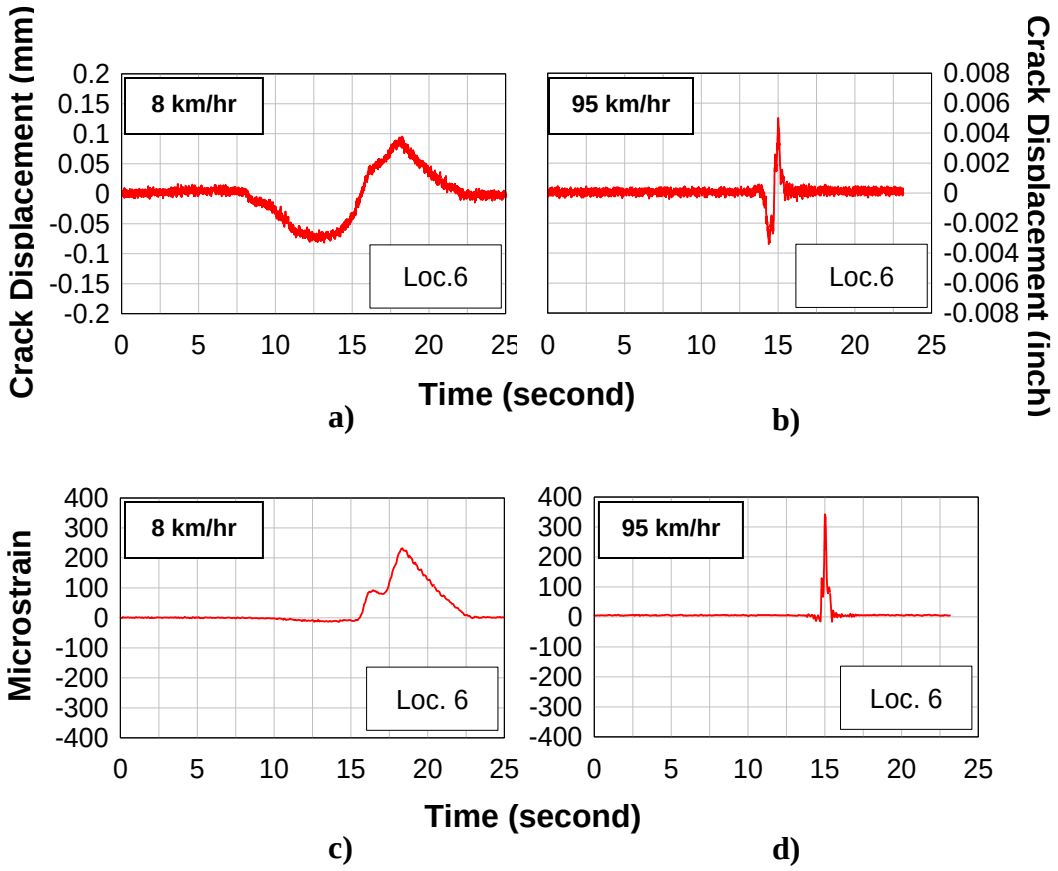

Figure 10.9: Effect of different test truck speeds at Location #6 for the northbound passage across the bridge: a), c) creep speed; b), d) posted speed

Table 10.3: Maximum strain measured for each truck passage and impact factors

	Max. Strain (με)	Impact Factor	Max. Strain (με)	Impact Factor	Max. Strain (με)	Impact Factor	Max. Strain (με)	Impact Factor	Max. Strain (με)	Impact Factor	Max. Strain (με)	Impact Factor	Max. Strain (με)	Impact Factor	Max. Strain (με)	Impact Factor
Location	1		2		3		4		5		6		7		8	
5N	130	-	98	-	89	-	6	-	213	-	235	-	266	-	48	-
50N	139	1.071	117	1.190	105	1.181	6	1.104	215	1.010	267	1.134	307	1.153	50	1.033
56N	143	1.097	115	1.171	100	1.129	7	1.219	279	1.309	317	1.347	358	1.344	62	1.295
59N	147	1.132	109	1.113	96	1.086	8	1.385	254	1.191	345	1.463	356	1.335	66	1.379
Avg.		1.100		1.158		1.132		1.236		1.170		1.315		1.278		1.236

10.4 LOAD DISTRIBUTION

Distribution of shear across the four girders on the two-span continuous portion of the bridge was inferred from the measured stirrup strains. The distribution was obtained using the rebar strain measurements at Locations #6 (exterior girder) and #7 (interior girder) for northbound and southbound truck passages at a creep speed. The maximum measured stirrup strains are shown in Table 10.4 and Figure 10.10.

Table 10.4: Strain measured for northbound truck passages at 5 mph and inferred distribution of shear in girders

Girder #	1	2	3	4
Max. Strain as Measured	235 με	266 με	86 με	63 με
Max. Strain Corrected for Truck Orientation	235 με	266 με	94.6 με	69.3 με
Distribution for Single Truck	35.3%	40.0%	14.2%	10.4%
Distribution for Two Trucks	22.9%	27.1%	27.1%	22.9%

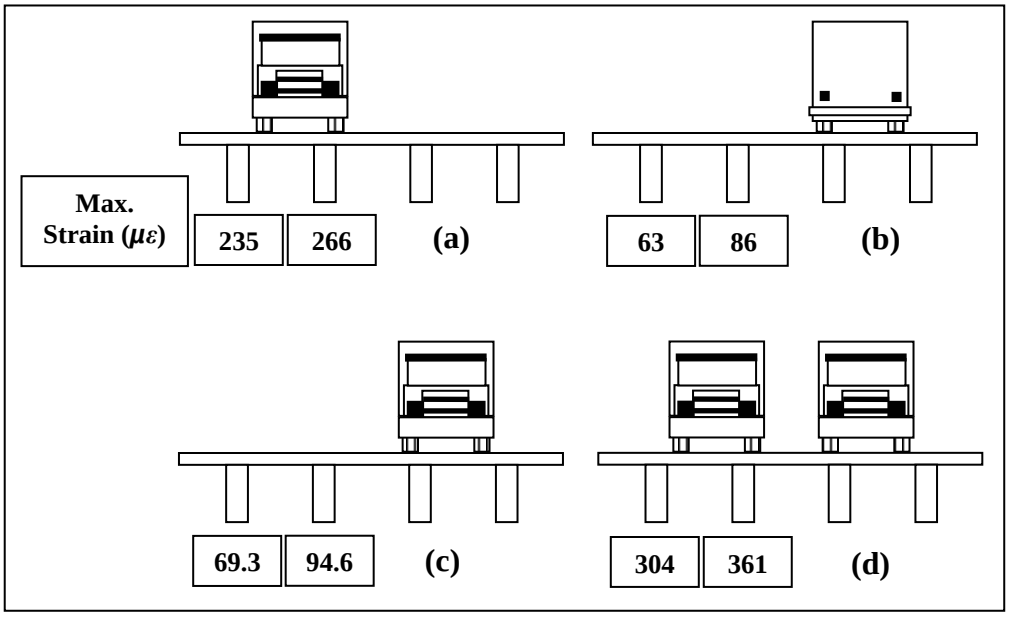

Figure 10.10: Legend for measurements shown in Table 10.4 – (a) northbound and (b) southbound as measured; (c) corrected for truck direction of travel; and (d) superposition of 2 trucks in northbound direction

To account for the truck axle orientations being different for the northbound and southbound directions relative to the instrumented locations, the strains for the southbound passage were amplified based on the shear magnitude produced at the location of interest using influence line ordinates as illustrated in Figure 10.11. This resulted in increasing the strains for the southbound passage by 10%. The resulting distribution for each of the girders in terms of the total shear force at this section from the test truck is shown in Table 10.3 for a single truck in the northbound lane or trucks in both lanes.

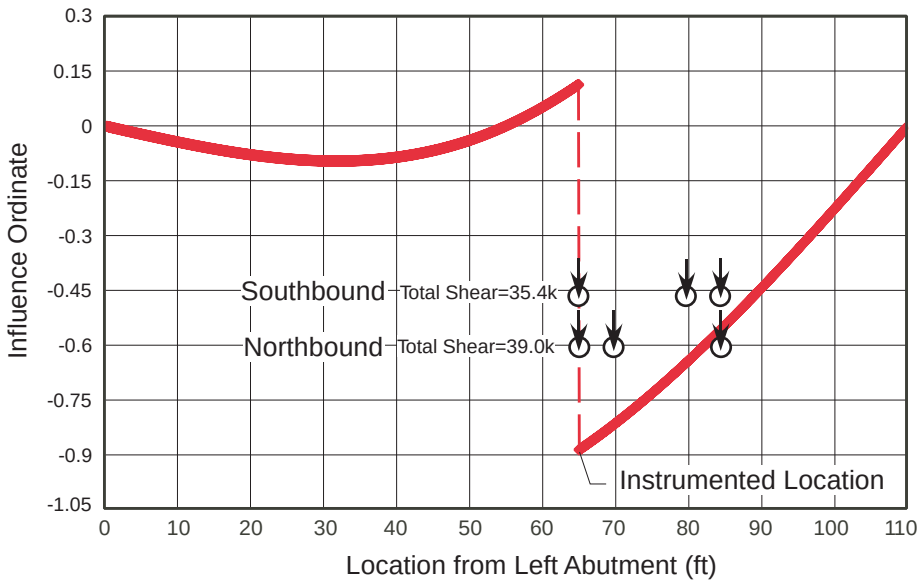

Figure 10.11: Influence ordinates for shear at 10 ft from center support (location of instrumentation on girders)

Distribution of loads for shear and moment in the 1953 Standard Specification were based on the spacing of girders (*AASHO 1953*). A wheel load fraction of S/5 was applied for interior girders with concrete floors on bridges supporting two or more traffic lanes, where S (ft) is the average spacing of girders. Exterior girders were designed assuming wheel loads were distributed by the deck acting as a simple beam between the girders. This technique is referred to as the "lever rule." No distribution was permitted for the wheel/axle load located at the end of the girder. The current AASHTO Standard Specification employs the same basic provisions for shear load distribution but now uses a wheel load fraction of S/6 for similar bridges with two or more traffic lanes (*AASHTO 2002*).

For the girder spacing and the AASHTO HS25 design truck, the shear forces and equivalent distribution factors were determined for the interior and exterior girders at instrumentation Locations #6 and #7. No distribution was used for the wheel/axle load located directly over the location where the shear force was computed and the other wheel loads were distributed as permitted by the code (S/5 for 1953 and S/6 for 2002). The code values are for two or more traffic lanes and thus multiple presence of load is implied in the distribution values. The load distribution for axle(s) at the location where shear is calculated is illustrated in Figure 10.12.

As seen in this figure, the controlling axle positions are orientation A for the interior girder and ExA for the exterior girder. For two design trucks positioned on the bridge to produce the highest shear at the location of interest (10 ft from center support), the total shear force produced on this section is 105 kips. The shear carried by the interior girder using the 1953 AASHO Standard Specification is 47.2 kips or 45.0% of the total shear. The exterior girders use the lever rule for all the axles (1.385 from Figure 10.12), and the total shear is 36.5 kips or 34.8% of the total shear.

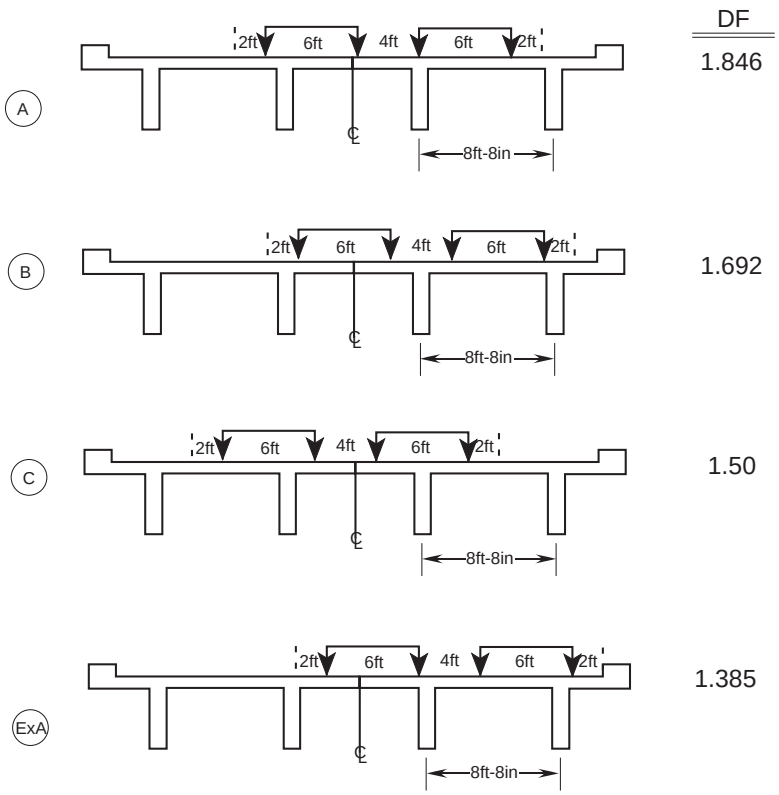

Figure 10.12: Wheel positions for distribution of shear according to “lever rule”

The 1953 AASHO provisions did not require that exterior girders carry at least the amount of shear for the interior girders, but did require all girders to be able to carry the statical shear at all sections. The shear carried by the interior girder using the current AASHTO Standard Specification is 43.7 kips or 41.7% of the total shear. The exterior girders again use the lever rule for all the axles (1.385 from Figure 10.12), and the total shear is 36.5 kips or 34.8% of the total shear. The current specification would require that the exterior girder carry the same or greater magnitude of shear as the interior girders.

Using the shear produced by two design trucks at the section (105 kips) and the measured girder distribution percentages in Table 10.4, the interior girders would carry 28.4 kips and the exterior girders would carry 24.0 kips. These are about 60.2% and 65.8% of the 1953 based design shears for the interior and exterior girders, respectively. The 1953 AASHO load distribution method produced girder design shear forces substantially larger than the actual shear produced across the bridge section by the design trucks, based on distributions obtained from field measurements.

10.5 PROPORTION OF SHEAR CARRIED BY STIRRUPS

The amount of the applied shear from the test truck carried by the stirrups was estimated based on the measured strains at instrumentation Locations #6 and #7, combined with the load distribution determined previously. Based on strain results corrected for the northbound truck

orientation shown in Table 10.4, for a single test truck in the northbound lane, stirrup stresses for each of the girders was computed.

The number of stirrups crossing the diagonal cracks at Locations #6 and #7 was determined from field observations shown in Appendix A. Each crack was crossed by three (3) stirrups. It was assumed that all stirrup legs crossing the crack carried the same stress level. For the 0.5 in. diameter stirrups, the vertical force component of the steel stirrups in each girder was determined as shown in Table 10.5. The statical shear produced across the bridge section under consideration (approximately 10 ft from the center support) was computed from statics using the test truck axle weights and spacing as 39.0 kips. As seen from Table 10.5, the stirrups account for approximately 58% of the applied shear.

Table 10.5: Estimated shear force in stirrups from test truck

Girder	1	2	3	4	Sum
Corrected Strain (με)	235	266	94.6	69.3	664.9
Distribution	35%	40%	14%	10%	
Stress (ksi)	6.82	7.71	2.74	2.01	
Av (in^2)	0.3927	0.3927	0.3927	0.3927	
No. of stirrups crossing crack	3	3	3	3	
Force at Crack in Stirrups (kips)	8.0	9.1	3.2	2.4	22.7

The remaining shear force is attributed to the other vertical force carrying components of the girder at the crack interface and through the compression zone, as well as the deck contribution and nonidealized support conditions. Dowel action was not considered, as the cracks were very fine or zero at the level of the flexural tension steel.

The dead load stress magnitude in the stirrups was estimated using the percentage of live load stress carried by the stirrups, assuming the dead and live load shear are carried similarly in the girders. The dead load shear in each girder (using 4 in. asphalt wearing surface) was estimated as 44.0 kips for the location 10 ft from the center support. This corresponds to a dead load stress in each stirrup of 21.3 ksi. Combined dead and live load stress in the stirrups becomes 29.0 ksi. When impact is added to the live load portion of the load (using the largest measured impact factor of 1.46), the combined stress in the stirrups becomes 32.6 ksi. This is significantly above the allowable stress of 20 ksi prescribed in the Standard Specification, but below the specified material yield stress of 40 ksi (*AASHO 1953, AASHTO 2002*).

11.0 COMPARISON OF AASHTO ALLOWABLE STRESS DESIGNS

A comparison of the AASHTO Standard Specification allowable stress design methodologies was performed for the continuous span portion of the bridge that exhibited the more significant diagonal tension cracking. The 6th and 17th editions of the Standard Specification were used for this comparison. Design trucks weights, axle spacings, and wheel patterns are the same for both editions (HS20-44 and H20-S16-44) (*AASHO 1953, AASHTO 2002*). The controlling axle configuration for maximum shear uses both axles spaced at 14 ft. Impact factors for live load are the same in both editions (28%) per Equation 10-3. Live load distribution for shear was performed using the procedure described previously. Interior girders used S/5 (1953) and S/6 (2002) for distribution of wheel loads along the span. Wheel loads at the point where shear was calculated were distributed according to the lever rule as illustrated in Figure 10.12. Total dead load of the bridge including the girders, deck, diaphragms, and curbs was computed and distributed evenly to all girders. A 102mm (4 in.) asphalt overlay was included in the dead load calculation.

The allowable shear force for the girders was calculated using the specified allowable concrete stress in shear as:

$$v_c = 0.03f'_c \qquad \text{1953 AASHO} \qquad \textbf{(11-1a)}$$

$$v_c = 0.95\sqrt{f'_c} \qquad \text{2002 AASHTO} \qquad \textbf{(11-1b)}$$

where f'_c is the specified compressive strength of the concrete (3300 psi).

The concrete contribution was computed as:

$$V_c = v_c bd \qquad \textbf{(11-2)}$$

where b is the beam width and d is the beam depth.

The beam depth varies depending on the amount of flexural steel as shown in Table 10.6. The stirrup allowable stress was 20,000 psi in both the 1953 and 2002 editions. The steel contribution to shear was calculated as:

$$V_s = \frac{A_v f_v d}{s} \qquad \textbf{(11-3)}$$

where A_v is the area of the stirrups (1/2 in. diameter bars), f_v is the allowable steel stress (20,000 psi), d is the beam depth, and s is the stirrup spacing.

Concrete and steel contributions are superimposed to determine the allowable shear. The allowable shear and the applied shear are shown in Figure 11.1 and 11.2 and are summarized in Table 10.6 for the 1953 and 2002 AASHTO Standard Specifications.

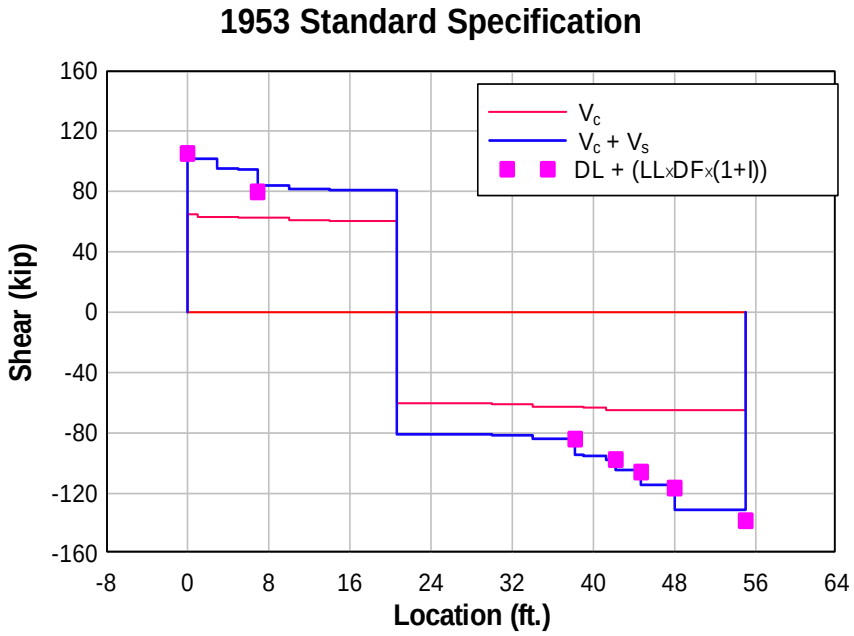

Figure 11.1: Allowable shear and applied service level shear for 1953 AASHO allowable stress design

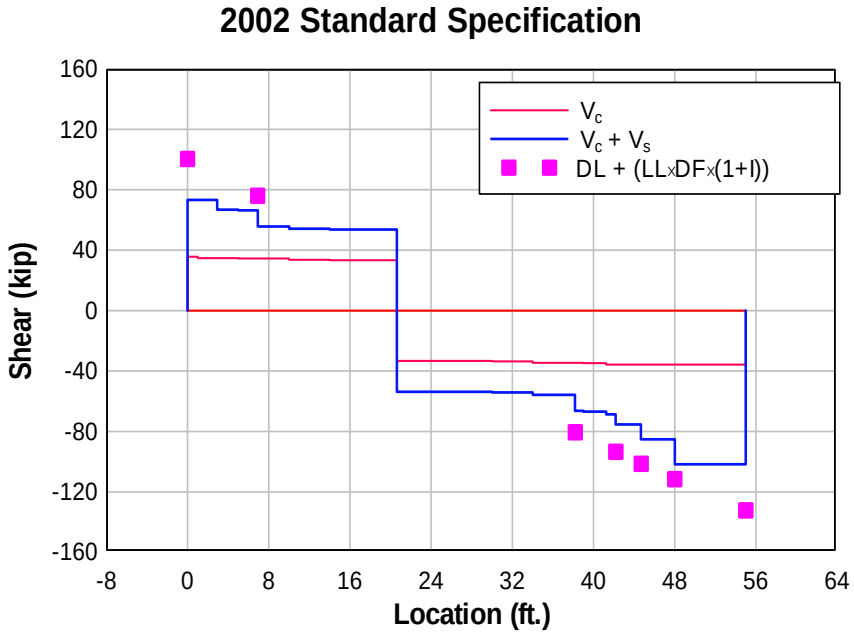

Figure 11.2: Allowable shear and applied service level shear for 2002 AASHTO allowable stress design

As seen in these figures, the 1953 and 2002 versions have identical stirrup contributions to shear resistance. The 1953 design load is larger than the 2002 design load for the interior girder due to the larger factor used for load distribution. The 1953 design was adequate for the time but relies on an unconservative concrete allowable stress to meet the design criteria. The as-designed bridge would not be considered adequate for the working stress design according to current standards, as seen in Figure 11.2, where the design loads exceed the allowable load in the high-shear regions.

Table 10.6: Design values for bridge girders according to 1953 and 2002 versions of AASHTO Standard Specification

Location from Left Support (in)	Effective Depth (in)	1953 V_c (kip)	Stirrup Spacing (in)	2002 V_c (kip)	V_s (kip)	1953 V_{total} (kip)	2002 V_{tota} (kip)
0 -12"	50.4	64.8	N/A	35.7	0	64.8	35.7
12" - 15"	49.0	63.0	N/A	34.7	0	63.0	34.7
15" - 35"	49.0	63.0	10	34.7	38.5	101.5	73.2
35" - 60"	49.0	63.0	12	34.7	32.1	95.1	66.8
60" - 83"	48.6	62.6	12	34.5	31.8	94.4	66.3
83" - 120"	48.6	62.6	18	34.5	21.2	83.8	55.7
120" - 168"	47.3	60.9	18	33.6	20.6	81.5	54.2
168" - 360"	46.9	60.3	18	33.3	20.5	80.8	53.7
360" - 408"	47.3	60.9	18	33.6	20.6	81.5	54.2
408" - 458"	48.6	62.6	18	34.5	21.2	83.8	55.7
458" - 468"	48.6	62.6	12	34.5	31.8	94.4	66.3
468" - 495"	49.0	63.1	12	34.8	32.1	95.1	66.8
495" - 506"	50.4	64.8	12	35.7	33.0	97.8	68.7
506" - 536"	50.4	64.8	10	35.7	39.6	104.4	75.3
536" - 576"	50.4	64.8	8	35.7	49.5	114.3	85.2
576" - 648"	50.4	64.8	6	35.7	65.9	130.8	101.7
648" - 660"	50.4	64.8	N/A	35.7	0	64.8	35.7

12.0 FINITE ELEMENT MODELING OF SOUTH APPROACH SPANS

12.1 MODEL DESCRIPTION

Field measured strains from the bridge were used for comparisons with linear finite element (FE) analysis. A finite element model was developed using ANSYS 7.0, a commercially available finite element analysis program. The south approach spans of the Willamette River Bridge on OR 219 were modeled with three-dimensional shell and beam elements. Shell elements incorporated both bending and membrane stiffnesses and were used for modeling deck, diaphragm, and girder components. Beam elements were used to model the columns at Bent 4. Total numbers of nodes and elements in the approach-span model were 13371 nodes and 13280 elements, respectively. The FE model is shown in Figure 11.3. FE analysis was performed for service level response; therefore the concrete elements were assumed to behave within a linear elastic range of concrete material properties and the contribution of reinforcing steel was neglected.

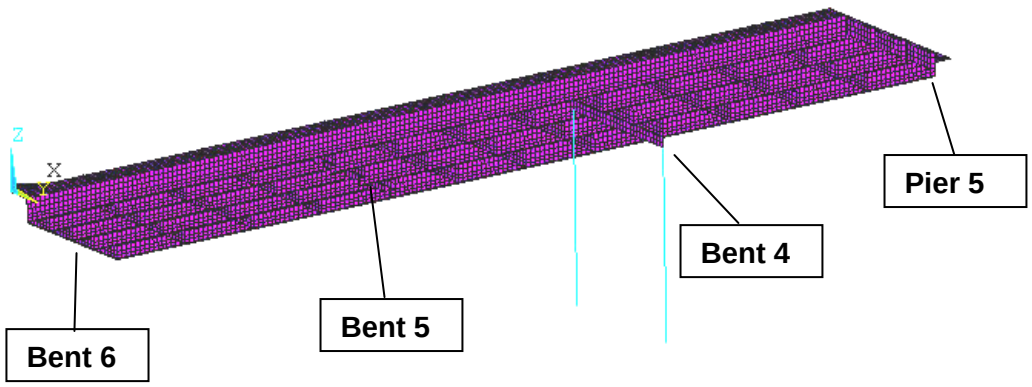

Figure 11.3: Finite element model of south approach spans

Concrete material properties were based on cores taken from the bridge. An average compressive strength (f'_c) of the concrete cores was 31.0 MPa (4500 psi) with a 7.34 MPa (1065 psi) standard deviation. The lowest and highest compressive strengths obtained from core tests were 23.1 MPa (3350 psi) and 42.2 MPa (6119 psi), respectively. Elastic modulus for the concrete was calculated as 26.4 GPa (3823 ksi) using Equation 12-1 (*ACI 318-2002*). Poisson's ratio was assumed to be 0.2.

$$E_c = 4733\sqrt{f'_c} \qquad \textbf{(12-1)}$$

where E_c is the elastic modulus of concrete (MPa) and f_c' = compressive strength (MPa).

12.2 SIMULATION OF TEST TRUCK PASSAGE

Truck loading consisted of a group of six point loads applied to the bridge model. The locations of the point loads followed the footprint of the test truck shown in Figure 10.7. Twenty-eight positions of truck wheel loads were separately applied to the bridge model in the bridge longitudinal direction to simulate test truck Passage #2 (passenger-side wheels located on the fog line). The distance from the fog line to the edge of the bridge was approximately 1753 mm (69 in). The driver-side truck wheel loads were applied to the bridge model at a distance of 1676 mm (66 in) from the edge. Result locations in the FE model were taken from positions close to the instrumented locations in the bridge and are shown in Table 9.1.

Shear stresses at the middle plane of shell elements were used for result comparisons. In order to make comparisons between the FE analysis results and the field-testing data, shear stresses illustrated in Figure 12.1b distributed along the height of girder sections from FE analyses were integrated over the section to obtain shear forces. The calculated shear force distributions obtained from the FE analyses were compared to stirrup strain distributions obtained from the field tests.

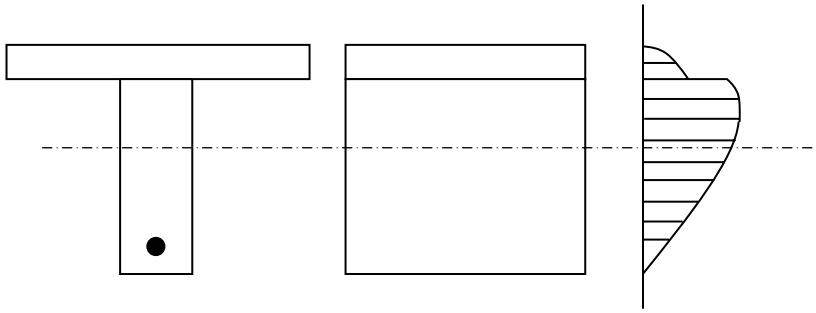

a)

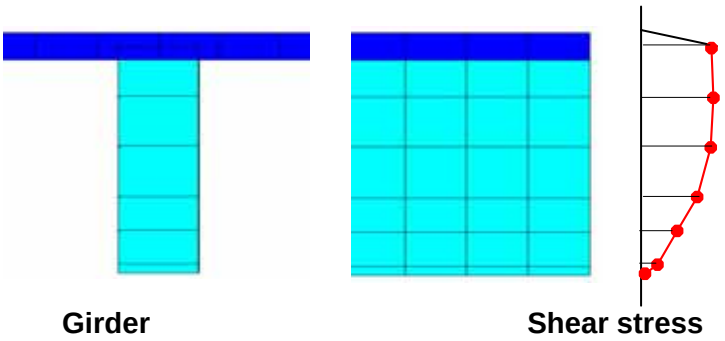

b)

Figure 12.1: Shear stress distribution at a section – a) theoretical distribution; b) FEA distribution

Comparisons of the shear distribution from field measured strains in the steel stirrups and from calculated FE analysis shear forces were made for seven locations as shown in Figure 12.2. The field-testing results at Location #4 were neglected, because both the strain and crack displacement data obtained from the tests were very small and the crack orientation was almost vertical.

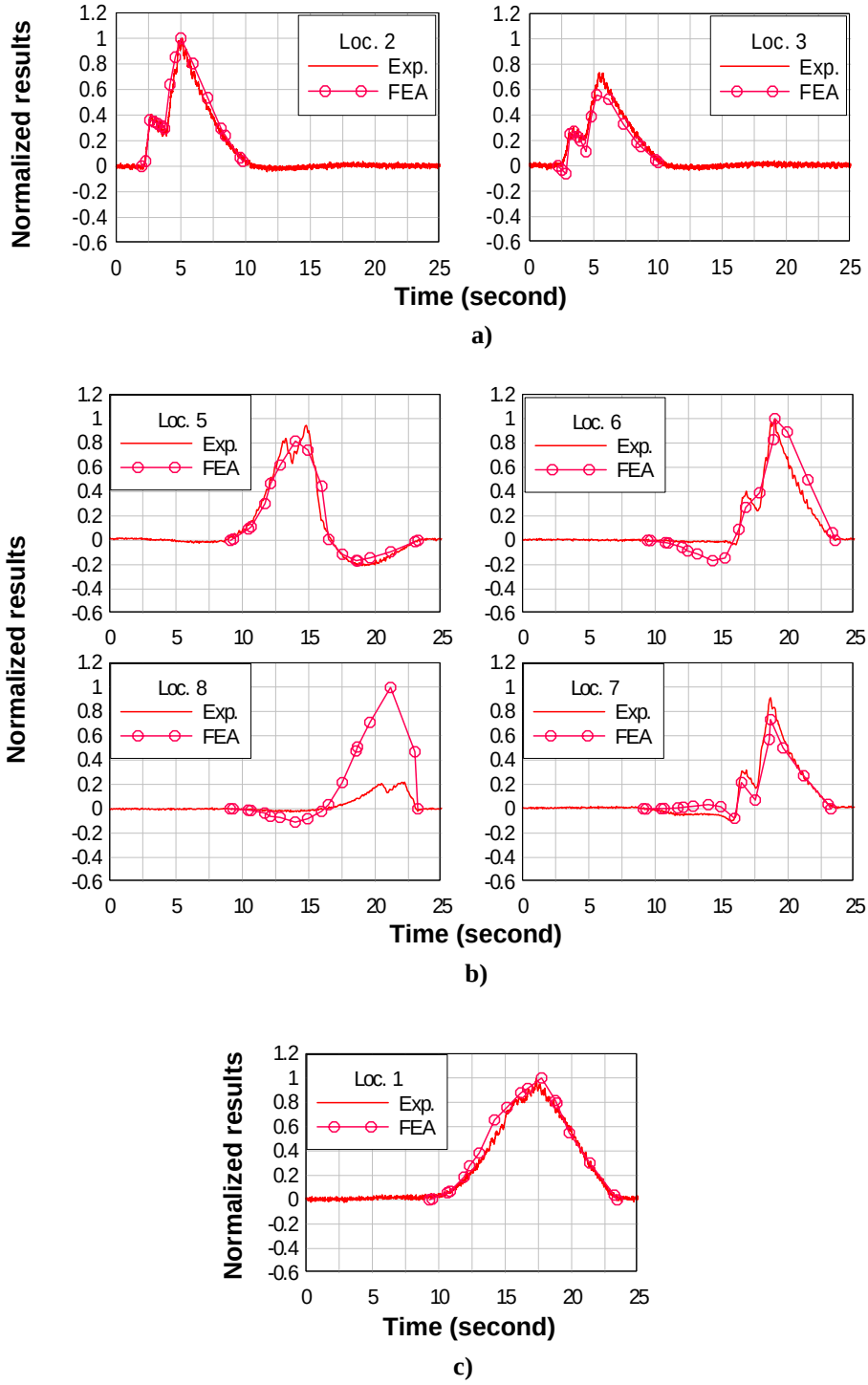

Figure 12.2: Truck passage simulation using finite element analysis – a) simple span; b) continuous spans; c) transverse beam at Bent 4

Comparisons between field-testing and FE analysis results were divided into three groups, i.e. simple span (Figure 12.2a), continuous span (Figure 12.2b), and transverse beam at Bent 4 (Figure 12.2c). For each group, measured strains from the field tests and calculated shears from the FE analyses were normalized by dividing each result by the largest result value for the group. For both field-testing and FE results, the largest results occurred at the same locations – Location #2 for the simple span and Location #6 for the continuous span. Good correlation between field-testing and FE analysis results was observed; however results from the FE analyses did not show effects of the test truck axle passing, front and tandem axles, which generated two close peaks. Adding additional truck positions to the FE model would likely capture these effects.

12.3 INFLUENCE OF DECK THICKNESS AND DIAPHRAGM STIFFNESS ON LOAD DISTRIBUTION

The most common deck thickness for 1950's vintage CRC deck-girder bridges in Oregon is 152 mm (6 in) thick, based on a database of cracked bridges in the State (see Part I of this report). To investigate the influence of deck thickness on load distribution, three different deck thicknesses, 152 mm (6 in), 254 mm (10 in), and 356 mm (14 in), were modeled to observe a change of shear forces in the four girders across a transverse section. The effect of the deck thicknesses on shear distribution is shown in Figure 12.3.

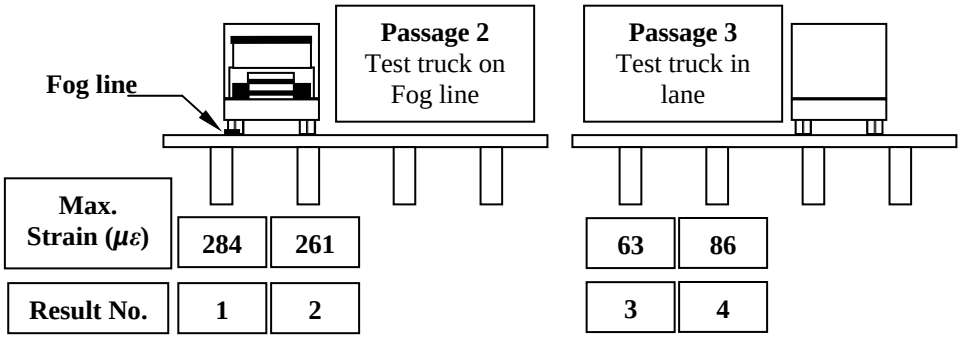

	Result No.			
	1	2	3	4
6-inch Deck - Field test, με (%)	284 (40.9)	261 (37.6)	86 (12.4)	63 (9.1)
6-inch Deck - FEM, %	47.0	28.7	18.1	6.2
10-inch Deck - FEM, %	46.4	29.2	18.0	6.4
14-inch - FEM, %	45.1	29.7	17.9	7.3

Figure 12.3: Influence of slab thickness on shear force distribution across a transverse section

The FE results were used to calculate shear forces in the four girders near result Location #6, when the last axle of the test truck (one side on the fog line) was positioned over Location #6. For field-test data, strain gages were installed on the two girders in the northbound lane, therefore measurements at Locations #6 and #7 for Passages #2 and #3 were used for

comparisons. Comparisons among the FE models show that as the deck thickness increases, the differences of the shear forces in the four girders decrease. The thicker deck mobilizes the entire bridge section and produces one-way bending of the bridge with both deck and girders resisting the applied load together.

Two FE models with different diaphragm stiffnesses were developed by changing the elastic modulus of the diaphragm elements, multiplied by 0.5 and 2, respectively. Results from the analysis were compared to those of the FE model with a 152 mm (6 in) thick deck and the as-designed diaphragm stiffness. The same loading and result locations were employed as for the different slab thickness study. No significant difference in shear forces for the four girders across the transverse section was observed for these different diaphragm stiffnesses.

12.4 PREDICTION OF DIAGONAL-TENSION CRACKING IN TWO-SPAN CONTINUOUS GIRDERS

A prediction of diagonal-tension cracking was made for the exterior girder in Span 8 between Bent 4 (center support) and the first diaphragm indicated with a circle shown in Figure 12.4. The largest diagonal-tension stress magnitude as a result of permanent loads can be observed in this region. Field-testing results (strain gage at Location #6) near this region also measured the largest live load strains. Permanent and live loads, i.e. structure self weight, wearing surface material weight, and truck loads, as well as forces caused by temperature gradients, shrinkage, creep, and support displacements were considered in the cracking prediction.

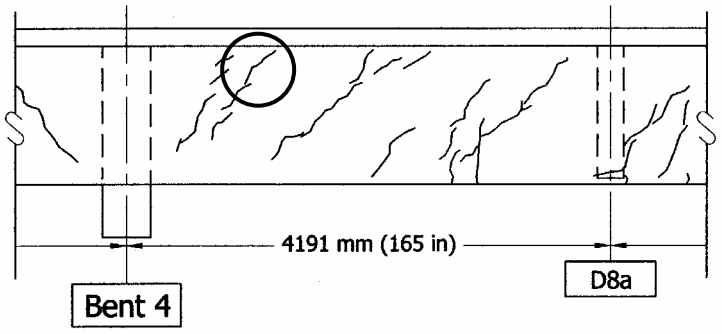

Figure 12.4: Cracks in the exterior girder between Bent 4 and the first diaphragm

Tensile strength of concrete (MPa) was determined as (*ACI 318-2002*):

$$f_t = 0.498\sqrt{f'_c} \qquad \textbf{(12-2)}$$

Again, core tests were used for the compressive strength of the concrete. The lowest concrete strength obtained from the core tests was 23.1 MPa (3350 psi) resulting in a concrete tensile strength of 2.39 MPa (347.3 psi). This value was used to determine when diagonal-tension cracking occurred in the girders.

12.4.1 Stresses due to permanent loads

Self weight of the bridge and wearing surface weight were considered. A unit weight of 23.6 kN/m^3 (150 lb/ft^3) was assumed for the reinforced concrete. An asphalt wearing surface with a total thickness of 101mm (4 in.), 50.5mm (2 in.) for the original wearing surface and 50.5mm (2 in.) from an overlay, were assumed to exist on the deck of the approach spans from curb to curb, 9144 mm (30 ft) wide. A unit weight of 20.4 kN/m^3 (130 lb/ft^3) was used for the wearing surface material.

12.4.2 Stresses due to deformations

Thermal loading, creep, and shrinkage produce concrete volume changes, which may contribute to cracking in CRC bridges due to restraint of the deformations. Added stresses caused by the deformations may produce combined stresses in the girder close to or exceeding the tensile strength of the concrete and lead to cracking.

12.4.2.1 Thermal

Two types of temperature changes, uniform and nonuniform temperature changes, may induce forces in the bridge girder. Uniform temperature change lengthens or shortens the entire bridge superstructure, while the nonuniform temperature change due to a temperature gradient between the bridge deck and girder underneath may cause the girder to bow upward. Forces may be introduced to the bridge members due to restraint at support locations.

At the bridge location, Newberg, Oregon, the average highest and lowest temperatures occurring in a year are 81 °F and 33 °F, respectively (*Oregon Climate Service 2003*). These values were used in the uniform temperature change analysis. A reference temperature during bridge construction was assumed to be 55 °F, which produced a 22 °F temperature change for contraction and 26 °F temperature change for expansion.

For the nonuniform temperature change analysis, an average temperature difference between seasonal maximum and minimum temperatures was considered to account for a daily temperature difference. During a typical 24-hour period the deck is heated more significantly than the other components during the day and the entire bridge cools at night. An average daily temperature range for the site was 27 °F in the summer and 13 °F in the winter (*Oregon Climate Service 2003*).

For both analyses, negligible time lag between air and concrete temperatures was assumed. A coefficient of thermal expansion or contraction for normal-weight concrete was chosen as 5.5×10^{-6} / °F (*MacGregor 1997*). The coefficient was consistently assigned to all elements in the bridge model for the uniform temperature change analysis. For the nonuniform temperature change analysis, only deck elements were allowed to expand with increasing temperature.

12.4.2.2 Shrinkage

Drying shrinkage, which occurs as the concrete cures, was also considered. Several empirical equations have been developed to predict drying shrinkage. Shrinkage strains were predicted using the CEB-FIP method as (*CEB-FIP Code 1990*):

$$\varepsilon_{cs}(t,t_s)=\varepsilon_{cso}\,\beta_s(t,t_s) \quad \textbf{(12-3)}$$

$$\varepsilon_{cso}=\varepsilon_s(f_{cm})\beta_{RH} \quad \textbf{(12-4)}$$

$$\varepsilon_s(f_{cm})=[160+\beta_{sc}(9-f_{cm}/f_{cmo})]\times 10^{-6} \quad \textbf{(12-5)}$$

$$\beta_{RH}=-1.55\left[1-\left(\frac{RH}{RH_0}\right)^3\right] \quad \textbf{(12-6)}$$

$$\beta_s(t,t_s)=\left[\frac{(t-t_s)/t_1}{350(h_e/h_o)^2+(t-t_s)/t_1}\right]^{0.5} \quad \textbf{(12-7)}$$

$$h_e=2A_c/u \quad \textbf{(12-8)}$$

where ε_{cs} is the axial shrinkage strain, ε_{cso} is the basic shrinkage strain, $\beta_s(t,t_s)$ is a coefficient describing development of shrinkage with time, β_{RH} is a coefficient that accounts for the effect of the relative humidity on shrinkage, β_{sc} is 50 for Type I cement, f_{cm} is the average 28-day compressive strength of the concrete (psi), f_{cmo} is 1450 psi, RH is the relative humidity of the ambient atmosphere (%), RH_o is 100%, h_e is the effective thickness to account for volume/surface ratio (in.), A_c is the cross sectional area (in.^{2}), u is the perimeter of the cross section exposed to the atmosphere (in.), h_o is 4 in., t is the age of the concrete (days), t_s is the age of the concrete at the end of moist curing (days), and t_1 is 1 day.

The prediction method accounts for member size, age of concrete, relative humidity, moist curing time, and concrete strength. The lowest relative humidity (*RH*) for the site is about 40% (*Oregon Climate Service 2003*). Moist curing time (t_s) and age of concrete (t) were assumed to be 14 and 365 days, respectively. Several elements within the bridge were considered, i.e. girders, the bent beam, slab, and columns. Shrinkage strains for the elements were calculated using Equations 12-3 through 12-8 and are summarized in Table 12.1.

Table 12.1: Shrinkage and creep strains in bridge elements

Bridge Member	Shrinkage Strain	Creep Strain*
Girders (13 in. x 53 in.)	-0.000218	0.000914
Deck (12 in. strip x 6 in. thick)	-0.000366	0.001088
Bent beam (16.5 in. x 71 in.)	-0.000174	0.000850
Columns (24 in. x 36 in.)	-0.000177	0.000854

* based on applied stress of 1500 psi.

Shrinkage of the concrete was simulated in the FE analysis using temperature changes in the elements of the model. Different thermal expansion coefficients were assigned to the various elements in the model to induce the volume changes based on the shrinkage strains computed in Equations 12-3 through 12-8. Temperature reduction was applied to the model causing the elements to contract thereby producing shrinkage strains.

12.4.2.3 Creep

Concrete exhibits a material behavior called creep whereby deformations increase with time when subjected to a constant load. Creep strains occur in the regions of beams and columns containing compressive stresses. Creep strains in each member were estimated as (*CEB-FIP Code 1990*):

$$\varepsilon_{cc}(t,t_0)=\frac{\sigma_c(t_0)}{E_c(28)}\phi(t,t_0) \quad \textbf{(12-9)}$$

$$\phi(t,t_0)=\phi_0\,\beta_c(t,t_0) \quad \textbf{(12-10)}$$

$$\phi_0=\phi_{RH}\,\beta(f_{cm})\beta(t_0) \quad \textbf{(12-11)}$$

$$\phi_{RH}=1+\frac{1-RH/RH_0}{0.46(h_e/h_0)^{1/3}} \quad \textbf{(12-12)}$$

$$\beta(f_{cm})=\frac{5.3}{(f_{cm}/f_{cm0})^{0.5}} \quad \textbf{(12-13)}$$

$$\beta(t_0)=\frac{1}{0.1+(t_0/t_1)^{0.2}} \quad \textbf{(12-14)}$$

$$\beta_c(t,t_0)=\left[\frac{(t-t_0)/t_1}{\beta_H+(t-t_0)/t_1}\right]^{0.3} \quad \textbf{(12-15)}$$

$$\beta_H=150\left[1+\left(1.2\frac{RH}{RH_0}\right)^{18}\right]\frac{h_e}{h_0}+250\le 1500 \quad \textbf{(12-16)}$$

where $\varepsilon_{cc}(t,t_0)$ is the creep strain between time t_0 and t, $\sigma_c(t_0)$ is the stress applied at time t_0 (psi), $E_c(28)$ is the modulus of elasticity for the concrete at an age of 28 days (psi), $\phi(t,t_0)$ is the creep coefficient, ϕ_0 is the basic creep coefficient, $\beta_c(t,t_0)$ is a coefficient accounting for the development of creep with time, and t_0 is the age of the concrete at initial loading (days).

The relative humidity (*RH*) was assumed to be 40%. Concrete strength (f_{cm}) was assumed to be constant and equal to 31.0 MPa (4500 psi) based on average core strengths. Age of concrete at initial loading (t_0) and age of concrete (t) are assumed to be 14 and 365 days, respectively. Creep strains for the various members are shown in Table 12.1. For this analysis, creep was assumed to be linearly related to stress, which is valid for compressive stresses less than 40% of concrete strength. Based on the FE analysis, the largest compressive stress in the bridge model under the permanent load was 9.55 MPa (1385 psi) and occurred at the bottom of the center support in the exterior girder.

For the FE model, the creep properties were assigned to elements that contained only principal compressive stresses. Selected elements of the FE bridge model for creep simulation are shown in Figure 12.5.

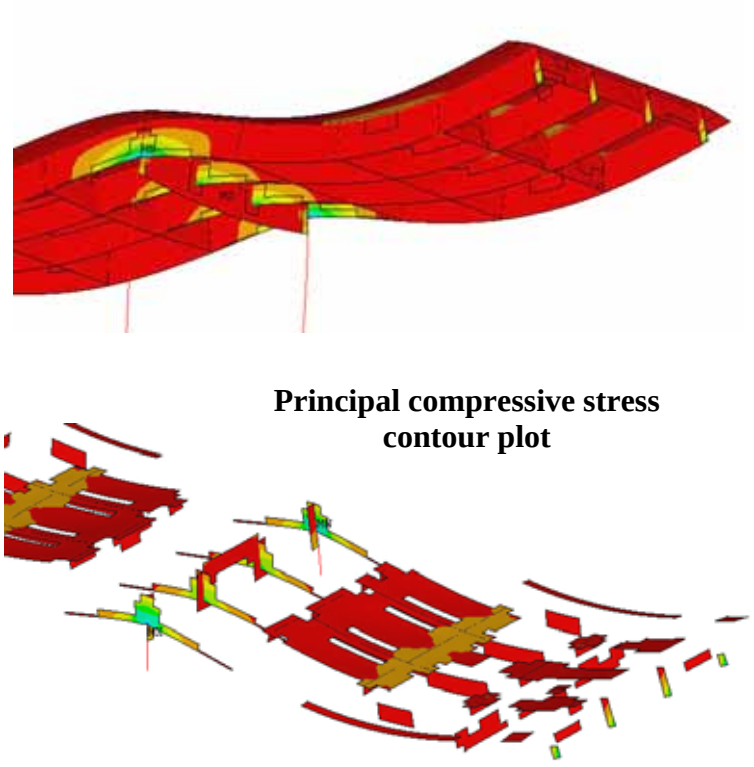

Figure 12.5: Selected elements for creep simulation

12.5 SUPPORT DISPLACEMENT

To assess the role of possible support deformations on diagonal-tension cracking, two FE models were developed with imposed support displacements. Movements of the end and middle supports were considered with a vertical displacement of 2.54 mm (0.10 in) applied individually at the end supports and at the center support. Changes in the diagonal–tension stresses near the middle bent were monitored.

12.6 SUPPORT RESTRAINTS

Based on the bridge design drawings, restraints at the north and south end supports were designed as a rocker (Figure 12.6a) and a vertical support (Figure 12.6b), respectively. At the middle support (Bent 4), the girders were cast monolithically with a transverse bent cap beam, which is supported by two columns. These supports provide actual boundary conditions that are different than idealized frictionless bearings.

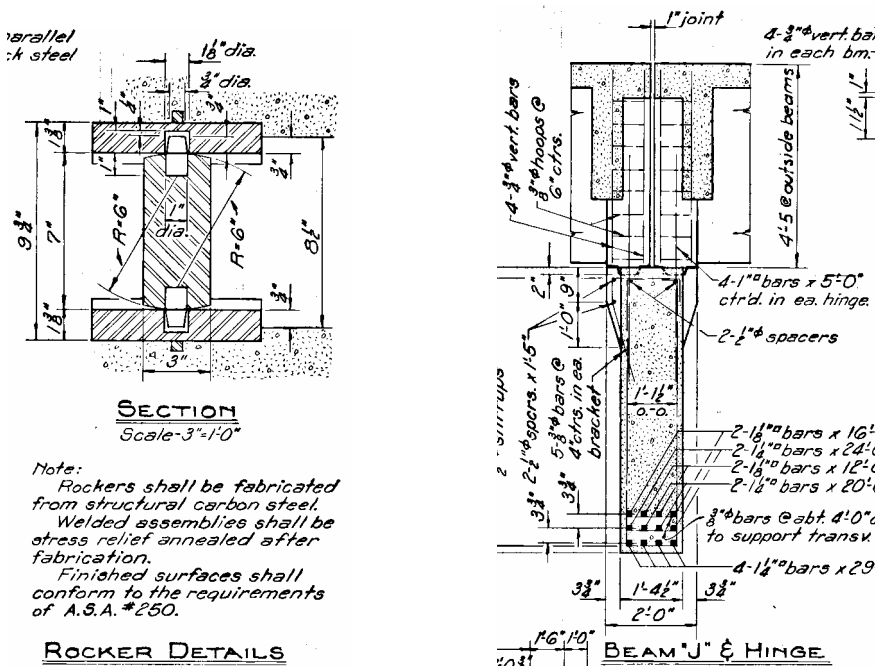

Figure 12.6: Detail of as-designed supports – a) north end; b) south end

The role of the boundary conditions at the ends of the girders was considered in the FE model. Supports at both ends were considered to be the similar and were idealized as roller supports with friction. The roller supports were modeled to have some degree of restraint to free movement due to friction at the bearing locations. Translation in the vertical direction was fully constrained, while rotations and transverse translations were free to move. Linear spring

elements were added to the bottom of the girders at the bearing locations to simulate static friction in the longitudinal direction as shown in Figure 12.7.

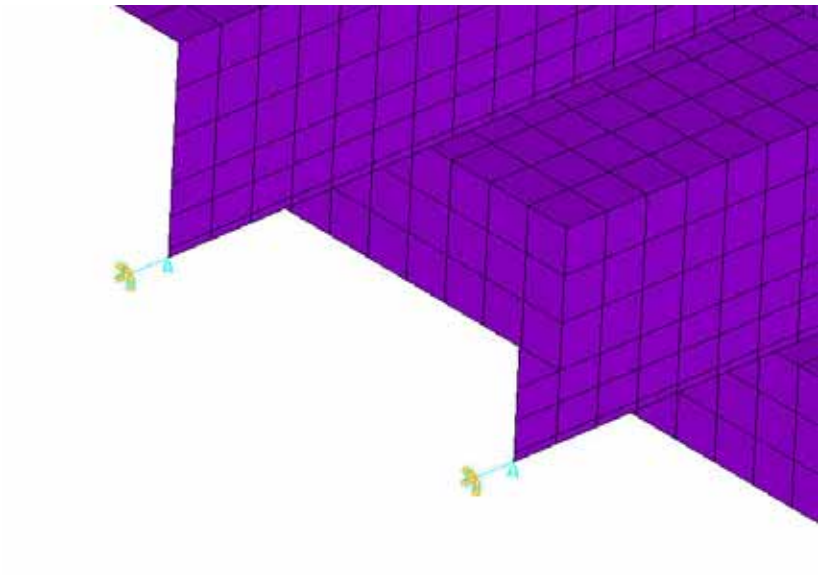

Figure 12.7: Linear spring elements for simulation of friction

Support displacements in both longitudinal and transverse directions were produced by permanent loads and loads due to deformations. For this analysis, only longitudinal friction was considered and described using a coefficient of friction. The friction coefficients were obtained by dividing longitudinal reactions at the end supports by vertical reaction force. The relationship between end-support movement and different coefficients of friction for the FE model subjected to a uniform thermal loading (contraction) is shown in Figure 12.8.

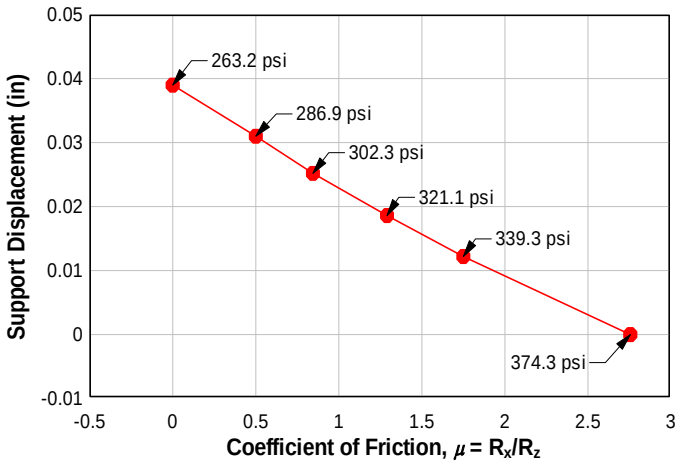

Figure 12.8: Relationship between end-support movement and different coefficients of friction for FE model subjected to a uniform thermal loading (contraction)

As shown in the figure, when the coefficient of friction equals zero, the supports freely moved by 1 mm (0.04 in). On the other hand, when the supports were prevented from moving, the corresponding coefficient of friction was 2.8.

The diagonal-tension stress near the center support is also shown in Figure 12.8 for the different levels of support friction. The stress was equal to 1.81 MPa (263.2 psi) for no friction and 2.58 MPa (374.3 psi) for fixed supports, a 42% increase. As the coefficient of friction increased, smaller end-support displacements were produced and greater diagonal-tension stresses developed near the center support. To estimate the support movement due to the specified bearings, the spring stiffness was varied until a coefficient of static friction of 0.5 was obtained. This value approximates a concrete-steel interface (*AUSTROADS 1992*).

13.0 FINITE ELEMENTS RESULTS SUMMARY

FE analysis results for the different loading cases are shown in Table 13.1. Stresses at several locations in the girder were considered. Diagonal-tension stress near the center support was located at the centroid of the shell element, 1257 mm (49.5 in) from the center support and 1130 mm (44.5 in) from the girder bottom. Diagonal-tension stress near the end support was located at 1251 mm (49.3 in) from the end support and 572 mm (22.5 in) from the girder bottom. At the same distance from the end support, flexural stress in the shell element was located at 25 mm (1 in) from the girder bottom.

Model 1 had only permanent loads including bridge self weight and weight of the wearing surface material. Models 2 - 5 had additional loads including thermal loading, drying shrinkage, creep, and support displacement, individually simultaneously with the permanent loads. For Model 6, shrinkage and nonuniform temperature change were combined with the permanent loads to simulate the most likely in-service load condition for the bridge at least one year after completion of construction.

Table 13.1: Summary of finite element analysis results

Model	Principal Stress, MPa (psi)			% Difference to Model 1 (Permanent Loads)		
	Diagonal Tension		Flexural			
	Near Center Support (1)	Near End Support (2)	Near End Support (3)	1	2	3
1) Permanent Loads	1.73 (250.8)	0.45 (65.7)	0.93 (135.2)	0.0	0.0	0.0
2) Temperature Change						
2.1) Uniform Contraction	1.98 (286.9)	0.71 (103.2)	2.09 (303.6)	14.4	57.1	124.6
2.2) Uniform Expansion	1.84 (266.4)	0.44 (64.0)	0.91 (132.1)	6.2	-2.6	-2.3
2.3) Nonuniform	3.27 (473.8)	1.23 (178.6)	0.38 (55.1)	88.9	171.9	-59.3
3) Shrinkage	0.80 (116.2)	0.18 (26.6)	2.26 (323.0)	-53.7	-59.5	139.0
4) Creep	1.69 (245.2)	0.51 (73.3)	0.91 (131.9)	-2.2	11.6	-2.4
5) Support Displacement						
5.1) Center Support	1.55 (224.8)	0.47 (68.4)	0.97 (140.0)	-10.3	4.2	3.6
5.2) End Support	1.83 (266.1)	0.44 (64.0)	0.91 (131.6)	6.1	-2.5	-2.6
6) Load Combination:						
Shrinkage and Nonuniform Temperature Change	1.95 (282.7)	0.72 (104.8)	2.11 (306.3)	12.7	59.5	126.7

Results for each of the cases are compared to the model under permanent loads only. Uniform contraction due to the temperature decrease (Model 2.1) caused a higher diagonal-tension stress by 14% and 57% near the center support and near the end support, respectively. Uniform contraction due to the temperature decrease also provided higher flexural stress near the end support by 125%.

Uniform expansion due to the temperature increase (Model 2.2) had a relatively small effect on the stresses, 6% higher for the diagonal-tension stress near the center support, 3% lower for the diagonal-tension stress near the end support, and 2% lower for the flexural stress near the end support.

Temperature gradient between the girder and deck (Model 2.3) had the greatest influence on the diagonal-tension stresses near the center and end supports with stress increases of 89% and 172%, respectively. However, flexural stress near the end support was reduced by 60%.

Simulated drying shrinkage (Model 3) produced 54% and 60% lower diagonal-tension stresses near the center support and near the end support, respectively, while it produced the biggest change in the flexural stress near the end support with an increase of 139%.

Creep (Model 4) caused a slightly lower diagonal-tension stress of 2% near the center support and flexural stress near the end support, while the diagonal-tension stress near the end support increased by 12%.

The center-support vertical settlement (Model 5.1) decreased the diagonal-tension stress by 10%, while the end-support settlement (Model 5.2) increased the same stress by 6%. The end-support displacement produced similar effects as the uniform expansion due to temperature change. This is reasonable, because both loads caused similar deformations of the girders.

The combined load model (Model 6) had 13% higher diagonal-tension stress near the center support, 60% higher diagonal-tension stress near the end support, and a 127% higher flexural stress near the end support compared to the model subjected to permanent loads only. This model was employed to predict cracking of the bridge with further superposition of live loads.

13.1 ESTIMATE OF TRUCK LOAD MAGNITUDE FOR DIAGONAL CRACKING

The FE model subjected to permanent loads, shrinkage and nonuniform temperature change was also loaded using point loads corresponding to the HS standard truck pattern. The spacing between the tandem and trailer axles of the HS truck was 4267 mm (14 ft) to produce maximum shear on the bridge. The passenger-side wheel loads of the HS truck were placed on the exterior girder line. The HS truck loads were moved incrementally over the deck starting from the center support toward the end support. The average maximum impact factor for Locations 5 - 7 was 37% based on field test results and was used in the analysis. A magnification factor of 27% from two truck loads based on the field measurement was considered as shown in Figure 13.1. These two factors were added to the FE model for the cracking prediction.

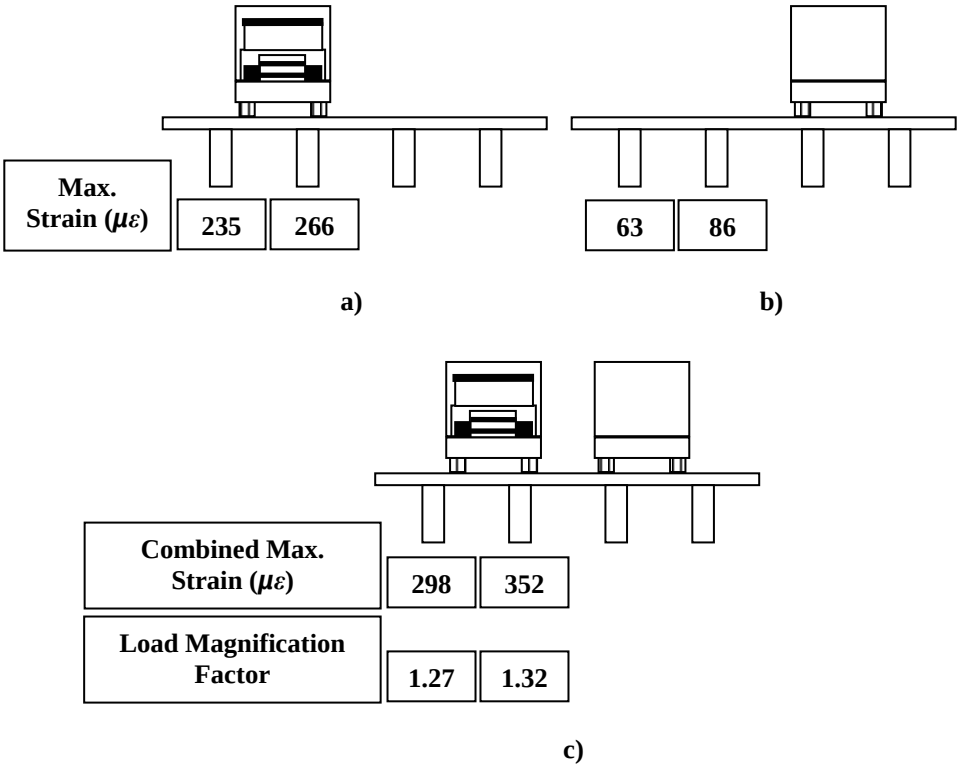

Figure 13.1: Load magnification factor due to two test truck loads considering stirrup strains in the exterior and interior girders at result Locations 6 and 7 near Bent 4 – a) maximum strains from the test truck moving north; b) maximum strains from the test truck moving south; c) combined strains (to simulate two truck loads)

The field measured crack pattern on the exterior bridge girder is shown in Figure 13.2a. Vector plots of principal stresses from the finite element analysis results are shown in Figure 13.2b and Figure 13.2c for the exterior girder shell elements under the HS truck loads. The size of the arrows represents the magnitude of principal stresses, and orientation of the arrows indicates the angle of principal stresses.

The location and weight of the HS truck configuration that generated stresses sufficient to produce diagonal-tension cracking in the girder are shown in Figure 13.2b with a dashed line. The diagonal-tension crack was located near the top of the girder web 1257 mm (49.5 in) away from the center support. The potential crack location was identified based on the stress magnitude and the angle of principal stresses corresponding to approximately 45 degrees from horizontal. From the FE analysis, the HS truck sufficient to cause a diagonal-tension crack corresponded to HS12 with a total weight of 192.2 kN (43.2 kip). The trailer axle of HS truck was located 3632 mm (143 in.) away from the Bent 4.

To predict a subsequent diagonal-tension crack caused by the HS truck configuration, the concrete elastic modulus for the elements containing the predicted first crack was reduced to 0.69 MPa (100 psi) to model cracking and associated local softening. Due to symmetry, diagonal-tension cracking could occur on the other side of Bent 4 in the exterior girder as well as on both sides of Bent 4 in the interior girder. Therefore, the stiffness of those elements was

reduced as well. The FE model used for prediction of subsequent diagonal-tension cracking is shown in Figure 13.3.

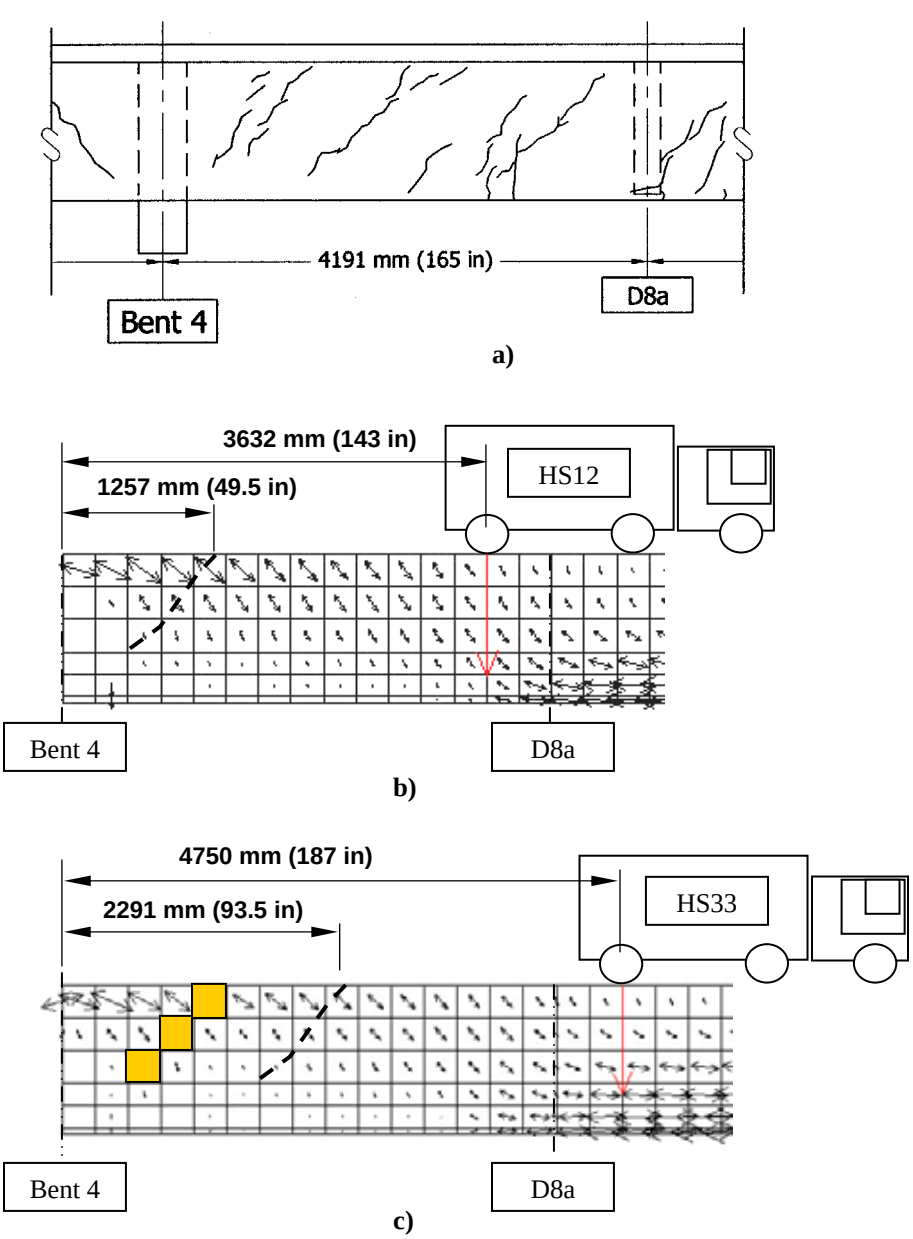

Figure 13.2: Diagonal-tension cracking prediction using finite element analyses – a) crack pattern existing in the bridge exterior girder; b) first cracking prediction; c) second cracking prediction

Results from the analysis of the subsequent diagonal-tension cracking prediction are shown in Figure 13.2c. The reduced stiffness elements are shown in gray. As seen in this figure, stresses in the elements at the top of the girder adjacent to the modified elements were reduced. A second potential crack was observed to occur at a distance of 2375 mm (93.5 in) from the center support (Bent 4) corresponding to 1118 mm (44 in) from the first crack. An HS truck

configuration with axle loads corresponding to HS33 with a total weight of 528.4 kN (118.8 kip) located a distance of 4191 mm (165 in) from Bent 4 was required to produced the subsequent crack.

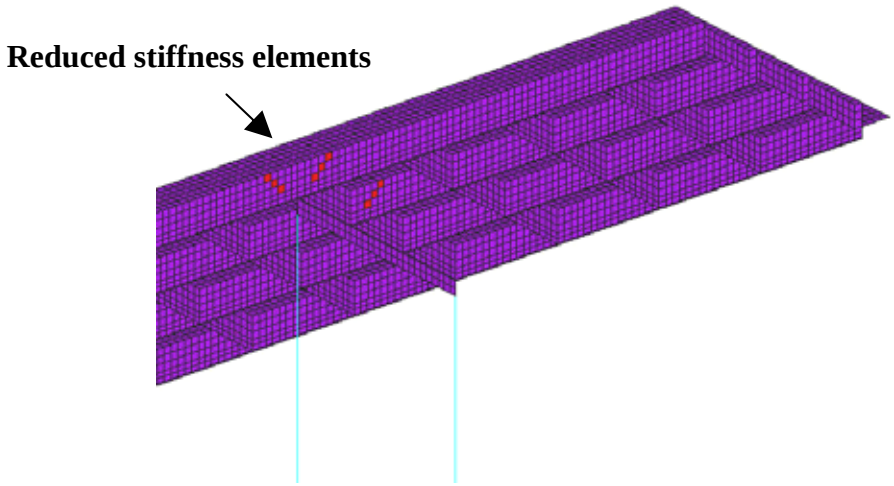

Figure 13.3: FE model of south approach spans for a subsequent diagonal-tension cracking prediction

The FE analyses gave a reasonable prediction of cracking corresponding to the existing diagonal-tension cracks in the bridge girders. However, the predicted crack location and corresponding loading are only approximate, due to the large element sizes in the approach span model. More detailed predictions could be made, if the bridge was modeled with finer element meshing and incorporation of nonlinear material models with added steel reinforcement elements. Other techniques, such as the smeared cracking approach or discrete cracking method, could also give more detailed results. However, such techniques require additional computational time, modeling requirements, or accurate load distribution to facilitate detailed substructure analysis compared to the linear elastic finite element analysis.

14.0 CONCLUSIONS

Field inspection and instrumentation of a 1950's vintage CRC deck-girder bridge have been completed. Strains in the stirrups and diagonal crack displacements were measured under ambient traffic conditions and a known test truck. A finite element model of the bridge was developed using linear elastic shell elements. The bridge behavior under permanent loads, loads due to deformations, and simulated truck loading was predicted. Prediction of initial diagonal cracking and subsequent cracking were made. Based on the field test and finite element analyses results, the following conclusions are presented:

1. The bridge girders do not meet modern design requirements for shear. This is due to overestimation of the concrete contribution to shear that was permissible in the design specification at the time.

2. Equivalent constant amplitude stirrup strains from measured ambient traffic induced strains at all instrumented locations were well below the fatigue limit for long life of reinforcing steel. The maximum strain was 10.6 ksi at Location #5. Metal fatigue leading to fracture of the stirrups is unlikely. However, at the time of data collection, the bridge was load posted.

3. Cracks were observed to open for all instrumented locations and open and close for instrumented locations on the continuous spans. This may have implications for epoxy injection of cracks and bond fatigue of stirrups.

4. Stirrup strains and crack displacements in the continuous spans were generally higher than those in the simple span for the controlled test truck loading due to a fewer number of girders and the structural indeterminacy.

5. Peak strain measurements in stirrups tended to increase with increasing test truck speed. The average for all instrumented locations was a 20% increase in strain for the truck traveling near the posted speed compared to the slow speed (5 mph). The largest increase observed was 46% at Location #6.

6. The maximum stress range in the steel stirrups calculated using the strain results due to the test truckload was equal to 76.6 MPa (11.1 ksi), which is less than the safe stress range of 163 MPa (23.6 ksi) based on the AASHTO standard specification. The test truck produced higher strains than those observed under ambient traffic conditions.

7. Stirrup stresses under combined live load with impact and permanent load were estimated to be considerably above the allowable stress of 20 ksi. Permanent loads contributed significantly to the stress magnitude. Careful consideration should be given when an overlay of the wearing surface is contemplated for these types of bridges, so as not to significantly increase the stirrup stress under permanent loads.

8. Load distribution for the bridge girders was estimated from measured stirrup strains. The interior girder carries approximately 40% of the statical shear produced on the bridge section from a single test truck in the marked lane and approximately 27% of the statical shear produced on the bridge section from two test trucks. The AASHTO Standard Specification load distribution methods conservatively over-estimate the live load shear force on the individual girders.

9. The finite element analyses reasonably predicted the relative magnitude of vertical force in the girders as compared to the field measured stirrup strains under service-level moving loads. This indicates that load distribution in the service-level range may be reasonably predicted using elastic finite element analysis for these types of bridges containing diagonal cracks in the girders.

10. Greater load distribution of shear forces across the girders is achieved as the slab thickness increased.

11. Diaphragm stiffness had little effect on the shear force distribution.

12. Nonuniform temperature change produced the greatest increase of diagonal-tension stress near the center support, with a 90% increase compared to the FE model without the temperature change effect. Nonuniform temperature change caused a 172% higher diagonal-tension stress near the end support.

13. The simulated drying shrinkage yielded a much higher flexural stress near the end support, with a 139% increase.

14. The center-support settlement decreased the diagonal-tension stress near the center support by 10%, while the end-support settlement increased the stress by 6%.

15. The FE model subjected to truck loads, permanent loads, and loads due to drying shrinkage and nonuniform temperature predicted diagonal-tension cracking of the girders. Analysis results estimated that an HS truck configuration corresponding to HS12 caused the initial diagonal-tension cracking near the center support. A heavier truck, HS33, generated a subsequent diagonal crack next to the first crack located a distance of approximately the girder's effective depth away.

16. It is anticipated that the bridge would exhibit diagonal cracks from actual truck loads operating on the bridge from combined effects of the truck loads with permanent loads as well as temperature and drying shrinkage effects.

15.0 REFERENCES

AASHO, American Association of State Highway Officials. *Standard Specifications for Highway bridges, 4th Edition*. Washington, DC. 1944.

AASHO, American Association of State Highway Officials. *Standard Specifications for Highway bridges, 5th Edition*. Washington, DC. 1949.

AASHO, American Association of State Highway Officials. *Standard Specifications for Highway bridges, 6th Edition*. Washington, DC. 1953.

AASHO, American Association of State Highway Officials. *Standard Specifications for Highway bridges, 7th Edition*. Washington, DC. 1957.

AASHO, American Association of State Highway Officials. *Standard Specifications for Highway bridges, 8th Edition*. Washington, DC. 1961.

AASHO, American Association of State Highway Officials. *Standard Specifications for Highway bridges, 9th Edition*. Washington, DC. 1965.

AASHTO, American Association of State Highway and Transportation Officials. *Standard Specifications for Highway bridges, 16th Edition*. Washington, DC. 1996.

AASHTO, American Association of State Highway and Transportation Officials. *Standard Specifications for Highway bridges, 17th Edition*. Washington, DC. 2002.

ACI 318-02. American Concrete Institute. *Building Code Requirements for Structural Concrete*. American Concrete Institute. Farmington Hills, Michigan. 2002.

ACI 318-63. American Concrete Institute. *Building Code Requirements for Structural Concrete*. American Concrete Institute. Farmington Hills, Michigan. 1963.

AUSTROADS. *Australian Bridge Design Code, Part 4: Bearings and Deck Joints*. Sydney, Australia. 1992.

Comité Euro-International du Béton. CEB-FIP Model Code 1990. Thomas Telford Services Ltd. London. 1993.

Downing, S. A. and D. F. Socie. "Simple Rainflow Counting Algorithms." *Int. J. of Fatigue*. 4:1, 31-40. 1982.

MacGregor, J. G. *Reinforced Concrete Mechanics and Design*. 3rd Edition. Prentice Hall. Upper Saddle River, New Jersey. 1997.

Miner, M. A. "Cumulative Damage in Fatigue." *Journal of Applied Mechanics*. Vol. 12. Trans. ASME Vol. 67. pp. A159-A164. 1945.

Nilson, A. H. *Design of Concrete Structures*. McGraw-Hill, Inc. New York, New York. 1997.

Oregon Climate Service (OCS). “The Climate of Oregon.” College of Oceanic and Atmospheric Sciences. Oregon State University. Corvallis, OR. 2003.